The physics of fast Z pinches

D.D. Ryutov
Lawrence Livermore National Laboratory, Livermore, CA 94551, USA
M.S. Derzon
Sandia National Laboratories, Albuquerque, NM , 87185, USA
M.K. Matzen
Sandia National Laboratories, Albuquerque, NM , 87185, USA

Abstract

The spectacular progress made during the last few years in reaching high energy densities in fast implosions of annular current sheaths (fast Z pinches) opens new possibilities for a broad spectrum of experiments, from x-ray generation to controlled thermonuclear fusion and astrophysics. Presently Z pinches are the most intense laboratory X ray sources (1.8 MJ in 5 ns from a volume 2 mm in diameter and 2 cm tall). Powers in excess of 200 TW have been obtained. This warrants summarizing the present knowledge of physics that governs the behavior of radiating current-carrying plasma in fast Z pinches. This survey covers essentially all aspects of the physics of fast Z pinches: initiation, instabilities of the early stage, magnetic Rayleigh-Taylor instability in the implosion phase, formation of a transient quasi-equilibrium near the stagnation point, and rebound. Considerable attention is paid to the analysis of hydrodynamic instabilities governing the implosion symmetry. Possible ways of mitigating these instabilities are discussed. Non-magnetohydrodynamic effects (anomalous resistivity, generation of particle beams, etc.) are summarized. Various applications of fast Z pinches are briefly described. Scaling laws governing development of more powerful Z pinches are presented. The survey contains 36 figures and more than 300 references.

CONTENTS

DISCLAIMER

BASIC NOTATIONS

Throughout this paper we use predominantly the SI system of units. The temperature is measured in the energy units (for instance, we write the equation of state for the ideal gas as $p=nT$, with T measured in *Joules*, and not $p=nkT$, with k being the Boltzmann constant and T measured in *Kelvin*). In the "practical" formulas we use mixed system of units (for instance, the temperature will be measured in electron-volts).

B	magnetic field induction
C	radial convergence
E	electric field
D_m	magnetic diffusivity
I	pinch current
I_w	current in an individual wire
I_Z	ionization energy of an ion in a charge-state Z
L	anode-cathode distance
T	temperature
Z	the charge of a fully stripped ion
Z_{eff}	average charge of the ions in a plasma
a	Alfven velocity
c	speed of light
g	effective gravity acceleration
h	characteristic thickness of the imploding shell
k	wave vector
m	azimuthal mode number
$\hat{m}$	mass per unit length of the pinch
$\hat{m}_w$	mass per unit length of an individual wire
n	particle number density
p	pressure
r_0	initial pinch radius
r_{min}	pinch radius at a maximum compression
s	sound speed
t	time
v_{Te}	electron thermal velocity
v_{Ti}	ion thermal velocity
Γ	growth rate
Λ	the Coulomb logarithm
Π	dimensionless pinch parameter
α	angle between the wave vector and the magnetic field
β	ratio of the plasma pressure and the magnetic field pressure
γ	specific heat ratio
ε	electric permittivity of the vacuum
η	electrical resistivity
λ	wavelength of the perturbation, $\lambda=2\pi/k$.
$\lambda\!\!\!^{-}$	characteristic length-scale of the perturbation, $\lambda\!\!\!^{-}=1/k$.
μ	permeability of the vacuum

ν kinematic viscosity
ρ mass density
χ thermal diffusivity
ω angular frequency
$\omega_{Ce,i}$ electron (ion) gyrofrequency
ω_{LH} lower-hybrid frequency
$\omega_{pe,i}$ electron (ion) plasma frequency

I. INTRODUCTION

A. A piece of history

Self-constricted plasma configurations are among the most fascinating objects in plasma physics, both because of their natural occurrence in a number of situations, including geophysics (lightning) and astrophysics (current channels at galactic scales), and because of their importance for a variety of applications. The first systematic attempts in the analysis of these configurations began in 1934, with the publication of a paper by J. Bennett (1934) on the equilibrium of streams of charged particles with a finite temperature. L. Tonks (1937) introduced the term "pinch" to describe these configurations.[1] Later, in the 1950s, the prefix "Z" was added to distinguish self-constriction by the axial (z) current from compression of a plasma column by an inductively driven azimuthal (θ) current. Only the former configuration, Z pinch, will be considered in our paper. We note in passing that the other configuration is called a θ pinch.

A broad attack on the study of Z pinches began at the early 1950s in conjunction with research on controlled thermonuclear fusion. The idea was to heat a deuterium-tritium mixture by an adiabatic and/or shock compression in a Z pinch and then sustain this system in the equilibrium state until a sufficient amount of fusion energy was released. This early stage of pinch research is covered in a book by Bishop (1958). It was soon discovered,

[1] Note the title of Sec.V of his more detailed paper (Tonks, 1939): "Constriction of Arc under its Own Magnetic Field - Pinch Effect." According to J.A. Phillips (1987), the term "pinch effect" was in fact first used in 1907 by C. Hering, to describe what would be now called "a sausage instability" of a liquid metal conductor in induction furnaces.

however, that the equilibrium pinch suffers from a large number of magnetohydrodynamic instabilities, including sausage and kink. Current disruptions caused by the development of these instabilities gave rise to voltage surges and the generation of accelerated deuterons that, in turn, produced bursts of neutron radiation. Realization that the neutrons were not of a "noble" thermal origin but were rather a side effect of a disastrous instability, led to widespread pessimism with regard to the chances for Z pinches to produce fusion-relevant plasmas. As a result, Z pinches virtually disappeared from the research programs of large fusion laboratories.

As a legacy of these years, there remained extensive theoretical analyses of the stability of pinch equilibria, summarized in particular in the survey by Kadomtsev (1966), and realization of the role of a so-called "Pease-Braginski current" (Pease, 1956; Braginski, 1958; see also a nice compact derivation in Pereira, 1990), a current at which radiative losses can be fully compensated by the Ohmic heating (1.4 MA for hydrogen, independent of the density and the pinch radius). References to the early studies of Z and θ pinches can be found in Kolb (1960).

B. What are "fast" Z pinches? (What is the scope of this review?)

Interest in Z pinches revived in the mid-1970s and early 1980s, initiated by a rapid development of pulsed-power technology. Various versions of Z pinches were tried, most notably fiber pinches and imploding gas-puffs. For the fiber pinches (see, e.g., Haines, 1982; Hammel, 1983), whose diameter ranged typically from tens of micrometers to a couple of hundred micrometers, the time for establishing the radial equilibrium (a few nanoseconds) was short compared to the duration of the current pulse. In other words, they were evolving along a sequence of the Bennett-type equilibria, where the plasma pressure is approximately balanced against the magnetic forces.

By contrast, the annular gas-puffs (see, e.g., Stallings et al., 1979; Spielman et al., 1985a; Smirnov, 1991) had an initial diameter of a few centimeters, and the driving current

pulsewidth was comparable to the implosion time (which is the time between initial current flow through the gas puff and stagnation of the plasma on axis). In this case, a free acceleration of the gaseous shell towards the axis occupies the major part of the total current pulsewidth. After having reached a certain minimum radius, the plasma bounces back and ceases to exist; the Bennett-type equilibrium has never been reached. The word "fast" used in the title of this survey refers just to this class of pinch discharges and specifies the scope of the survey: our prime focus will be discussion of the properties of those pinches where a run-in stage is definitive and duration of the whole process is too short to reach the Bennett-type state.

There is a significant difference in the important plasma instabilities for these two systems. Instabilities with an e-folding growth time much longer than the time of the propagation of acoustic signal over the pinch radius are important when considering quasi-equilibrium systems and are, obviously, of much less importance in the behavior of imploding systems. On the other hand, instabilities caused by the presence of large inertial forces (in particular, Rayleigh-Taylor instability, which will be discussed in much detail in this paper) are insignificant for quasi-equilibrium systems and become of a paramount importance for fast Z pinches. A nice discussion of various physics issues related to implosions of thin shells can be found in Turchi and Baker (1973), perhaps the first paper specifically devoted to fast Z-pinches.

Despite a short life-time (of order 10 ns in some cases), the plasma assembled by a fast Z pinch implosion provides unique possibilities for experimentation in a number of areas of physics. The growing interest in this area of research is reflected in particular by the fact that, at a recent conference on high-density Z pinches (Pereira, Davis, Pulsifer - Eds, AIP Conf. Proc., v. 409, 1997), more than half of the papers were directly related to fast (in the aforementioned sense) Z pinches. The quasi-equilibrium self-constricted plasma configurations, of the type of fiber pinches, have their own merits and probably deserve a separate survey. We feel that it would be difficult to cover both subjects in one

paper, partly because of the differences in the dominant physical processes, and partly just because of the space limits.

As has already been mentioned, the recent progress in fast Z pinches has been reached, to great extent, because of major breakthroughs in the pulsed-power technology. Pulsed power technology will not be discussed in this survey in any detail. A very brief summary of the pertinent information will be presented in Sec. I D. This review will concentrate on the physics issues of fast Z pinches. We will discuss in some detail simple models of various effects important for pinch performance, so that this survey could be used as a first introduction to the subject. On the other hand, we will consider also more subtle and complicated issues which could be skipped during the first reading of this paper.

TABLE 1. Characteristic parameters of a fast Z pinch

Height of the column, L (cm)	1-2
Initial radius of imploding cylinder, r_0 (cm)	2
Convergence, $C \equiv r_0/r_{min}$	10
Mass per unit length, $\hat{m}$ (mg/cm)	1-2
Maximum pinch current, I_{max} (MA)	10
Maximum voltage, V_{max} (MV)	1
Maximum magnetic field on the pinch surface, B_{max} (T)	10^3
Implosion time, t_{imp} (ns)	100
Maximum kinetic energy of the implosion, W_{max} (MJ)	1

The physics of fast Z pinches is an active area of research. Many elements of this complex phenomenon are still not well understood and are the source of scientific disputes. Sometimes, the lack of experimental data and/or of a clear theoretical picture does not allow the discussion to rise above a qualitative, semi-speculative level. Still, even on such occasions, the authors take the risk of presenting their thoughts, with the humble hope that a reader will benefit from comparing her or his viewpoint with authors'.

To give some general impression of the parameter domain of the present-day fast Z pinch experiments, we provide in Table 1 some numbers (a much more detailed discussion will be presented later) that relate not to any specific experiment but rather to some "generic" fast Z pinches. In every particular experiment parameters may vary by a factor of a few.

By convergence (the third line in Table 1) we mean the ratio of the initial pinch radius to the final pinch radius,

$$C=r_0/r_{min}. \tag{1.1}$$

Note that, because of the skin-effect, the voltage is not a well-defined quantity (for instance, inside a highly conducting shell there is no axial electric field at all); in Table 1 we are referring to the integral Edl between the anode and cathode at the distance from the axis equal to the initial pinch radius.

In addition to the most commonly studied parameter domain shown in Table 1, there exists another group of experiments, involving implosions of much heavier liners (with $\hat{m}\sim$ a few gram/cm), with a characteristic implosion time in the range of microseconds (see the end of Sec. I C). These pinches fall under our definition of "fast" pinches but will be discussed only very briefly in our survey.

The imploding load is often called a "target," similar to the term used in ICF research (e.g., Lindl, 1995). The other traditionally used term is "the liner," which designates a thin imploding annular shell of whatever nature (gas puff, foil, foam, wire-array plasma, etc).

We have tried to limit the references to books and papers in scientific journals that would be easily accessible to the reader. However, in some cases we had to cite conference proceedings.

C. Specific types of fast Z pinches

There exists a variety of initial configurations that are imploded in fast Z pinches. Depending on the application (as will be discussed in more detail in later sections) the initial density profile is chosen to be uniform, annular, or peaked on axis. One initial configuration that we have already mentioned is a supersonic gas jet, with either an annular or uniformly-filled gas density profile, originating from a nozzle situated at one of the electrodes. The gas jet then flows through a fine mesh that serves as the opposite electrode, or there may be simply a hole that receives the jet (Fig. 1a). More complex multi-shell gaseous jets are also possible.

To create an initial density profile that is more uniform axially between the electrodes, thin annular shells made of metal and plastic foils have also been used for the initial load configuration. Another way of creating the initial configuration is by machining a cylinder from a low-density foam (Fig. 1b). Development of the aerogel technology allowed experimentalists to produce solid cylinders with average mass density as low as ~1 mg/cm^3 (3 mg/cm^3 have actually been used in experiments) and having very small deviations from cylindrical symmetry (Antolak et al., 1997). Other foams, such as agar have a more coarse structure but have the advantage of being more easily machineable; this allows one to make both uniform and hollow annular cylinders of agar.

For the loads shown in Figs. 1a and 1b, the substance is initially nonconducting. Before the current will flow through the pinch, the breakdown of the material should occur. Because a breakdown is a statistical process, it may cause considerable initial non-uniformities of the pinch. To try to have a more predictable initiation of the discharge in a foam, one sometimes uses thin conducting coatings on the surface of the foam. In the case of gaseous jets, one or another method of pre-ionization can be used.

More recently (e.g., Matzen, 1997), considerable progress in the technology of fabricating very fine wire arrays has allowed assembling highly symmetrical cylindrical shells consisting of hundreds of very fine (several micrometers in diameter) metal wires

(Fig. 1c). The initial state of the imploding shell is in this case, obviously, conducting. One may therefore expect a more symmetric initiation of the discharge. For specific applications, a foam cylinder, uniform or annular, or a more complex structure may be inserted into the wire array (Fig. 1d).

Thus far we have been discussing Z pinches with an implosion time in the range of tens of nanoseconds. There exist devices where the imploding objects are relatively heavy metal shells and where the implosion time is as long as hundreds of nanoseconds to microseconds. This kind of Z pinch also falls under the aforementioned definition of "fast" Z pinches and will be covered by our survey. As an example, one can mention spherical implosions of metal shells (Baker et al, 1978; Degnan et al., 1995). A schematic of the latter experiment, where quasi-spherical implosions were successfully realized, is shown in Fig. 1e. Quasispherical targets may also be pursued in lower-mass configurations.

D. Pulsed power

Remarkable progress made during the last few years in fast Z pinch parameters became possible by progress in pulsed-power technology and in the development of sophisticated diagnostics instrumentation. As has already been emphasized, this review is directed to the discussion of the physics of Z pinches and will not address the equally important issues of pulsed-power technology and pinch diagnostics. However, to give an interested reader some guidance in the pertinent work, we briefly summarize the status of both areas.

The power and current available for Z pinch implosions reached new heights during the last decade: the pulsed-power generator Saturn (Spielman et al., 1989) allowed reaching electrical power of 20 TW and a maximum current of ~10 MA; the 50-TW Particle Beam Fusion Accelerator (PBFA II, now called "Z") was modified to drive fast Z-pinch implosions and at currents of ~20 MA (Spielman et al., 1996). Both generators are situated at Sandia National Laboratories (Albuquerque, New Mexico, USA). The kinetic energy in

imploding liners that were 2-cm long at an initial radius of 2 cm reached ~0.35 MJ at Saturn and ~1.2 MJ at Z. A schematic of the Z facility is shown in Fig. 2. There are other high-power generators used in Z-pinch research. In Russia, the best known is the Angara-5 generator (Al'bikov et al., 1990), with a maximum current of ~4 MA and a maximum power to the load of ~10 TW. Generators of a similar size include Double Eagle at Physics International, Blackjack 5 at Maxwell Laboratories, and Proto II at Sandia National Laboratories. Worldwide, about 15 generators operating at the current level of 1-3 MA and power to the load of ~1-5 TW are used in Z-pinch research (some of them are described in Camarcat et al., 1985). There are also numerous smaller generators. Most of larger generators use so-called magnetically insulated transmission lines (MITL) to deliver the power to the axisymmetric diode assembly. These magnetically insulated lines are, in turn, fed by transmission lines insulated with water. The power to the water transmission lines is supplied by high-voltage Marx generators. A wealth of information on these issues can be found in the proceedings of pulsed power conferences. A typical geometry of the diode assembly, where the Z-pinch target is situated, is shown in Fig. 3.

To drive the slower and heavier loads of the type shown in Fig. 1e with the implosion time of the order of 1 μs, slower generators are required. Examples of such generators are Shiva Star situated at Phillips Labs, Albuquerque, New Mexico, USA (Degnan et al., 1995), and Pegasus situated at Los Alamos Nat. Lab, USA.

E. Diagnostic instrumentation

Electric parameters of the discharge and the current through the pinch are inferred by measuring the electric and magnetic fields at specific points of the device in the generator with millimeter-size magnetic loops and capacitive probes. To measure the current through the pinch column, it would be necessary to measure the magnetic field inside the return current conductor (Fig. 3). This is difficult to do because of very large magnetic fields in a region of strong radiation and heat fluxes. Therefore, the magnetic field (and the current)

are usually measured in the MITL, at distances larger than ~3 cm from the axis of the Z pinch. The voltage is measured at the insulator stack. A description of the probes and further references can be found in Stygar et al. (1997). A possible way of measuring the magnetic field in the plasma column is the use of a Faraday rotation technique (Branitskii et al., 1992 a,b; Sarkisov et al, 1995 c).

Optical measurements are useful for the characterization of the early stage of the Z-pinch implosion, when the X-ray radiation doesn't yet overwhelm the optical detection system. Optical interferometry and holography allow one to detect low-density blow-off plasma at an early stage, as well as to observe instabilities of individual wires in the wire arrays. These measurements have a spatial resolution of a few tens of micrometers to millimeters and temporal resolution ~1 ns. Further details and references can be found, e.g., in Haines et al. (1997); Muron, Hurst, and Derzon (1997); and Deeney, et al. (1997a). Emission tomography is described by Veretennikov et al. (1992).

For later stages of the Z-pinch implosion, the x radiation becomes significant and is successfully used for characterization of the pinch. Total radiation intensity is typically measured with bolometers, with a temporal resolution of ~0.5 ns. Calorimeters can be used to measure the total radiation energy. X-ray diodes (XRDs) and photoconducting detectors (PCDs) are used to make broadband time-resolved measurements of x-ray spectra (Spielman et al., 1997). Multichannel scintillation detectors have also been developed for this purpose (Averkiev et al., 1992).To characterize the radiation in x-ray lines, plasma temperatures, and ionization states, x-ray spectroscopy is used (Leeper et al., 1997; Pikuz et al., 1997). X-ray pinhole framing cameras provide a spatial resolution as small as 100 micrometers, with time duration of the exposure as small as 100 picoseconds.

The high-energy electron beams sometimes generated in Z pinches can be detected by the gamma radiation from electrodes, and high-energy ion production can be observed by gamma spectroscopy of activated materials. The presence of fast deuterons is inferred from neutron radiation.

A complete description of the status of diagnostic instrumentation would require the inclusion of many tens if not hundreds of additional references and would lead us well beyond the intended scope of this paper. We point out that many diagnostics papers can be found in the January 1997 and January 1999 issues of the *Review of Scientific Instruments* and in the proceedings of the 1997 Conference on Dense Z Pinches (Pereira, Davis, Pulsifer - Eds, AIP Conf. Proc., v. 409, 1997).

II. IMPLOSION IN THE IDEAL CASE OF THE ABSENCE OF INSTABILITIES

In this section we discuss the case of an "ideal" implosion that might occur in the absence of instabilities. This will give us a kind of a reference point that would allow us to more clearly see effects of possible complications caused by instabilities. Stable purely cylindrical implosion can be numerically simulated with a great deal of detail and a considerable amount of information obtained in such simulations is available in published literature (e.g., Hammer et al, 1996; Peterson et al, 1996). However, we prefer to concentrate on simple analytical models that allow the reader to more easily follow the chain of causes and effects. Working in this spirit, we start from the analysis of the simplest possible system, the structureless perfectly conducting thin shell. After that, we gradually add complicating factors, like the finite conductivity, possible rotation, etc.

A. Implosion of a thin shell

In the simplest case of a thin annular shell (like the one formed by the wire array), the equation of the radial motion can be written as:

$$\frac{\hat{m}}{2\pi r}\ddot{r} = -\frac{B^2}{2\mu} = -\frac{\mu I^2}{8\pi^2 r^2}, \qquad (2.1)$$

where $B=B(t)$ is the magnetic field at surface of the pinch, and $I=I(t)$ is the pinch current. Let us measure the current in the units of the maximum current, I_{max}, the time in the units of

the time τ within which the current reaches its maximum, and the radius in the units of the initial radius r_0. In other words, we introduce dimensionless variables

$$\tilde{r} = r/r_0, \ \tilde{t} = t/\tau, \ \tilde{I} = I/I_{\max}. \tag{2.2}$$

Rewritten in these variables, Eq. (2.1) converts to:

$$\tilde{r}\ddot{\tilde{r}} = -\Pi\tilde{I}^2, \tag{2.3}$$

where

$$\Pi = \frac{\mu I_{\max}^2 \tau^2}{4\pi \hat{m} r_0^2} \tag{2.4}$$

is a dimensionless scaling parameter of the problem. Two implosions with the same functional dependence of the current vs. time (i.e., with the same dependence $\tilde{I} = \tilde{I}(\tilde{t})$) occur in a similar fashion if the parameter Π for them is the same. In particular, the time instant when the pinch collapses on the axis, measured in the units of τ, is the same for both implosions.

To provide a good efficiency for converting the energy stored in the pulsed power generator into kinetic energy of the imploding pinch, one should choose an optimum mass of the pinch material. This mass should be such that the implosion time be approximately equal to the time within which the current reaches its maximum value: if the mass is too large, the current pulse ends before the pinching occurs; if the mass is too small, the pinching occurs before the current reaches its maximum, also implying a poor efficiency. In other words, for every current pulse shape there exists an optimum value of the parameter Π.

Consider in some more detail the initial stage of the implosion of a thin shell (Eq. 2.1). When the pinch radius has not yet decreased considerably with respect to its initial value r_0, one can represent r as $r=r_0-\Delta r$, with Δr small. In all our semi-quantitative estimates we will use a simple model of the current through the pinch,

$$I = I_{\max} \sin^2\left(\frac{\pi t}{2\tau}\right). \tag{2.5}$$

At an early stage of the implosion, the pinch current can be with a reasonable accuracy approximated by a parabolic dependence vs time,

$$I = I_{\max}\left(\frac{\pi t}{2\tau}\right)^2, \tag{2.6}$$

For the dependence (2.6) one easily obtains for Δr:

$$\frac{\Delta r}{r} = \frac{\pi^4 \Pi}{480}\left(\frac{t}{\tau}\right)^6. \tag{2.7}$$

Note that the pinch radius departs from its initial value very slowly, $\sim t^6$. For a load with a mass corresponding to the collapse at $t=\tau$, even at $t=(2/3)\tau$ the pinch radius is decreased by a mere 10 % of its initial value. This discussion shows that a pinch has a long "latent" phase followed by a very fast collapse that occurs within a small fraction (~0.1-0.2) of the total implosion time τ. Calculated time-histories of the wire array radius and the pinch current in one of the shots at the Saturn accelerator are shown in Fig. 4.

An important characteristics of the system is the kinetic energy W_{kin} of the shell at the point where it reaches some desired minimum radius r_{min}. This can be a radius determined by a finite thickness h of the shell (i.e., $r_{min} \sim h$), or a radius of an inner cylinder as in the scheme shown in Fig. 3. To find W_{kin}, one can use the energy relationship that can be obtained by multiplying Eq. (2.1) by $\dot{r}$ and integrating by part, from $t=0$ to $t=t^*$, where t^* corresponds to the point where $r=r_{min}$. One finds:

$$W_{kin} = \frac{\mu}{4\pi}\int_0^{t^*} \frac{dI^2}{dt}\ln\left(\frac{r}{r_{\min}}\right)dt; \tag{2.8}$$

W_{kin} is a kinetic energy per unit length of the pinch at $t=t^*$. The mass of the liner enters Eq. (2.8) only implicitly through the implosion time $t^*=t^*(\hat{m})$, and through the dependence of the radius vs. time, $r=r(t, \hat{m})$.

At large convergences, one can obtain a simple approximate expression for W_{kin}. To do that, one should note that the logarithm in the integrand of Eq. (2.8) is almost constant and equal to $\ln C$ for the most part of the implosion. The contribution of the part where the logarithm begins to change (roughly speaking, after the pinch radius reaches $r_0/2$) is small

because the time within which the pinch implodes from $r_0/2$ to r_{min} is very short compared to the total current pulse-width (see Fig. 4 and comments after Eq. (2.7)). So, replacing the logarithm in the integrand of (2.8) by a constant value $\ln C$ (corresponding to the final convergence $C=r_0/r_{min}$, i.e., typically, to C~10-20) , one finds:

$$W_{kin} \approx \frac{\mu I^2(t^*)\ln C}{4\pi} \ . \tag{2.9}$$

One sees that the maximum of the transferred energy corresponds to such a mass that the time t^* roughly corresponds to the maximum of the current. This statement has a so called "logarithmic accuracy," i.e., it is valid up to the terms of order of $1/\ln C$. To make a more accurate estimate of the optimum implosion time, one should take a derivative of W_{kin} over $\hat{m}$. From Eq. (2.8) one finds:

$$\frac{\partial W_{kin}}{\partial \hat{m}} = \frac{\mu}{4\pi}\int_0^{t^*} \frac{dI^2}{dt}\frac{1}{r}\frac{\partial r}{\partial \hat{m}}dt \ . \tag{2.10}$$

Obviously, the derivative $\partial r/\partial \hat{m}$ is positive: a heavier liner implodes slower and, at a given time, has a larger radius. Therefore, if t^* corresponds to the current maximum, the derivative $\partial W_{kin}/\partial \hat{m}$ is positive. It reaches zero (i.e., the kinetic energy reaches a maximum) at some point beyond the maximum of the current. This point usually corresponds to the current that is 20-30% less than the current maximum. For the current waveform as in Eq.(2.5), the optimum value of the parameter Π is equal to approximately 4.

In a real life, for a given pulse-power generator, the current waveform cannot be considered as independent of the parameters of the load (because of the contribution of the load impedance to the overall impedance of the circuit). This circumstance can be taken into account by solving equations for the pinch together with the circuit equations (see, e.g., Katzenstein, 1981; Struve et al., 1997). One should also emphasize that the kinetic energy is not necessarily an appropriate figure of merit. For example, in the experiments on generation of radiation the figure of merit could be the radiated energy. The contribution to the radiated energy comes not only from the kinetic energy of the pinch but also from Joule heating (see Sec. VIII A) and pdV work on the plasma during the stagnation phase

(Peterson et al, 1997, 1998). Still, the kinetic energy is an important and easily tractable characteristics of the implosion and we will concentrate our discussion on it.

Using Eq. (2.9), one can derive an expression for the volume density of the kinetic energy w_{kin} at the stagnation point in the case of an empty liner:

$$w_{kin} = \frac{W_{kin}}{\pi r_{\min}^2} \approx 2p_m^* \ln C\,, \tag{2.11}$$

where p_m* is the magnetic pressure at the surface of the pinch at $r=r_{min}$. If this energy is converted to the thermal energy of the monatomic ideal gas, then the gas pressure will be $p=(2/3)w_{kin}$, or

$$p = \frac{4}{3} p_m^* \ln C \tag{2.12}$$

On sees that, with such a scenario, the gas pressure is indeed considerably higher than the magnetic pressure, and the pinch will rapidly expand after stagnation. The pinch rebound was detected in the experiments with aluminum wire arrays on the Saturn facility (Sanford et al., 1997a).

If one deals with a liner made of heavy elements, then, in fact, a considerable amount of energy will be spent on the ionization, reducing p compared to the estimate (2.12). In the implosions of wire arrays, temperatures in the range of hundreds electron-volts and electron densities in the range of 10^{22} are typical (Sanford et al., 1997b; Maxon et al., 1996; Matzen, 1997; Deeney et al., 1997b). The radiative losses also lead to smaller than (2.12) pressures.

If the radiation loss time is considerably shorter than the acoustic time r_{min}/c_s (where c_s is the sound speed), then, in the absence of instabilities, the pinch might experience a collapse to ever smaller radii (a radiative collapse, see, e.g., Meierovich, 1986). The Joule heating, especially with the anomalous resistance included, works in the opposite direction (Robson, 1991), as well as the radiation imprisonment and effects of electron degeneracy (Haines, 1989; Chittenden, Haines, 1990). The radiative collapse in a real situation may be prevented from happening also by the constraints imposed by circuit equations (a fast

increase of the pinch inductance may decrease the current, Haines, 1989; Choi & Dumitrescu-Zoita, 1997).

B. Targets with initially uniform density distribution

In this section we switch to the discussion of implosions of the targets with initially uniform density distribution, like foam cylinders, or smooth radial density distributions, like, e.g., gas puffs. In this case, a shock wave propagates ahead the current-carrying sheath and reaches the axis considerably earlier than the sheath. We assume that the skin-depth is small compared to the radius of the column, as is the case in real situations.

The converging cylindrical shock, if it possesses a good symmetry, can by itself produce a strong increase of density and temperature on axis, formally singular (Guderley, 1942; see also Whitham, 1974). After the shock is reflected from the axis and again reaches the surface of the cylinder, a kind of an adiabatic compression begins, where the plasma pressure is approximately equal to the magnetic pressure, and the sound speed in the plasma is comparable to the Alfven velocity. This means that a kind of a transient Bennett-type equilibrium is formed for a few acoustic transit times.

In this discussion of the implosion of a uniform density column, we ignored the role of radiation. This can be the case with imploding DT gas puffs. If, however, one deals with implosions of heavier elements, then the radiation of the plasma behind the shock can become important. In the extreme case of very strong radiation losses, the plasma behind the shock radiates its energy much faster than the time within which the shock could propagate across the radius of the pinch. In this extreme case the shock will not be formed at all, and all the material impacted by the magnetic piston will just stick to the piston. It corresponds to a so-called snow-plow model studied in much detail in the early years of pinch research (1950's). We will use the term "snow-plow" just in this sense, to designate a simple model where all the material swept by the magnetic piston merely sticks to it. This

case is similar to the one discussed in the previous section and we will start from it, leaving discussion of the second possibility (weak radiation) until the next section.

In the case where mixtures of gases are used, and the densities are low enough, the picture may be complicated by a radial separation of the ion species under the action of the ambipolar radial electric field (Bailey et al, 1982; Barak & Rostoker, 1982; Rahman, Amendt, & Rostoker, 1985). Gordeev (1987) contends that in a low-density gas-puff implosion of a multi-spices plasma, the mutual friction between the ion components may cause an enhanced penetration of the magnetic field.

1. A snow-plow model (strongly radiating column)

Equations of motion of the magnetic piston sweeping the plasma as a snow-plow read as:

$$\frac{\hat{m}^*}{2\pi r}\ddot{r} - \rho(r)\dot{r}^2 = -\frac{\mu I^2}{8\pi^2 r^2} \qquad (2.13)$$

$$\dot{\hat{m}}^* = -2\pi r\dot{r}\rho(r) \qquad (2.14)$$

where $\rho(r)$ is the initial density distribution and $\hat{m}^* = \hat{m}^*(t)$is the instantaneous mass accreted at the piston. The second term in the l.h.s. of Eq. (2.13) describes the momentum imparted to the piston by the accreting material. We assume that the density at a certain radius remains unchanged until the very moment of the magnetic piston arrival. For two implosions with the initial density distributions having the same functional dependence on r/r_0, there exists the same similarity law as for the equation (2.14), i.e., the two implosions are similar if the parameter Π for them is the same.

Consider an early stage of the implosion of a uniform cylinder in the framework of the snow-plow model. In this case, at the same mass per unit length as in a thin shell, the current sheath moves towards the axis faster than in the case of a thin shell. The reason is merely the smaller mass involved in the implosion at an early stage. To illustrate this point

more quantitatively, consider an analog of Eq. (2.7) assuming that the initial density distribution is uniform, i.e., $\rho = \hat{m}/\pi r_0^2$. One now has:

$$\frac{\Delta r}{r_0} = \frac{\pi^2}{4}\sqrt{\frac{\Pi}{30}}\left(\frac{t}{\tau}\right)^3 \qquad (2.15)$$

This solution is valid until Δr is less than, roughly speaking, $r_0/3$. We see that the implosion begins faster than for a thin shell. The collapse on axis also occurs earlier than for the thin shell of the same mass per unit length. Still, the latent period is present in this case, too.

For the snow-plow model [Eq. (2.13)], the analog of Eq. (2.1) reads as:

$$W_{kin} = \frac{\mu}{4\pi\hat{m}}\int_0^{t^*}\frac{d(\hat{m}^* I^2)}{dt}\ln\frac{r}{r_{\min}}dt\ , \qquad (2.16)$$

where $\hat{m}$ is the total mass per unit length, and $\hat{m}^*$ is the mass swept by the current sheath by the time t,

$$\hat{m}^* = 2\pi\int_r^{r_0} r'\rho(r')dr'. \qquad (2.17)$$

We assume here that one deals with the implosion of a simple gas-puff or a foam cylinder, without an external shell (otherwise, one would have to add the mass of this shell both to $\hat{m}$ and $\hat{m}^*$ in Eq. (2.13)). Using the same arguments as in the case of a thin shell, one can show, that, at high convergences and smooth density distributions, W_{kin} is still approximately determined by Eq. (2.9). From elementary mechanical considerations one can find that the power released in the inelastic interaction of the initially resting substance with a moving piston is (per unit length) $\dot{\hat{m}}^* \dot{r}^2/2$. Integrating this expression over time, one finds that, at $C>>1$, the part of the energy that was radiated from the accreted mass is, within an order of magnitude, $1/\ln C$ of the final kinetic energy (i.e., relatively small). This is so because most of the mass is accreted before the liner reaches the radius, say, $r_0/3$, when the liner velocity is still small compared to its final velocity at $r=r_{min}$.

An interesting feature of Eq. (2.13) consists in that, at the properly chosen radial density distribution, one can provide conditions where the surface of the pinch does not

experience radial acceleration. Such a regime may be desirable for the reason that it may be stable with respect to the Rayleigh-Taylor instability. This idea has been explored by Hammer et al. (1996). To approach the state of a constant velocity, the outermost part of the pinch should experience a sudden kick that would impart to it the desired velocity v. As soon as this state has been reached, the further evolution of the system is described by Eq. (2.13) with the first term in the left-hand-side of this equation omitted. One obtains the following equation for the desired density profile (Hammer et al., 1996):

$$\rho(r) = \frac{\mu I^2 \left(\frac{r_0 - r}{\mathrm{v}} \right)}{16\pi^2 \mathrm{v}^2 r^2} \qquad (2.18)$$

The density should rapidly increase near the axis ($\propto 1/r^2$), and essentially all the mass should be concentrated within the radius $r \sim 2r_{min}$. Fig.5 depicts the required density distributions. For such sharply varying density distributions one cannot use Eq.(2.9) to estimate the kinetic energy. The final kinetic energy in this case is:

$$W_{kin} = \frac{\hat{m}\mathrm{v}^2}{2}, \qquad (2.19)$$

with the mass $\hat{m}$ related to the implosion velocity by Eqs. (2.17) and (2.18), with $r=r_{min}$ in the former equation. The optimum velocity (at which W_{kin} is maximum) is the velocity at which $r=r_{min}$ is reached at the current maximum. It is also important to note that the radiative losses W_{rad} in this case are considerable. Using the same arguments as the ones that followed Eq. (2.17) one can show that the total radiated energy is $W_{rad}=W_{kin}$ (Cf. Hammer et al., 1996).

2. Weakly radiating plasma

In this case, the shock wave splits from the piston and propagates in front of it, heating and compressing the plasma. As the initial temperature of the pre-shocked plasma is small, the shock has a very large Mach number and can be considered as a strong shock

(Landau and Lifshitz, 1987). For the gas with adiabatic index γ, the plasma density (ρ_1) and plasma pressure (p_1) behind the shock are:

$$\rho_1 = \frac{\gamma+1}{\gamma-1}\rho, \quad p_1 = \frac{2}{\gamma+1}\rho u^2, \tag{2.20}$$

where u is the shock velocity. If the magnetic piston is moving with some constant velocity v, there is a simple relationship between u and v, a direct consequence of the mass conservation equation, $\rho u=\rho_1(u\text{-v})$: $u = (\gamma+1)\mathrm{v}/2$. For the ideal monatomic gas ($\gamma=5/3$), $u=(4/3)$v, i.e., the shock velocity is approximately 30% higher than the velocity of the piston. This means that the shock converges on axis when the pinch radius is equal, roughly speaking, to $r_0/3$. This is a crude estimate, as it doesn't take into account variation of v and effects of the cylindrical geometry. Still, it doesn't differ strongly from more elaborate analyses, in particular from the "slug" model by Potter (1978) and from the energy analysis by Miyamoto (1984).

Potter's model assumes that the plasma behind the shock is uniform, with parameters related to the parameters in front of the shock by Eqs. (2.20). The pressure p_1 is, on the other hand, equal to the magnetic pressure. This allows one to close the set of equations and to find position of the shock and the piston as a function of time. The prediction is that the shock reaches the axis at $r\approx 0.3r_0$. After the shock is reflected from the axis and reaches the piston, a quasi-equilibrium state is formed in which the plasma pressure is approximately equal to the magnetic pressure. One sees that this is quite a different situation from implosions of thin shells where the particle pressure in the final state is much higher than the magnetic pressure.

Such solutions are of interest in the implosions of low-Z targets, in particular, DT gas-puffs and deuterated carbon foams. If one deals with the targets of heavier materials, they may remain not fully ionized behind the shock. In this case the use of the power law adiabats may break down. As a considerable amount of energy is spent on the ionization, the temperature behind the shock is lower than in the fully ionized case, and the density

higher (Zeldovich, Raizer, 1967). In such a situation, the separation between the piston and the shock front reduces compared to what has been discussed above, and the snow-plow model of Sec. II B.1 becomes relevant.

As in a plasma with non-fully stripped ions the tail of the electron distribution function experiences losses caused by excitation and ionization events, the tail may get depleted, affecting the rate of the excitation and the radiation intensity (e.g., Clark, Davis & Cochran, 1986; DeGroot et al., 1997a). An example of the analysis of the experimental data on x-ray spectra from implosions of the foam loads on the Saturn device, with non-equilibrium effects included, can be found in MacFarlane et al (1997). In quasistatic pinches, an important channel of the heat loss is an enthalpy flow to the electrodes related to the pinch current (Haines, 1960). In fast pinches this channel is usually sub-dominant.

We have discussed three limiting cases of the implosion: that of a thin shell, that of a non-radiating uniform (not annular) column and that of a strongly radiating uniform column (snow-plow model). Of course, a whole range of intermediate cases is also possible. In particular, in the gas-puff implosions with annular gas-puffs, the initial density on axis is never zero, because of a finite angular divergence of the jet. A converging shock would then propagate in a relatively low-density gas in front of the main shell, and would cause a significant density and temperature increase on axis prior to arrival of the main shell. This is a possible explanation of an early formation of a dense on-axis column in the experiments by Shiloh, Fisher, and Bar-Aavraham (1979).

C. 3D implosions

As has been already mentioned in Sec. I C, one may deliberately implode shells with a geometry different from cylindrical. Fig. 1 e depicts an implosion of an approximately spherical shell whose polar areas are sliding along the conical electrodes. This scheme was successfully realized in experiments by Degnan et al. (1995). The magnetic pressure at the surface of the shell is larger in the polar areas (because of the

smaller distance from the axis). To compensate this effect (that would lead to deviations from the spherical implosion) the shell thickness was made larger in the polar parts. To avoid jetting at the point of the sliding contacts of the shell with the electrodes, the angle at their apex was made greater than 45°.

The other technique for producing quasi-spherical implosions is a proper tailoring of the thickness of the initially cylindrical liner, with the thickness decreasing from the equatorial plane to the ends (Fig. 6). The liner implosion then occurs as shown in Figs. 6 a-d, with the volume inside the liner experiencing (at the stages following Fig. 6 c) a 3-D compression. Such scheme has been successfully tested in experiments with relatively massive aluminum liners by Alikhanov et al. (1977). Numerical simulations of 3D implosions have been recently performed by Lisitsyn, Katsuki, and Akiyama (1999).

D. Electrode phenomena

So far, we have been considering problems with a pure cylindrical symmetry, i.e., problems where all parameters depend only on r. A perfect cylindrical symmetry cannot be reproduced in a real life, even if the system is MHD-stable. Indeed, the pinch always has a finite length, and there is a contact between the pinch plasma and the electrodes. This creates some axial non-uniformity and thereby violates pure cylindrical symmetry. The presence of the electrodes may affect the pinch performance in a number of ways.

First, there is some friction between the liner and the surface of the electrode. This effect may be significant for high temperature and low density pinch plasmas. The presence of the tangential shear flow in the transition region between the electrode and the liner may excite the Kelvin-Helmholtz instability (see Chandrasekhar, 1961) and shear-flow turbulence. This will be a turbulence of supersonic flow (the plasma velocity far from the wall is much higher than the sound speed in the plasma shell), with strong radiative losses. Very little is known about the turbulent momentum transfer under such circumstances. First

observation of the Kelvin-Helmholtz instability in the ICF-relevant environment has been reported by Hammel et al (1994).

Second, there is a heat flux to cold massive electrodes. Its significance is again determined by the density and temperature of the liner. This heat flux causes an axial variation of the plasma temperature near the electrodes thereby violating the cylindrical symmetry of the implosion.

Third, there may occur some mass influx from the surface of the electrode that makes the end part of the pinch heavier and causes its lagging with respect to the equatorial part of the pinch.

Fourth, conducting electrodes impose a "frozen-in" condition on the normal component of the magnetic field. To illustrate the possible role of this effect, consider a liner implosion in the presence of a weak initial axial magnetic field B_{z0} (such geometries are supposed to be used in experiments on the generation of strong magnetic fields; see, e.g., Alikhanov et al., 1967). If (as it usually is) the bias magnetic field is small compared to the azimuthal magnetic field of the pinch, it does not considerably affect the pinch dynamics during the run-in phase. Consider, however, what happens to the magnetic field itself. The axial magnetic flux through every element of the electrode and liner is conserved (because of their high conductivity). This creates a situation shown in Fig. 7: a thin near-electrode layer appears where the embedded magnetic field becomes almost radial in direction; the thickness of this layer is of the order of the skin-depth δ, which is very small compared to the pinch radius. From the conservation of the magnetic flux, the following estimate of the radial magnetic field inside the skin-layer follows: $B_r \sim B_{z0} r/\delta$. This estimate corresponds to the intermediate stage of the run-in, where the pinch radius is equal to, say, a half of the initial radius. For a typical implosion at a time of ~30 ns, the skin-depth in the electrode material is of the order of 10^{-3} cm and, for r~1cm, one obtains $B_r \sim 10^3 B_{z0}$. Even if the bias magnetic field is small, say, 10^4 G, the magnetic field in the skin is very large and may become comparable with the self magnetic field of the pinch.

This, in turn, will cause a thermal explosion of the electrode skin-layer (because of very high current density), and also change in the dynamics of the liner implosion near the surface of the electrodes.

In some experimental settings, in order to provide a better diagnostic access, one of the electrodes is made with a hollow central part (Fig. 8). This may lead to a different phenomenon, similar in some sense to the plasma focus effect (for the description of the latter see, e.g., Sec. 4 in Vikhrev and Braginskiĭ, 1986). When, in the course of the implosion, the liner slides past the edge of the hole, some current-carrying "bridge" should be formed from the materials of both the liner and the electrode (panel 2). The density of this bridge is presumably less than the density of the liner itself. Anomalous resistivity may turn on causing considerable heating and radiation from this region. The bridge experiences a magnetic pressure directed downward and begins to evolve as shown in (panels 3-4). The further evolution of the bridge should lead to its early self-implosion in some axial point, formation of the "neck" (panel 5) and, possibly, the break-up of the current channel, with generation of high-energy particle beams. The collapse should be accompanied by injection of the material in both directions from the collapse point. Bright features appearing near the anode hole relatively early in the pulse were observed by Derzon, et al. (1997a) and they persisted till late time (Fig. 9).

E. Structure of the imploding shell.

The knowledge of the structure of an imploding shell is required for the stability analysis that will be made in the further sections of this report. Consider the implosion of a thin shell whose thickness h is such that the time of propagation of the compression wave through the distance h, is small compared to the characteristic time of the implosion process. This assumption is certainly valid for thin enough shells. Then the shell can be considered as being in a quasi-steady-state mechanical equilibrium which is governed by the following equation:

$$\rho g = -\frac{\partial}{\partial x}\left(p + \frac{B^2}{2\mu}\right), \tag{2.21}$$

where g is the effective gravity acceleration (in the co-moving frame) and x is a coordinate directed towards the axis. We are using here a planar model - because of a small thickness of the shell. The geometry of the problem is illustrated by Fig. 10.

There is no magnetic field at the inner surface of the shell (no current inside the shell) and, therefore, the acceleration is related to the magnetic field B_0 at the outer surface of the shell via equation:

$$\rho g h \sim B_0^2 / 2\mu, \tag{2.22}$$

where h is the shell thickness.

First assume that the temperature of the shell is determined by the Ohmic heating. A rough estimate of the thermal energy delivered to the unit area of the shell can be made by multiplying the Poynting vector by the characteristic time τ of the implosion process:

$$E_0 B_0 \tau / \mu. \tag{2.23}$$

The electric field on the surface of the shell depends on the relationship between the skin-depth h_{skin} and the total thickness h of the shell:

$$E_0 \sim \frac{B_0 h_{skin}}{\tau} \max\left(1, \frac{h_{skin}}{h}\right). \tag{2.24}$$

Assume first that heat losses via radiation are negligible. Then, the thermal energy per unit area of the shell is

$$\frac{B_0^2}{2\mu} h_{skin} \max\left(1, \frac{h_{skin}}{h}\right). \tag{2.25}$$

This thermal energy determines the plasma pressure inside the shell. For the thickness of the skin-layer we take its value in some characteristic point halfway through the implosion. Note that the estimate (2.25) provides only a general scaling law; the specific numerical factor depends on the current waveform.

If ionization energy is small, so that the thermal energy per unit volume is of the order of the plasma pressure (later in this section, we discuss the situation where ionization

energy is significant), Eqs. (2.22) and (2.25) show that, in a quasi-equilibrium state, the shell thickness is necessarily of the order of the skin-depth h_{skin} (Fig. 11 a).

Consider, now the other possibilities. If the shell experiences some turbulent motions produced by hydrodynamic instabilities, then a new source of heating becomes available and may deliver much more thermal energy to the shell than follows from Eq. (2.25). One more situation where thermal energy may be large is an implosion of sufficiently thick gas-puff or foam annulus, where the shock wave propagates before the piston and heats the plasma. When the thermal energy of the shell is considerably greater than the energy delivered by the Ohmic heating, an equilibrium with the shell thickness much greater than the skin-depth h_{skin} becomes possible (Fig. 11 b). In the region beyond the skin-layer, the magnetic pressure in Eq. (2.21) is negligible. At a uniform temperature and a uniform plasma composition, one then obtains a familiar exponential density distribution,

$$\rho \propto \exp(-x/h), \tag{2.26}$$

with the scale-length h defined as

$$h = T/\overline{m}g\ , \tag{2.27}$$

and $\overline{m}$ being an average atomic weight (half a proton mass for the hydrogen plasma).

The opposite limiting case is that of very fast radiative losses and/or of a large ionization energy, as it may be in a plasma of high-Z elements. This case is of a particular interest for the shells formed from wire arrays and we discuss it in some detail, following general ideas of the papers by Hussey, Roderick and Kloc (1980), Hussey and Roderick (1981), Grigor'ev and Zakharov (1987), Chukbar (1993a) and Hammer et al. (1996).

The plasma thermal energy in this case is much smaller than that determined by Eq. (2.25), leading to a corresponding decrease of the plasma temperature. At low temperatures, the skin-depth becomes greater than the shell thickness, $h_{skin}>h$. The axial electric field is then uniform over the shell thickness. We assume that the temperature is also uniform, providing a uniform conductivity and a uniform axial current. The latter, in

turn, means that the magnetic field varies linearly over x. As it must vanish at the inner side of the shell (we assume that there is no axial current inside the imploding shell), we find that

$$B = B_0\left(1-\frac{x}{h}\right) \qquad (2.28)$$

where h is the shell thickness. For the further analysis, it is convenient to introduce the relationship $p=s_{iso}^2\rho$, with $s_{iso}=\sqrt{T/\overline{m}}$ being a speed of the isothermal sound waves. As follows from Eq. (2.27), the assumption of the skin-depth being greater than the shell thickness implies that almost all the energy delivered to the shell by Ohmic heating is radiated to make plasma pressure less than the magnetic pressure, $\rho s_{iso}^2 << B_0^2/2\mu$. In this case, as follows from Eqs. (2.21), one automatically has $gh>> s^2_{iso}$. With this observation made, one can find the following solution of Eq. (2.21) (with B as in Eq. (2.28)):

$$\rho=\rho_0\left[\left(1+\frac{s_{iso}^2}{gh}\right)\left(1-\exp\left(-\frac{gx}{s_{iso}^2}\right)\right)-\frac{x}{h}\right];\ \rho_0=\frac{B_0^2}{\mu gh}. \qquad (2.29)$$

We have taken into account that the density should become zero at x=0; then, at x=h, it is small (in the parameter s_{iso}^2/gh<<1), as it should be. Our simple model does not resolve the structure of the further transition to the zero density near the inner side of the shell. The density distribution (2.29) is shown in Fig. 11 c. Note that h now is *not* determined by (2.27), because the magnetic force is now dominant in the pressure balance.

For the solution (2.29) the mass per unit area of the shell is approximately equal to $\rho_0 h/2$; it is determined by the initial conditions of the experiment. However, the solution (2.29) does not allow one to determine ρ_0 and h separately. The additional equation needed is provided by a condition of a thermal balance, which equates Joule heating and radiative losses. This condition, generally speaking, contains a different combination of the parameters ρ_0 and h and can, therefore, serve as a second equation (provided the temperature is determined experimentally).

III. AN EARLY STAGE OF THE DISCHARGE

A. Breakdown of gas-puffs

Although at present fast Z-pinch research is concentrated on wire array implosions, other fast Z pinches, in particular, gas-puffs (see, e.g., Stallings et al, 1979; Branitskii et al, 1991, 1992a,b; Deeney et al, 1993; Baksht, Datsko, Kim, et al, 1995) and pinches with foam targets (Derzon, Nash, Allhouse et al, 1997) are also of a considerable interest. Therefore, we start this section with the issues of initializing these types of pinches. What we present here is not a quantitative theory: it is rather a broad qualitative discussion aimed at the identifying critical physics issues.

In our discussion of gas-puffs, we will present most of the numerical estimates for the density range ~$3\cdot10^{17}$-$3\cdot10^{18}$ cm^{-3}. We mean here peak densities, in the middle of the gas stream. Taking as a representative value for the cross-section of electron scattering on atoms, σ_a~10^{-15} cm^2, one finds that the mean-free path for electron scattering, $\lambda_{ea}=1/n_a\sigma_a$, where n_a is a neutral atom density, is much shorter than the typical height of the pinch. If the applied voltage is such that the energy acquired by the electron between two collisions is small compared to the ionization potential, the electron avalanches would develop quite slowly. The seed electron would experience a random walk with a superimposed average drift in the direction of the anode; its energy would gradually increase and reach the excitation threshold; at this point, with a high probability, it would lose energy through excitation and only with a small probability would reach the ionization threshold I_{ion} (this, incidentally, is a standard picture of the gas breakdown at densities above the Paschen pressure minimum, see Meek and Craggs, 1978; Raizer, 1991). In the situation of fast Z pinches, where the voltage is rapidly growing, before the aforementioned process produces sufficient electron multiplication, the voltage reaches the level where electrons acquire the ionization energy between two successive collisions:

$$eE\lambda_{ea} > I_{ion}, \tag{3.1}$$

where E is the electric field strength. Then, a typical e-folding time for avalanching will be only $1/\mathrm{v}_e n_a \sigma_i$, where σ_i is the ionization cross-section).

Before going further, we note that in gas-puff experiments the radial density distribution is relatively smooth, with a gradual transition from the nominal density inside the jet to much lower density at the jet periphery (Fig. 1a). Therefore, with voltage growing, the condition (3.1) will be first satisfied at low densities. But the density cannot be too low: in order to produce a considerable charge multiplication on its way to the anode, the electron would have to experience at least several ionizing collisions, i.e., the product $Ln_a\sigma_i$ (where L is an anode-cathode distance) should be greater than, say, 10:

$$Ln_a\sigma_i > 10. \qquad (3.2)$$

Eq. (3.2) imposes a lower limit on the density. At $\sigma_i \sim 3\cdot10^{-16}$ cm^2 and $L\sim1.5$ cm the required densities are $\sim 2\cdot10^{16}$ cm^{-3}, and this is where breakdown will occur first. The time for developing a considerable ionization is $\sim 10/\mathrm{v}_e n_a \sigma_i$ (~5 ns at $n_a=2\cdot10^{16}$ cm^{-3}).

With applied voltage rapidly growing, the inequality in Eq. (3.1) will be met in the deeper layers of the jet and the ionization front will move towards the higher densities. Eventually, the conductivity of the outer current-carrying shell becomes so high that the skin-effect becomes important. After this time the further increase of the current occurs in the outer layers of the gas-puff (this skin-dominated stage of ionization has been analyzed by Vikhrev and Braginski, 1986). At this stage, the further ionization of the inner layers is produced by radiation from the current-carrying shell and, at the later stages of the implosion, by the shock heating.

In gas-puffs, the isodensity surfaces are usually not cylindrical but rather conical, because of the divergence of the jet (see Hussey, Matzen and Roderick, 1986). Deeney et al (1994), and Barnier et al (1998) developed special nozzles producing almost cylindrical jets. Superimposed on the regular flow, smaller-scale density fluctuations produced by the hydrodynamic turbulence may be present. This brings additional complications to the picture of the breakdown.

In very low density pinches, where even the maximum density of the jet is less than roughly 10^{16} cm^{-3}, the electron multiplication factor becomes insufficient (see Eq. (3.2)) and a different mechanism of breakdown should come into action. It should strongly depend on the generation of electrons at the cathode (Baksht, Russkikh, Chagin, 1997), via, probably, photoemission.

Note that, at low gas densities, even a very weak current may cause the magnetization of electrons, thereby affecting the avalanching process. At the density 10^{16} cm^{-3} the electron-neutral elastic collision frequency of, say, 30-eV electrons is $3 \cdot 10^9$ s^{-1}, and becomes lower than electron gyrofrequency at a magnetic field of only 0.015 T. In a 4-cm diameter column such a magnetic field would be created by the current of only ~ 1.5 kA (!). Therefore, even relatively weak axial magnetic field (weak compared to the pinch azimuthal field at the maximum current) may affect the breakdown process and, thereby, the overall pinch performance. The favorable effect of an axial magnetic field ~0.3 T has been recorded in experiments by Baksht, Russkikh, and Chagin (1997), and Gasque et al. (1996). Of course, we do not claim that the bias magnetic field does not have other effects on the pinch physics (in particular, on the pinch stability at the later stages of the implosion, where it increases because of the radial compression). We just emphasize that even a very weak field can influence breakdown of the gas-puffs and make it more "regular".

The gas breakdown itself is a statistical process and may lead to a formation of azimuthally-asymmetric current-carrying channels, especially at lower densities where electrode effects become important (and bring about a new source of non-uniformities). Therefore, the pre-ionization of the gas by some external source might be beneficial. This is shown in the papers by Stallings et al. (1979), Ruden et al. (1987), Baksht, Russkikh, and Fedyunin (1995), and Baksht, Russkikh, and Chagin (1997).

The presence of a long enough pre-pulse may also be beneficial for creating a uniformly ionized column. Effect of the pre-pulse is determined by its time duration and its voltage. In particular, in Baksht, Russkikh, and Fedyunin (1995) the prepulse (1.5 μs, 1

kV) did not cause the breakdown because the axial line density $n_0 L < 3.6 \cdot 10^{15}$ cm^{-2} was well below the Paschen optimum for Ar. Such a prepulse would have caused a breakdown of Ar with a density an order of magnitude higher. Whether this would be beneficial for the further fast implosion is not quite clear, because during the long pre-pulse numerous ionization-radiation instabilities (see Sec. III C) could develop and lead to strong perturbation of the initial state. The pre-pulse breakdown was reported by Smith and Dogget (1985) who also studied the current distribution of argon gas-puffs with a density below 10^{16} cm^{-3} during the first 20 ns of the discharge. They correctly identified an important role of the early electron magnetization, although their use of the magnetized resistivity to explain a large skin depth does not look right: the fact that the electron collision frequency ν_{ei} is much less than the electron gyrofrequency ω_{Ce} does not mean that the axial resistivity increases by a factor $(\omega_{Ce}/\nu_{ei})^2$; the resistivity does change significantly, and a radial electric field is established in a plasma (see, e.g., Braginski, 1965).

B. Breakdown of the foam

As the commonly used foams of CH_x, SiO_2, and agar ($\approx CH_2O$) are insulators, the question of the time and quality of the breakdown exists for these loads, too. In particular, it would be important to know whether breakdown occurs at the outer surface or some discharge channels are formed in the bulk of the foam. Very little is known at the moment on these issues and we have to limit ourselves to merely a verbal discussion.

To be more specific, we discuss breakdown of SiO_2 foam. Breakdown voltage for the SiO_2 foam could be quite large. This can be understood from the following qualitative considerations. If we substitute the foam with a gas with the same average particle density, i.e., with $6 \cdot 10^{20} \rho_0$ (mg/cm^3)/A particles per cm^3, the gas density would be quite high. For example, for ρ_0=5 mg/cm^3, and A=20 the particle density would be $1.5 \cdot 10^{20}$ cm^{-3}. At room temperature, this density would correspond to a pressure of approximately 5.5 atm; the Paschen product (pressure times length) will be then, roughly speaking, 1000 times

higher than its optimum value for the majority of gases. This would correspond to breakdown voltages in the range of a hundred kilovolts. High voltages needed for initiation of discharge in the foam loads and the corresponding delay for the onset of the current flow may cause strong leaks and even a closure of the gap in the magnetically insulating transmission line (see Fig. 3).

As soon as the voltage reaches ~100 kV, breakdown occurs. At high densities, it has a tendency to develop in the form of a narrow channel which, generally speaking, is not straight (Raizer, 1991). The energy required to ionize a breakdown channel to a singly-charged state is very small. An estimate from below for this quantity can be presented as:

$$W_{ion} > \pi L a_0^2 I_{ion} \rho / A m_p \ , \qquad (3.3)$$

where L is the column length, a_0 is its radius, I_{ion} is the ionization energy, ρ_0 is the foam density, m_p is proton mass and A is an average atomic weight. In "practical" units,

$$W_{ion}(J) \approx 3 \cdot 10^3 L(cm)[a_0(cm)]^2 \rho_0(mg/cm^3)/A. \qquad (3.4)$$

Taking L=1 cm, a_0=0.05 cm, ρ_0=5mg/cm^3 and A=20, one obtains $W_{ion} \approx$ 0.2 J. After the first breakdown channel is formed, new breakdowns may still occur, because the inductive voltage induced in the bulk of the dielectric can be quite high until 3-5 channels are formed. So, one can expect that, after this first phase of the current pulse, the column will carry several discharge channels. Though the energy released in the breakdown is very small compared to the total energy delivered to the pinch during the whole implosion process, the consequences of the formation of non-axisymmetric breakdown channels can be quite severe because the channel will have a density different from that of the external medium and will serve as a strong perturbation during the MHD phase of the implosion. The role of appearance of thin breakdown channels in fiber pinches with dielectric (frozen deuterium) fibers was discussed by Meierovich and Sukhorukov (1991).

In the state of single ionization, the plasma should have temperature ~2-3 eV. This would correspond to relatively low magnetic diffusivity (Huba, 1994), $D_M \sim 5 \cdot 10^5$ cm^2/s. With this diffusivity, the resistive broadening of the current channel should be slow (for

t=10 ns the broadening would be ~1 mm). In other words, as soon as several highly conducting channels are formed, the initial current will be trapped in them. With the continuing ionization of the column, the further current build-up will occur in a thin skin-layer at the surface of the column. But, as we have already emphasized, the initial current will remain trapped within several narrow channels inside the column. The presence of this current will cause some distortions of the equilibrium; the trapped magnetic field will grow proportionally to the convergence. Formation of several channels was observed in the experiments with gaseous liners on ANGARA-5-1 facility (Volkov, Utyugov, and Frolov, 1993). The reason for their formation and persistence during the whole implosion event could be just the one suggested above.

An ideal situation would be, of course, the one where breakdown is produced uniformly over the surface of the cylinder and intercepts so much current that the voltage drop inside the cylinder becomes insufficient to produce any internal breakdowns. In this sense, an interesting option is the use of a thin conducting coating. The coating should not necessarily be thicker than the skin-depth. What is sufficient (and relatively easily achievable even for the metal coatings with a thickness of order a fraction of a micron), is that the L/R time of the circuit is considerably greater than 10-20 ns. There are experimental evidences that conductive coatings and prepulse had a favorable effect on the quality of the discharge (Nash et al., 1997a).

The presence of a pre-pulse can have a considerable effect on the breakdown of the coated foam. Even if the voltage during the prepulse is in the range of only a few kilovolts, it is sufficient, in the time-frame ~1 μs, to fully evaporate conducting coating. Depending on the voltage and the pre-pulse length, the evaporated material can expand by a few millimeters. The conductivity of this relatively cold vapor will be low and, probably, insufficient to inductively shield the liner. On the other hand, the presence of a gaseous corona around the foam load may turn on the same breakdown mechanism as in the case of

gas puffs (Sec. III A). A small axial magnetic field (~0.3 T) may be beneficial in producing a more symmetric current-carrying shell.

The aforementioned scenario of evaporation of the coating without its ionization corresponds just to one possible shape of the prepulse, with a long "pedestal" of a low voltage. If the prepulse is shorter and with a higher voltage, then a fast transition from vapor to a highly ionized plasma may occur.

The effect of a current pre-pulse on the explosion of a single carbon fiber was studied by Lebedev et al. (1998a) and Aliaga-Rossel et al. (1998). During the first 80 ns after arrival of the main pulse, the fiber exposed to a pre-pulse showed a less developed coronal plasma; later on, the differences between the wires exposed and not exposed to a pre-pulse became insignificant. Mosher et al. (1998) reported of a better uniformity of discharges in preheated white hot wires.

C. Thermal instabilities; filamentation and striations

It has been known since the mid 1980s that, early in the pulse, surface layers of the gas-puff pinch experience fast instabilities that cause formation of bright stripes perpendicular to the axis and (usually later) parallel to the axis. We call first of them "striations" and the second of them "filaments". Such patterns, for instance, have been clearly observed in the study by Branitskii et al. (1991) at the Angara-5-1 facility (Fig. 12). In this particular experiment the maximum current was 3 MA, voltage 0.4-0.6 MV and current rise-time~100 ns. The loads were usually Xe gas puffs with a height of 1 cm, initial diameter 3 cm, and mass per unit length of ~0.1 mg/cm. Ripples with a wave-length ~1 mm were formed immediately after arrival of the current pulse and were gradually replaced by filamentary structure with the same wave length; these filaments persisted half-way to current maximum. Azimuthal instabilities were not affected by replacing Xe with Ne.

These modes develop very rapidly compared to Rayleigh-Taylor instability and should have a different nature. They are usually identified with thermal instabilities where,

once the temperature in some fluid element increases (decreases), it continues to increase (decrease). Possible causes of such behavior are: increase of radiation losses at decreasing temperature, and positive feed-back in the Joule heating. In its "pure" form this instability does not require mass redistribution and may occur at times short compared to the acoustic time for the spatial scale of the instability (e.g., Afonin, 1995).

If parameters of the system are such that the growth rate of the thermal instability becomes comparable with the growth rate of Rayleigh-Taylor instability, they get coupled. Such a situation was, in particular, discussed by Imshennik and Neudachin (1987, 1988). In the absence of the gravity force (and, whence, the R-T instability), the slow thermal instability gets coupled with acoustic motions. This instability can be called "radiative-condensation instability" because of the formation of clumps of colder matter at its non-linear stage (Aranson, Meerson, and Sasorov, 1993). Various aspects of these instabilities have been considered by Velikhov et al. (1972), and Haines, (1974).

We discuss here these instabilities for the case where the thickness of the cylindrical conducting shell is much less than the skin-depth, and where the mechanical motions of the shell can be neglected ("fast" thermal instability). First, by solving Maxwell equations we relate the current perturbation to the perturbation of the resistivity and then we plug the thus found current perturbation into the thermal balance equation.

For a thin shell, its properties can be characterized by the "surface conductivity" σ_s which is the product of the shell thickness and the conductivity proper, or by a "surface resistivity" $\eta_s \equiv 1/\sigma_s$. The surface current can be presented as

$$J_t = E_t/\eta_s, \tag{3.5}$$

where E_t is the tangential component of the electric field. For perturbations, one has:

$$\delta J_t = \delta E_t/\eta_s - (\delta \eta_s/\eta_s^2) E_t, \tag{3.6}$$

where the sign "δ" designates the perturbations, and the unperturbed quantities do not bear this sign. As we are going to consider perturbations with the scale length shorter than the shell radius, we replace the cylindrical geometry by the planar one, with the axis x

corresponding to the radial coordinate, and the axis y corresponding to the azimuthal coordinate. In the unperturbed state, the current and the electric field have only the z components, while the magnetic field has only the y component. The unperturbed magnetic field is zero inside the shell (in our geometry, at $x<0$).

As there are no currents outside the shell, the magnetic field there is curl-free and can be represented as a gradient of some scalar function ψ, $\delta B=-\nabla\psi$. This function satisfies the Laplace equation, $\nabla^2\psi=0$. We consider the perturbations in the form $exp(\Gamma t+ik_y y+ik_z z)$, where $Re\Gamma$ is a growth rate. In addition to the Laplace equation for ψ, we will need the x component of Faraday's law,

$$ik_y\delta E_z - ik_z\delta E_y = -\Gamma\delta B_x. \tag{3.7}$$

The solution of the Laplace equation for the $x>0$ ($x<0$) half-space reads as:

$$\psi_\pm = A_\pm \exp(\mp kx), \tag{3.8}$$

where $k=\sqrt{k_y^2+k_z^2}$. We need to supplement these equations with the boundary conditions at the $x=0$ surface: the continuity of the normal component of the magnetic field (this yields $A_+=-A_-$ in (3.10)), and the jump condition for the tangential components of the magnetic field in terms of the surface current (3.8). Using these conditions, after some elementary algebra one finds the following expression for the perturbation of the current:

$$\delta J_z = -J_z \frac{k_y^2}{k^2}\frac{1}{1+(\Gamma/\Gamma_0)}\frac{\delta\eta_s}{\eta_s}, \tag{3.9}$$

where $1/\Gamma_0$ is a characteristic decay time for the current perturbations,

$$\Gamma_0 = \frac{2k\eta_s}{\mu} \equiv \frac{k\eta}{\mu h}. \tag{3.10}$$

where h is the shell thickness. The y component of the current perturbation is $\delta J_y=-(k_z/k_y)\delta J_z$, and k_y is related to the azimuthal mode number m: $k_y=m/r$. It is also convenient to introduce the angle α between the unperturbed magnetic field and the wave vector: $\sin\alpha=k_z/k$. Note that, according to (3.9), for highly conductive shells, where the resistive decay time is very long compared to the time of the process, the relative current

perturbation, $\delta J_z / J_z$, can be small even for considerable perturbation of the resistivity, $(\delta\eta_s/\eta_s) \sim 1$.

Now we switch to the equation of the thermal balance. It can be presented in the form:

$$\dot{Q}(T) = \eta_s(T) J^2 - q(T), \tag{3.11}$$

where Q is a plasma energy content per unit area of the shell, and q is the power loss (radiation) per unit area. The equilibrium state corresponds to the balance of the two terms in the r.h.s.:

$$\eta_s(T_0) J^2 - q(T_0) = 0. \tag{3.12}$$

The equation for the temperature perturbation, written with the account for the equilibrium condition (3.12), is:

$$C_V \frac{\partial \delta T}{\partial t} = 2q \frac{\delta J_z}{J_z} + q \frac{\eta_s'}{\eta_s} \delta T - q' \delta T, \tag{3.13}$$

where the prime designates the derivative of the corresponding quantity over the temperature, and C_V is the heat capacity per the unit area of the shell. Using Eq. (3.11), one then obtains the following dispersion relation:

$$\Gamma = \frac{q\eta_s'}{C_V \eta_s} \left[1 - \frac{2\cos^2 \alpha}{1 + (\Gamma/\Gamma_0)} \right] - \frac{q'}{C_V}, \tag{3.14}$$

with $\sin\alpha \equiv k_z / k$.

Instead of exactly solving this (quadratic) equation, we present a qualitative discussion of possible instabilities described by it in some limiting cases. One extreme case is that of a strong temperature dependence of the heat losses and a weak temperature dependence of the resistivity. In this case, one can neglect the first term in the r.h.s. of Eq. (3.14). The remaining term predicts the instability if $q' < 0$, in other words, if the radiative losses decrease with a temperature increase. This may happen in an optically thin plasma dominated by free-bound radiation or by line radiation, where some strong transitions disappear with the growing temperature because of the change of the ionization state.

In the opposite limiting case where the temperature dependence of the resistivity is dominant, one can neglect the last term in the r.h.s. Instabilities present in this case are driven by the temperature dependence of the resistivity. Somewhat paradoxically, these instabilities are present at either sign of η_s'; what depends on the sign is their spatial structure. At $\eta_s'>0$, to make the r.h.s. as large as possible (at Γ positive), one has to choose $\alpha=\pi/2$ ($m=0$). In other words, the fastest growing modes at a positive temperature dependence of the resistivity are axisymmetric modes ("striations"). At $\eta_s'<0$, the most unstable modes correspond to $\alpha=0$, in other words, to the purely azimuthal perturbations. For them one has (with $q'=0$):

$$\Gamma = \frac{q\,|\eta_s'|}{C_V \eta_s}\,\frac{1-(\Gamma/\Gamma_0)}{1+(\Gamma/\Gamma_0)}\,. \qquad (3.15)$$

The largest growth rate corresponds to $\Gamma_0 \to \infty$, in other words, according to (3.10), to large m number (thin filaments stretched along the axis). Our simple model does not include the thermal conductivity along the surface of a layer. If included, it will limit from below the size of both striations and filaments.

The positive dependence of resistivity vs temperature is typical for low temperatures, where the ionization degree grows and electron-neutral collisions get replaced by the Coulomb collisions with much higher cross-section. Accordingly, striations should form predominantly at the early stage of the pulse. This instability, as well as the other thermal instabilities, can reach a strongly non-linear stage. They will eventually cause redistribution of matter (the process that we have not included into the analysis presented above). Such nonlinear structures may exist much longer than η_s' is positive and seed the Rayleigh-Taylor instability.

The negative dependence of resistivity vs. temperature takes over later, when plasma gets singly ionized. Therefore, filamentation should develop later than striations - in agreement with the aforementioned experimental data by Branitskii et al. (1991) (Fig. 12). The presence of azimuthally asymmetric structures in the foam loads was recorded on the

Saturn device (Lazier et al., 1997), although in this case their appearance might also be caused by a discrete azimuthal structure of the return current conductor.

D. Early stage of the wire array discharge; merging of the wires.

Driving pulsed currents through single metal wires and dielectric fibers has been the subject of numerous experimental studies: Aliaga-Rossel et al (1998), Aranchuk et al. (1986); Bartnik et al. (1990), Beg et al. (1997), Mosher and Colombant (1992), Sarkisov and Etlicher (1995); Sarkisov et al. (1995 a,b), Sethian et al. (1987), Skowronek and Romeas (1985). Theoretical analyses were published by Coppins et al. (1988), Rosenau et al. (1988), Bud'ko, Liberman, & Kamenets (1990), Neudachin and Sasorov (1991), Sasorov (1991), and Bobrova et al. (1992).

An important feature of the discharge in a single wire is that the wire core, at least for thick wires, may remain cold and expand very slowly. The core is surrounded by a plasma "corona" that contains only a small fraction of mass but carries almost all the current. This conclusion was made in the paper by Aranchuk et al. (1986) specifically devoted to experimental studies of single wire explosions (see also an earlier paper by Aranchuk, Bogolyubskii and Tel'kovskaya, 1985). They have found that, in the explosions of 20-μm diameter copper wires, only 2-7% of the total mass was carrying the current and radiating. The rest of the mass remained cold. This corona was subject to violent unstable motions, while the core remained more or less cylindrical. The maximum current through the wire was 0.5 MA, the current rise time was approximately 100 ns. The halo plasma can be formed because of desorption during a pre-pulse (a point made in Bartnik et al, 1990) or just because of the evaporation of the whole wire. This relatively low-density halo provides better conditions for the breakdown (Cf. Sec. III A). A strong effect of the wire cleanliness on formation of the corona was reported by Bartnik et al (1994). A long lasting core of the exploded wire was observed by Kalantar and Hammer (1993). Sarkisov et al. (1995 a,b) detected a thick core in explosions of 20-μm copper

wires; they used absorption of the 532 nm laser light to detect the evolution of the exploding wire. Beg et al. (1997) performed a very detailed study of explosions of carbon (7- and 33-μm diameter) and aluminum wires (25-μm diameter) at the maximum current ~ 100 kA and current rise time 55 ns. For the thicker wires, the core existed at least until the current maximum, whereas for the 7-μm carbon wire it disappeared within ~ 10 ns (we note in passing that the paper by Beg et al. (1997) contains a wealth of information on the wire pinches, including detailed characterization of the instabilities in coronal plasma, and detection of electron beams). Detailed numerical simulations of development of the m=0 instability have been recently published by Chittenden et al (1997). The theory attributes formation of the corona to the Ohmic heating of the low-density plasma due to anomalous resistivity (Sasorov, 1991; Haines et al, 1996). We will return to this issue in Sec. VII A.

The behavior of the plasma corona of the wires assembled in a cylindrical array is very different from that of separate wires. The reason is the presence of a strong common magnetic field. As a curiosity, one can mention the following: the common magnetic field of the wire array near its surface is $\mu I/2\pi r$, where r is the array's radius. The magnetic field produced by a certain wire at the location of its closest neighbor (i.e., at the distance $2\pi r/N$, where N is the number of wires in the array), is $\mu I/(2\pi)^2 r$, i.e., universally smaller by a factor of 2π than the common field.

This common field accelerates the light coronal plasma past the wire cores towards the center of the array and forces the current to switch to the cores. Therefore, there is reason to believe that the current will be forced to flow in the wire cores. This assumption is supported by the fact that the dynamics of the wire array implosion corresponds, to a good accuracy, to a model in which the whole mass of the wire array is involved in the implosion, at least for a sufficiently large number of wires in the array (Cf. Sanford, et al., 1999 a,b). The systematic study of the effect of the number of wires on the pulsewidth of the radiation emission carried out in this paper points also at a significant decrease in precursor plasma at a large number of wires. There is a good agreement of the radiation

pulse with the simulations based on the assumption that all wire mass is involved in the implosion (e.g., Fig 11 in Spielman et al, 1998). It should be noted that, for a smaller number of thicker wires, the effect of current interception by the coronal plasma may be significant, with a large amount of a blow-off plasma accelerated to the center of the array (Aivazov et al., 1988; Lebedev, et al, 1998 b, 1999).

Limiting ourselves to the case of a large number of wires, we assume that essentially all the mass of the wire is involved into hydrodynamic motions. As is well known (see Kadomtsev, 1966; Bateman, 1980), a wire is unstable with respect to MHD sausage and kink modes. For perturbations with wavelengths exceeding the wire radius, $k_z<r_w^{-1}$, growth-rates are:

$$\Gamma \sim \sqrt{\frac{B_w^2 k_z^2}{\mu(\hat{m}/N\pi r_w^2)}}\,, \qquad (3.16)$$

where B_w is the magnetic field intensity at the surface of the wire (we ignore the factor 2-3 difference between the growth-rates of the kink and sausage modes). Numerical results pertaining to specific radial profiles of the current and the density can be found, e.g., in Felber (1982) and Pereira, Rostoker, and Pearlman (1984).

According to what has been said above, we assume that all the wire mass is involved in the hydrodynamic motion. The modes with $k_z \sim 1/r_w$, where r_w is the instantaneous radius of an individual wire, create perturbations randomly distributed over the wire length and cause a gradual broadening of the wire (the increase of the effective r_w). Assuming that the growth rate of short-wave perturbations is large compared to the characteristic times involved in the problem (so that the perturbations reach a nonlinear state), the expansion velocity is independent of initial perturbations. In this regime the expansion velocity can be evaluated (in particular from the dimensional considerations), as $v \sim \Gamma r_w$. Using expression (3.16) and noting that $B_w=\mu I/2\pi N r_w$, one finds:

$$v \sim I\sqrt{\frac{\mu}{4\pi\hat{m}N}}\,. \qquad (3.17)$$

In "practical" units,

$$\mathrm{v}(cm/s) \sim \frac{3\cdot 10^6 I(MA)}{\sqrt{N\cdot \hat{m}(mg/cm)}} \,. \qquad (3.18)$$

Solving equation $\dot{r} = \mathrm{v}$ with I as in (2.6), one finds that r_w reaches a half of the inter-wire gap, $\pi r/N$, at

$$\frac{t}{\tau} \sim 15\left[\frac{\hat{m}(mg/cm)}{N}\right]^{1/6}\left[\frac{r(cm)}{\tau(ns)I_0(MA)}\right]^{1/3} . \qquad (3.19)$$

For the wire array with the "standard" Z parameters, t/τ is ~0.5. Therefore, development of the MHD instabilities of the wires can, in principle, cause an early merging of the wires. Note that at t/τ ~0.5 the current in the wires reaches only a quarter of its maximum value, and the array's diameter experiences only a very small change. This is why we neglected change of r in the preceding discussion. In a more sophisticated version of this analysis, one should take convergence into account.

If the MHD mechanism of the wire merging is indeed the dominant one, one can make some predictions with regard to the initial state of the thus formed liner: it will be grossly non-uniform, with the spatial scale of the non-uniformities of the order of a half of the inter-wire distance. These non-uniformities will be both axial and azimuthal. This observation may be of some value for the numerical simulations of the R-T instability of the type carried out by Peterson et al. (1996, 1997, 1999). In a model suggested by Haines (1998), the perturbations developing in the wires are assumed to be uncorrelated. Based on this assumption, Haines comes to a conclusion that the amplitude of macroscopic axisymmetric perturbations (which has to be obtained by the averaging over the azimuth), should scale as $N^{-1/2}$, with N being a number of the wires in the array. Experimentally, an increase of the number of wires had a favorable effect on the implosion symmetry (Sanford et al, 1996, Deeney et al, 1997b, Deeney, et al., 1998a). The authors of these papers relate improved performance to an early formation of a continuous shell in the case of a large number of the wires (see also a more recent study by Sanford et al, 1999).

In summary, the merging of the wires most probably occurs in a turbulent fashion, with development of the perturbations with the scale of the order of the instantaneous wire radius. When merging occurs, the thus formed shell has a thickness of order of the inter-wire distance and non-uniformities of the same scale. The amplitude of non-uniformities is of order of 1. This sets the stage for the further evolution of the liner, where two competing processes occur: smoothing out the inhomogeneities by virtue of hydrodynamic motions and thermal conductivity, and enhancement of those modes that are Rayleigh-Taylor unstable.

IV. HYDRODYNAMIC STABILITY OF AN IMPLODING LINER

The Rayleigh-Taylor (R-T) instability plays an important role in essentially all high-energy-density experiments, including experiments with fast Z pinches and ICF capsules. This instability is universal and very difficult to stabilize. It is a key factor among those setting the limit for the performance of fast Z pinches and other pulsed power devices. As one might expect, there are hundreds of publications devoted to the studies of this instability in general and in the pulsed plasma systems in particular. We will certainly not be able to cover all the relevant results in this relatively compact paper. The interested reader can find further references in the surveys by Sharp (1984), Kull (1991), and Lindl (1995), the latter survey considering specifically the physics of ICF capsules. A summary of experimental results for ICF capsules was given by Kilkenny et al. (1994). As a good general introduction, one could recommend Chandrasekhar's book (1961) which, however, deals only with incompressible systems.

In this section we discuss the instability of an ideal fluid, without accounting for dissipative processes like viscosity, thermal conductivity, and electrical resistivity in the body of the fluid (although we allow for the presence of shock waves, which are, of course, dissipative structures). Dissipative effects are discussed in Sec. V.

Generally, theoretical analysis of the magnetic Rayleigh-Taylor instability involves very lengthy calculations which do not match the format of this survey. Still, to give the reader a possibility to follow more closely some important arguments, we present a complete derivation of the growth rates for one relatively simple system: a slab of a uniform, incompressible, perfectly-conducting fluid supported from below by a horizontal magnetic field (Harris, 1962). After that, mostly on the qualitative level, we will add new elements to the picture of stability.

One should remember that, in the implosions of thick metal shells of the type used by Degnan et al. (1995), the structural strength of the material can have a considerable stabilizing effect at the early stage of the implosion process. These effects have not yet been studied in great detail and we will not discuss them below. Some further information and pertinent references can be found in Atchinson et al. (1997).

A. Stability of a slab of an incompressible fluid.

The geometry of the problem is illustrated by Fig. 10: the slab thickness is h, the gravity force is directed downward in the x direction, with $\mathbf{g}_x=-\mathbf{e}_x g$, and $g>0$; the unperturbed magnetic field B occupies the lower half-space, $x<0$, and is parallel to the axis y. In the geometry of a cylindrical implosion of a thin shell, x would correspond to the radial coordinate (directed in this case to the axis), y would correspond to the azimuthal (θ) coordinate, and z, to the axial coordinate. The unperturbed magnetic field that supports the slab, is related to the gravity force and the fluid density by the obvious relationship:

$$\rho g h = \frac{B^2}{2\mu} \equiv p_m, \tag{4.1}$$

where we use the notation p_m to designate the magnetic pressure.

As the unperturbed state does not depend on time or the coordinates y and z, one can seek the solution of the problem in the form of the harmonic perturbations in these

variables, i.e., in the form $f(x)\exp(-i\omega t + ik_y y + ik_z z)$. The instability corresponds to $Im\omega > 0$. Sometimes, instead of ω, we use the growth rate,

$$\Gamma = -i\omega. \tag{4.2}$$

The linearized hydrodynamics equations are:

$$-\omega^2 \rho \xi = -\nabla \delta p, \tag{4.3}$$

$$\nabla \cdot \xi = 0, \tag{4.4}$$

where ξ is the displacement of the fluid element with respect to its unperturbed position, and δp is the pressure perturbation. These equations yield $\nabla^2 \delta p = 0$, with the solution

$$\delta p = A\exp(kx) + B\exp(-kx), \tag{4.5}$$

where

$$k = \sqrt{k_x^2 + k_y^2}, \tag{4.6}$$

and A and B are arbitrary constants. One finds then from (4.3) that

$$\xi_x = \frac{k}{\rho\omega^2}[A\exp(kx) - B\exp(-kx)]. \tag{4.7}$$

At the upper and lower boundaries of the slab, one should impose boundary conditions of the pressure balance at the perturbed boundary. These conditions are:

$$\delta p - \rho g \xi_x = 0, \text{ the upper boundary,} \tag{4.8}$$

$$\delta p - \rho g \xi_x = \delta p_m, \text{ the lower boundary,} \tag{4.9}$$

with $\delta p_m = B\delta B_y / \mu$. To find the magnetic field perturbation at the perfectly conducting surface, one should use the condition that the magnetic field has a zero normal component at the surface, or, in other words, that

$$\mathbf{n} \cdot \delta\mathbf{B} + \mathbf{B} \cdot \delta\mathbf{n} \equiv -\delta B_x + B\delta n_y = 0, \tag{4.10}$$

where $\boldsymbol{n}$ is the unperturbed outer normal to the lower surface, $\boldsymbol{n}$=(-1, 0, 0), and $\delta n_y = \partial \xi_x / \partial y = ik_y \xi_x$. Perturbation of the vacuum magnetic field is curl-free, whence

$$\delta\mathbf{B} = -\nabla\psi. \tag{4.11}$$

The scalar potential satisfies the Laplace equation,

$$\nabla^2\psi \equiv \frac{\partial^2\psi}{\partial x^2} - k^2\psi = 0 \tag{4.12}$$

Its solution evanescent at $x \to -\infty$ is

$$\psi = C\exp(kx) \tag{4.13}$$

where C is another arbitrary constant. Substituting this solution into (4.11) to find δB_x, substituting the resulting expression for δB_x into (4.10) to express C in terms of the value of ξ_x at the lower boundary, and returning to Eq. (4.11) to express δB_y in terms of ξ_x, one finds that the magnetic pressure perturbation, $\delta p_m = B\delta B_y / \mu$, at the lower boundary is:

$$\delta p_m = -2\frac{k_y^2}{k} p_m \xi_x. \tag{4.14}$$

This equation shows that magnetic pressure increases (decreases) at the bumps, $\xi_x<0$ (dips, $\xi_x>0$) of the sinusoidally perturbed surface. This can also be rephrased as a statement that the magnetic energy perturbation is positive, thereby providing a stabilizing effect (the perturbation of the gravitational energy, for the unstable perturbations, is negative).

Using relationship (4.14) and substituting solutions (4.5) and (4.7) into the boundary conditions (4.8) and (4.9), one finds two linear homogeneous equations for the constants A and B. From the condition that the determinant of this set of equations is zero, one obtains the following dispersion relation for the eigenfrequencies of the problem

$$\left(\frac{\omega^2}{kg}\right)^2 - \frac{2k_y^2 h}{k}\frac{1+\exp(-2kh)}{1-\exp(-2kh)}\frac{\omega^2}{kg} - 1 + \frac{2k_y^2 h}{k} = 0. \tag{4.15}$$

Introducing an angle α between the magnetic field and the wave vector,

$$\cos\alpha = k_y / k \tag{4.16}$$

one can present the roots of this dispersion relation as:

$$\frac{\omega^2}{kg} = kh\cos^2\alpha\frac{1+\exp(-2kh)}{1-\exp(-2kh)} \pm \left\{\left[kh\cos^2\alpha\frac{1+\exp(-2kh)}{1-\exp(-2kh)}\right]^2 + 1 - 2kh\cos^2\alpha\right\}^{1/2} \tag{4.17}$$

The sign "plus" corresponds to a stable root. The nature of a stable mode becomes particularly clear in the limit $k \to \infty$, where the eigenmode corresponding to this root gets strongly localized near the upper surface, with A/B in the equation (4.5) becoming of order of 1 (this means that, near the upper surface, the second term in the expression (4.5) is exponentially small compared to the first one). The stable mode is an analog of the gravity

wave on the surface of a fluid (see, e.g., Landau and Lifshitz, 1987). At smaller k, the eigenfunction of this mode encompasses the whole layer but still is somewhat stronger concentrated near the upper surface, where the gravity force is directed to the fluid, so that the stabilizing contribution dominates.

The second root corresponds to the mode that can be stable or unstable, depending on the wave number k. The mode is unstable at small k's and stable at large k's. The critical wave number k_0 at which the mode becomes stable, is:

$$k_0 = \frac{1}{2h\cos^2\alpha} \tag{4.18}$$

For $\alpha \sim 45^0$ the critical wave number is of the order of h^{-1}. At large k's, the magnetic energy perturbation (positive) overbalances the gravitational energy perturbation (negative, for a mode localized near the lower surface). Whence, the stability at large k's.

An exceptional role is played by the perturbations with $\alpha=\pi/2$. In this case, the system is unstable at all k's. A perturbation with $\alpha=\pi/2$ is sometimes called the flute mode. Its remarkable feature is that it does not perturb the vacuum magnetic field and therefore the positive (stabilizing) contribution of the magnetic energy perturbation vanishes. In cylindrical geometry this mode corresponds to axisymmetric perturbations, with no dependence on the azimuthal angle θ.

At small k's the growth rate reduces to

$$\Gamma = \sqrt{kg\left[\sqrt{1+\cos^4\alpha} - \cos^2\alpha\right]} \tag{4.19}$$

and becomes independent of the thickness of the layer. For these large-scale perturbations the layer can be considered just as a structureless infinitesimally thin gravitating sheet. The overall dependence of the growth-rate on the wave vector for several values of α is shown in Fig. 13. At $\alpha=0$ (a purely azimuthal mode in the cylindrical geometry) the growth rate is equal to $\sqrt{kg\left(\sqrt{2}-1\right)}$ (e.g., Harris, 1962; Kleev, Velikovich, 1990).

These results pertain to constant density distributions. A broader class of density distributions of incompressible fluids has been studied by Munro (1988). If the lower

surface of the fluid is free, then, there exist modes with the growth rate $(kg)^{1/2}$. At large k they are strongly localized near the interface and have large growth rate. If, however, the transition is smooth enough, the growth rate is limited from above. Some further discussion of these modes can be found in Inogamov (1985), Bychkov, Liberman, Velikovich (1990), and Bud'ko et al (1989).

B. Effects of compressibility

The most important new element that emerges from the finite compressibility is the presence of propagating acoustic waves. Various aspects of the R-T instability in compressible fluid have been discussed in Landau and Lifshitz (1987), Catto (1978), Parks (1983), Bernstein and Book (1983), Gonzales and Gratton (1990), Lezzi and Prosperitti (1989), Gratton, Gratton and Gonzales (1988), Budko and Liberman (1992), Ryutov and Toor (1998). We discuss here a slab of plasma whose temperature in the unperturbed state is constant, supported from below by a uniform magnetic field in the geometry identical to the one shown in Fig. 10, under the assumption of the perfect plasma conductivity and vanishingly thin transition layer between the plasma and the magnetic field. Later, in Sec. IV C, we address the issues related to the finite thickness of the transition layer.

If the composition of the plasma does not change in the vertical direction, then plasma density and pressure follow the exponential dependence (2.26), $p, \rho \propto \exp(-x/h)$ with the scale-length h (2.27). It turns out that the problem in the case of a sharp plasma-vacuum transition allows an exact solution (Parks, 1983, Bernstein and Book, 1983, Gratton, Gratton and Gonzales, 1988). When acoustic waves (that are present now in a fluid) propagate in a plasma with exponentially decreasing density (as is the case of a constant-temperature slab supported from below), their amplitude grows exponentially. Therefore, in the perturbation analysis one must allow for the presence of the solutions exponentially growing in the vertical direction and it would be incorrect to impose a

constraint of an exponentially decreasing solution. Further details related to this issue can be found in a comprehensive analysis by Gratton, Gratton and Gonzales (1988).

We present a dispersion relation for unstable modes in the form derived in Ryutov and Toor (1998). Using the same notation as in Sec. IV A, one can write it as:

$$\omega^4 - k^2 g^2 + 2\cos^2\alpha kg\left[\omega^2\left(2\cos^2\alpha\frac{kgh^2}{s^2} - 1\right) + 2k^2 gh\left(1 - kh\cos^2\alpha\right)\right] = 0 \quad (4.20)$$

where

$$s^2 = \frac{\gamma p}{\rho} = \frac{\gamma T}{\overline{m}} = \gamma gh \quad (4.21)$$

is the sound speed. Its unstable solution behaves very much in the same manner as the solution of Eq. (4.15): at small k's, $kh << 1$, the growth rate is determined by the same expression as for the incompressible fluid, i.e. by Eq. (4.19), while at larger k's it decreases and turns zero at some critical $k=k_0$, which is exactly the same as (4.18).

Formally, Eq. (4.20) has unstable solutions even at $k>k_0$. However, these solutions correspond to the modes whose amplitude grows in the vertical direction faster than $exp(x/2h)$, so that the energy density diverges at large x. On this basis, Gratton, Gratton and Gonzales (1988) (correctly) consider these solutions as unphysical. What happens with perturbations at $k>k_0$, can be more clearly demonstrated by the analysis of the initial value problem based on the use of the Laplace transform: if one stirs the plasma near the lower boundary and creates there perturbations with spatial scales much smaller than $1/h$, then a part of the perturbation is radiated as acoustic waves in the upward direction, and a part stays near the boundary as a stable surface wave.

Let us discuss in some more detail the reason why, at small k's, the scale-height h drops out from the dispersion relation so that all the information on the structure of the plasma slab disappears from the dispersion relation; the sound speed also disappears from it. First one notes that the sound speed s is related to the other parameters of the problem through the relationship (4.21). The sound propagation time over the distance $\sim 1/k$ is $1/ks$. Using Eq. (4.21), one can easily show that for long enough perturbations with $k<k_0 \sim 1/h$,

the instability e-folding time ($\sim 1/\sqrt{kg}$) becomes shorter than the sound propagation time ($1/ks$). Basically, this means that the parts of the slab that are separated by a distance exceeding $1/k_0$ cannot communicate to each other by acoustic signals propagating inside the slab; therefore, they evolve independently of each other.

From these considerations we see that, for the modes with a parallel scale-length exceeding the thickness of the layer, $k<1/h$, one can neglect the interaction between different points along the surface of the imploding shell. The shell itself, for such modes, can be considered as a thin structureless surface possessing some inertia (determined by the mass per unit area). This is a very important observation which helps one to make some clear predictions regarding the evolution of the modes with $k<1/h$ (see Sec. IV D).

These arguments allow one also to make some conclusions with regard to the stability of the wire array before the wire merging: if one considers the m=0 perturbation with wavelengths much greater than the inter-wire distance, the fact that the array consists of separate wires does not manifest itself in any way, and expression (4.19) correctly describes the growth rate. The stability of some modes with wavelengths comparable to the inter-wire distance has been studied by Felber and Rostoker (1981) and Samokhin (1988). Felber and Rostoker have shown that there exist two types of modes: the ones in which the wires remain within the meridianal planes (medial modes, according to terminology introduced by Hammer and Ryutov, 1999), and the ones where the wires bend along the surface of the cylinder (called lateral modes by Hammer and Ryutov). A complete linear stability analysis for arrays consisting of a large number of wires (Hammer and Ryutov, 1999) has shown that a $\sqrt{kg}$ scaling holds for surprisingly short wavelengths, approaching the interwire spacing. The growth rate for the lateral modes is as high as the growth rate for medial Rayleigh-Taylor modes. For wavelengths shorter than the interwire spacings, an approximately linear dependence on k takes over. For the $m=0$ medial mode, Desjarlais and Marder (1999) have considered both linear and nonlinear stages of the instability.

Amplitude of the initial perturbation for the m=0 mode was determined on the basis of Haines' theory (Haines, 1998) mentioned at the end of Sec. III D of this survey.

C. Smooth transition between the plasma and the magnetic field; local modes

The finiteness of the plasma resistivity smoothes the transition between the vacuum magnetic field and the plasma. Fast development of short-wavelength flute perturbations (for which the critical wave number is infinite) also smears out the transition. We will use notation h_1 to denote the thickness of the transition; h_1 can be smaller than or comparable to the total thickness of the shell h (Sec. II G). For perturbations with wave numbers below $1/h_1$, one can use the results of the previous section. In this section, we consider perturbations with the wave number much greater than $1/h_1$, so called local modes. The growth rate of these modes depends on the local value of the density gradient ρ'. Since within the transition layer the characteristic value of the magnetic field strength is of the order of the vacuum magnetic field, these short-wavelength perturbations can be unstable only if they are of a flute type (otherwise, perturbation of the magnetic energy becomes prohibitively high). The growth rate for the flute perturbations has been derived by Chen and Lykoudis (1972):

$$\Gamma^2 = \left(\frac{g^2}{a^2 + s^2} + \frac{g\rho'}{\rho} \right), \tag{4.22}$$

where $a^2=2p_m/\rho$ is the local value of the Alfven speed. For $\rho'>0$ the local modes are universally unstable. Taking into account rough estimates $\rho'/\rho \sim 1/h_1$ and $gh \sim a^2 + s^2$ that follow from the equilibrium condition, one can estimate the growth rate of the localized modes as

$$\Gamma^2 \sim g/h_1 . \tag{4.23}$$

Note that the presence of the magnetic field within the shell does not change the conclusion made in Sec. VI.B regarding the properties of the long-wavelength

perturbations: at $k<<1/h$, the instability e-folding time is shorter than the time needed for the Alfven wave to propagate over the distance $1/k$. Therefore, even if the magnetic field penetrates into the shell, the long-wave perturbations behave as perturbations of a massive structureless infinitesimally thin sheet.

Another comment is related to the perturbations localized near the interface between the plasma and the magnetic field. The growth rate of the modes localized near this interface, at large k's, doesn't reach a saturation, because the parameter ρ'/ρ near the interface becomes infinite. On the other hand, if the interface is smeared and the density decreases, say, exponentially, the growth rate at large k's reaches a saturation (see also comment at the end of Sec. IV A).

D. More on the stability of a thin shell; effects of accretion

As has been shown in Sections IV A, B, the analysis of perturbations with wavelengths exceeding the shell thickness can be carried out without account for the internal structure of the shell. This allows one to obtain a relatively simple description of the instability including effects of the cylindrical geometry of implosion (Harris, 1962), of the mass accretion effects (Gol'berg and Velikovich, 1993; DeGroot et al., 1997b), and even get some insights into nonlinear phase of the problem (Ott, 1972; Bashilov, Pokrovskii, 1976; Manheimer, Colombant and Ott, 1984; Basko, 1994; Book, 1996). We derive the corresponding equations in the planar case. Later, in Sec. IV F, we discuss effects of a cylindrical geometry.

Consider a thin shell accelerated by a magnetic pressure p in the x direction (Fig. 14). The horizontal line at $x=0$ depicts the initial position of the shell. We will analyze only most dangerous flute perturbations aligned with the magnetic field lines which are directed along the y axis. In other words, we consider perturbations which do not depend on the coordinate y. The motion occurs in the (x,z) plane. The magnetic pressure then is uniform even on the perturbed surface of the shell.

Following Ott, we denote by $\xi_x(z,t)$ and $\xi_z(z,t)$ the x and y displacements of a certain element of the shell (whose initial location on the shell surface was z). In other words, at this point we are using a Lagrangian description of the peturbations. These displacements are not assumed to be small: we are going to obtain a non-linear set of equations. We will also take into account the possibility of mass accretion on the shell from the gas initially situated at the $x>0$ half-space, assuming that the gas just sticks to the shell (strongly radiating plasma, see Sec. II B,C). In the unperturbed motion one obviously has $\xi_z=0$ and

$$\frac{\partial}{\partial t}\left(\sigma_0 \frac{\partial \xi_x^0}{\partial t}\right) = p, \quad \frac{\partial \sigma_0}{\partial t} = \rho \frac{\partial \xi_x^0}{\partial t}, \tag{4.24}$$

where ρ is the density of the cold resting gas swept by the shell, and σ_0 is the mass per unit area of the shell (varying with time because of the accretion).

Let us denote by Δz an initial distance between the two neighboring points at the surface (Fig. 14). One of them gets displaced to the point $(\xi_x(z,t), \xi_z(z,t))$, the other to the point $(\xi_x(z,t)+\Delta z \partial\, \xi_x(z,t)/\partial z,\ \xi_z(z,t)+\Delta z \partial\, \xi_z(z,t)/\partial z)$. Let the mass of this element of the surface be Δm . The change in the mass occurs because of the accretion. Using simple geometrical considerations (identical to the ones used by Ott (1972)), one finds:

$$\Delta \dot{m} = \rho\left(\frac{\partial \xi_z}{\partial z}\dot{\xi}_x - \frac{\partial \xi_x}{\partial z}\dot{\xi}_z\right)\Delta z, \tag{4.25}$$

or

$$\dot{\sigma} = \rho\left(\frac{\partial \xi_z}{\partial z}\dot{\xi}_x - \frac{\partial \xi_x}{\partial z}\dot{\xi}_z\right), \quad \sigma \equiv \frac{\Delta m}{\Delta z}, \tag{4.26}$$

where the dot designates a partial derivative over the time. Equations of motion can be obtained in the same way as in Ott (1972). They read as:

$$\frac{\partial}{\partial t}\left(\sigma \frac{\partial \xi_x}{\partial t}\right) = p\frac{\partial \xi_z}{\partial z}; \quad \frac{\partial}{\partial t}\left(\sigma \frac{\partial \xi_z}{\partial t}\right) = -p\frac{\partial \xi_x}{\partial z}. \tag{4.27}$$

If the shell is being accelerated into the vacuum, then σ does not depend on time, and one does not need Eq. (4.26) for σ. In this case Eqs. (4.27) become the linear equations. This observation was made by Ott: the Lagrangian formulation of the problem in

this case leads to linear equations describing even the finite-amplitude perturbations. Note that Bashilov and Pokrovskii (1976) generalized Ott's nonlinear solution to the cylindrical case. We will comment on the properties of the non-linear solution later and now will discuss small perturbations of the shell. To distinguish the perturbations, we will mark them by a symbol "δ". We get:

$$\frac{\partial}{\partial t}\left(\sigma_0 \frac{\partial \delta\xi_x}{\partial t}\right) = \left(p - \rho v^2\right)\frac{\partial \delta\xi_y}{\partial y} - \dot{v}\delta\sigma;$$
$$\frac{\partial}{\partial t}\left(\sigma_0 \frac{\partial \delta\xi_y}{\partial t}\right) = -p\frac{\partial \delta\xi_x}{\partial y}; \qquad (4.28)$$
$$\frac{\partial \delta\sigma}{\partial t} = \rho v \frac{\partial \delta\xi_y}{\partial y},$$

where $v=\partial\xi_x^0/\partial t$.

If there is no material in front of the accelerated shell ($\rho=0$), then the set of equations (4.28) becomes particularly simple:

$$\frac{\partial^2 \delta\xi_x}{\partial t^2} = g\frac{\partial \delta\xi_y}{\partial y}; \quad \frac{\partial^2 \delta\xi_y}{\partial t^2} = -g\frac{\partial \delta\xi_x}{\partial y}, \qquad (4.29)$$

Here $g \equiv p/\sigma_0$ is the effective gravity force. For the perturbations with exp(-*ikz*) dependence on the co-ordinates this equation yields a familiar expression for the growth rate (Cf. Eq. (4.19) with $\theta=\pi/2$): $\Gamma=(kg)^{1/2}$.

An interesting point here is the surface density perturbation of the shell. The quantity σ that we have been using so far was the Lagrangian density: a mass that corresponds to a segment of the shell whose end points originated at the ends of the initial segment Δz, divided by this Δz (see (4.26)). If there is no accretion, then the thus defined density is constant. But the real density of the shell defined as a mass Δm occupying some segment $\Delta\ell$ on the surface of the shell, divided by this $\Delta\ell$, is changing (because $\Delta\ell$ is changing). One can show that the surface density is redistributed over the shell in such a way that the density decreases on the tops of perturbations and increases on the bottoms (Fig. 15). This contains a hint on the process of a self-acceleration of the instability at the

non-linear stage: the areas of a lower (higher) density tend to move ahead (lag behind) faster than in a linear approximation. We will return to this issue in section IV G.

Consider now a linear instability in a more general case where accretion of the material is substantial and one has to use a general set of equations (4.28). A characteristic time of changing the parameters of the system, in particular, the mass per unit area and the acceleration is

$$\tau \equiv \sigma / \dot{\sigma} = \sigma / (\rho \mathrm{v}) \ . \tag{4.30}$$

As the e-folding time for short-wavelength perturbations decreases with k, at large enough k's it becomes much shorter than τ. This happens at $k >> \rho^2 \mathrm{v}^2 / g\sigma$. The magnetic pressure is related to the ram pressure of the accreted material via $\rho \mathrm{v}^2 \sim p$. Using this relationship, one finds that the limit of large growth rates corresponds to

$$k >> \rho / \sigma, \tag{4.31}$$

in agreement with DeGroot et al (1997b). At some medium point in the acceleration process the r.h.s. of (4.31) is of the order of the inverse path travelled by the shell, in other words, the inverse pinch radius. In this case one can consider all the unperturbed parameters entering the set (4.28) as constant. This yields the following expression for the instantaneous growth rate:

$$\Gamma = \left(\frac{k}{\sigma} \right)^{1/2} \left[p \left(p - \rho \mathrm{v}^2 \right) \right]^{1/4} . \tag{4.32}$$

This expression differs from the corresponding expression of DeGroot et al. (1997b); in particular, Eq. (4.32) predicts that the growth rate approaches zero at p close to $\rho \mathrm{v}^2$ when the shell is moving without acceleration.

For wavelengths that do not satisfy condition (4.31), the perturbation growth cannot be adequately defined in terms of the instantaneous growth rate; in this domain one has to solve a full set of differential equations (4.28). Qualitatively, in this domain the accretion still should lead to a decrease of the perturbation growth (Cf. Gol'berg and Velikovich, 1993). Cochran, Davis and Velikovich (1995) have shown by solving

numerically a 2-D set of equations of radiative hydrodynamics that uniform gas-puffs are more stable with respect to axisymmetric Rayleigh-Taylor instability than annular gas-puffs — in agreement with a general trend predicted by Eq. (4.32).

E. The case of a detached shock wave

In the previous section we have been discussing stability of a system where the gas just sticks to the surface of the piston. As we have mentioned in Sections II B,C such a model correctly reflects a situation where the gas collected by the piston is strongly radiating, so that the distance between the shock and the piston is negligible (an ultimate case of the snow-plow model). For the short current pulses typical for experiments on fast Z-pinches and low initial temperature of the matter, a strong shock will form that will propagate ahead of the piston. In this section, we discuss the situation of a weakly radiating plasma, where the plasma behind the shock remains hot, with the pressure at the surface of the magnetic piston equal to the magnetic pressure (Fig. 16). There exists a broad class of exact (self-similar) solutions describing plasma flow between the shock and the piston in the planar case, i.e., at the early stage of the implosion (see, e.g., Gol'berg and Velikovich, 1993). Stability of this solution with respect to Rayleigh-Taylor modes was discussed in Gol'berg and Velikovich (1993) (who, in particular, formulated boundary conditions at the surface of the shock wave) and later by DeGroot et al (1997b). We present here only (our own) qualitative discussion of the problem.

Denote by h the thickness of the layer between the shock and the piston. The modes with $k>>1/h$ localized near the piston do not differ significantly from the modes considered in Sec. IV B. Among those, only perturbations close to flute modes are unstable. However, for these unstable modes the growth-rate is large,~$(kg)^{1/2}$. These perturbations will cause a gradual broadening of the transition between the plasma and the magnetic field.

Consider now long-wavelength modes ($k<<1/h$). For these modes, the transition layer is "thin" and, according to the results of Sec. IV A-C , can be considered essentially

as a structureless surface. A growth rate could be estimated again as $\sim(kg)^{1/2}$. In the $k<<1/h$ case, unlike in the opposite case, the modes with an arbitrary orientation of the wave vector are unstable. The mass of the layer gradually increases because of the adding of material swept up by the shock wave. At small k's (small growth rates) the change of mass within one e-folding time may become considerable, and the concept of the instantaneous growth rate may break down (Gol'berg and Velikovich, 1993).

The thickness of the layer h is relatively small even for a non-radiating plasma: since the shock is strong, the density behind the shock is determined by Eq. (2.20); for a fully ionized gas with γ=5/3 the density is 4 times higher than the density before the shock and the thickness of the shocked material is, roughly speaking, 4 times less than the distance travelled by the shock. If one deals with a weakly ionized gas where a considerable fraction of energy is spent on the ionization of the shocked gas, "the effective γ " becomes smaller than 5/3 and the layer of the shocked material becomes even thinner.

At a convergence of~3-4 (for a gas with γ=5/3), the shock reaches the axis and upon rebounding returns to the piston, leaving behind a hot plasma with the pressure approximately equal to the magnetic pressure. The further compression of the hot material occurs in a quasistatic manner, almost adiabatically, with the plasma pressure equal to the magnetic pressure (Potter, 1978). This adiabatic compression (in the absence of radiative losses) may occur only if the current continues to grow. The plasma boundary at this phase decelerates, and stops at the current maximum. The pinch at this point is very similar to the equilibrium Bennett pinch. Of course, the Rayleigh-Taylor instability ceases to exist. Among the hydrodynamic instabilities, only the ones driven by the curvature of the magnetic field lines remain. Their e-folding time is of the order of r/s where s is the sound speed. Stability analysis of these modes goes beyond the scope of our survey. A discussion of this problem in a purely MHD approximation can be found in Kadomtsev (1966) and Bateman (1980); among possible equilibria there are diffuse equilibria stable with respect to the m=0 mode (so called "Kadomtsev equilibria"). Asymptotically, at large

radii, the pressure in these equilibria decreases as $r^{-10/3}$. Nonlinear evolution of the sausage instability for an incompressible fluid was studied by Book, Ott, and Lampe. (1976). It should be remembered that the plasma column after stagnation can be so hot that the MHD approximation breaks down, and non-MHD effects, in particular, the ones caused by the large ion orbits, become important. A general characterization of the parameter space for the stability problem of a Bennett-type pinch, with the identification of the sub-domains where various anomalies may surface, has been performed by Haines and Coppins (1991).

F. Effects of a cylindrical convergence

As we have seen, the most dangerous modes are flute modes with wave-numbers k of the order of the inverse shell thickness $1/h$. Until the very late stage of the implosion, when the liner is about to collapse on axis, the wavelengths of these modes are small compared to the liner radius ($kr>>1$). Therefore, their instantaneous growth rate should be adequately described by the planar model discussed in the previous three sections. Still, effects of the cylindrical convergence may become important earlier in the implosion; two reasons are discussed below.

The first is the effect of convergence on the mass σ per unit area: one obviously has $\sigma=\sigma_0(r_0/r)$. This may affect the sheath thickness, making it different from what it was in the case of the planar system with the same time-history of acceleration. Accordingly, the maximum growth rate changes compared to a planar case. In addition, there is a direct enhancement of the amplitude of even stable perturbations by the effect of a cylindrical convergence (like the growth of an amplitude of a cylindrically converging light wave).

The second effect is the increase of the azimuthal component of the wave vector, $k_\theta=m/r$: as the mode number m does not change with time, k_θ scales as $1/r$ (recall that, in our notations, $k_y\equiv k_\theta$). This causes a gradual decrease of the angle α between the wave vector and the direction of the magnetic field and may eventually lead to the stabilization of the mode by making the product

$$k\cos^2\alpha \equiv \frac{k_y^2}{\sqrt{k_z^2+k_y^2}} \tag{4.33}$$

less than $1/2h$, thereby causing stabilization of the mode (see Eq. (4.18)). Remember that, in a purely cylindrical system, k_z does not change with time.

The growth of perturbations at the linear stage of instability is determined by the exponentiation factor (see, e.g., Lindl, 1995),

$$\xi(t) = \xi_0 \exp G(t) \tag{4.34}$$

where

$$G(t) \equiv \int_0^t \Gamma(t')dt', \tag{4.35}$$

and Γ is an instantaneous growth rate (4.2).

A linear approach breaks down as soon as the amplitude reaches certain level $\xi=\xi_{NL}$. A rough estimate for ξ_{NL} is $\xi_{NL}\sim 1/h$ for the fastest growing perturbations (with $k\sim 1/h$) and $\xi_{NL}\sim 1/k$ for long-wavelength perturbations (with $k<<1/h$). The transition to the non-linear stage occurs at the time instant determined from equation:

$$G(t)=\ln(\xi_{NL}/\xi_0) \tag{4.36}$$

Since the initial perturbations are small, say, a couple of orders of magnitude less than ξ_{NL}, the logarithm is equal to 4-5, and weakly depends on both ξ_0 and ξ_{NL}.

For long-wavelength perturbations, the growth rate does not depend on the structure of the shell, and the function G has a universal dependence on time determined by the solution of Eq. (2.1). In this solution, the radius is a unique function of time and, therefore, G can also be expressed in terms of the instantaneous value of the radius. For the current given by Eq. (2.5), and parameter Π (Eq. 2.4) corresponding to stagnation at the point of the maximum current (i.e., $\Pi\approx 4$), the plot of $G/(kr_o)^{1/2}$ vs the convergence is presented in Fig. 17.

However, for the most dangerous perturbations with $k\sim 1/h$, the function G depends also on the thickness h of the shell which, in general, varies with time. A factor that acts

towards reducing h is the growing acceleration (the scale-height is inversely proportional to g, see Eq. (2.27), while factors acting in the opposite direction are the radial convergence (that increases a mass per unit area), possible onset of the anomalous resistivity, and the increase of the temperature. So, the issue of the transition to the non-linear regime for the fastest growing modes is more complicated. If one assumes that the thickness h remains constant during the implosion, one can use the plot of Fig. 17 to roughly find the transition point by assuming that $k \sim 1/h$ and imposing the condition that G is approximately equal to, say, 4. For a shell thickness equal to 0.1 of the initial liner radius (and, accordingly, $(kr_0)^{1/2}=3$), the non-linear effects become important (i.e., G becomes equal to approximately 5) at convergence equal to 4.

According to our previous discussion we considered here only the modes with small azimuthal numbers m; the modes with large m are stabilized at a moderate convergence because of the aforementioned effect of growing k_y ($k_y \sim 1/r$).

G. Nonlinear effects; turbulence and turbulent broadening of the shell

We start this discussion from the local modes with $k>1/h$. When the displacement ξ_x becomes greater than $1/k$, it changes the density gradient, which drives the instability and determines the growth rate, by the order of unity (Fig. 18). This signifies that the further development of the perturbations depends on their amplitude. In the case of short-wavelength perturbations, where the growth rate does not substantially depend on k, one can expect development of random motions with a broad spectrum of length-scales and the amplitude of a particular scale of the order of $1/k$. The characteristic time of turn-around of the vortices should be of the order of the inverse growth rate $1/\Gamma \sim (h/g)^{1/2}$. These random motions cause a kind of diffusion evolution of the density profile with the diffusion coefficient $\Gamma/k^2 \propto 1/k^2$. One sees that the greatest contribution comes from the largest length-scale compatible with the local approximation ($1/k \sim h$). But, this means that the diffusive approximation does not correctly describe the situation, that is, the characteristic

step-size is of the order of the gradient length-scale. This is a fundamental difficulty of a non-linear theory of the R-T- instability. A diffusive description may become relevant if the mode with the largest scale is, for one or another reason, suppressed. We will not discuss here this rather artificial possibility.

Dimensional arguments similar to the ones used in the theory of mixing at the interface of two semi-infinite fluids (Youngs, 1991) show that the broadening should occur according to the law:

$$h=\varepsilon g t^2 \tag{4.37}$$

where ε is some numerical factor. In Youngs' case ε is approximately equal to 0.07.

Let us now turn our attention to large-scale perturbations, with k much less than the inverse shell thickness. We consider only the most dangerous flute-like (axisymmetric) perturbations. This type of motion can be properly described by Ott's equations [Eq. (4.29)]. One can expect that, as there are no other scales in this problem, the non-linearity turns on when the amplitude of the perturbations becomes of the order of $1/k$. This hypothesis can be easily checked on the basis of the exact solution obtained by Ott (1972). For a single-mode initial perturbation the time evolution of the shell is illustrated by Fig. 19 (Basko, 1994). Strong deformations from a sinusoid appear indeed at $\xi_x \sim 1/k$.

For a long wavelength perturbation, entering the non-linear phase does not mean stabilization or slowing down. Quite the contrary, effects of the mass redistribution (Fig. 16) cause an acceleration of the mode development. This, in particular, manifests itself in formation of singular spikes within a finite time (Fig. 19). The time of the spike formation is equal to $2(kg)^{-1/2}\ln(2/k\xi_{x0})$. Although the Lagrangian description breaks down after the formation of singularities, there are no reasons why the lighter parts of the shell should not continue their accelerated motion to the axis. So, there are no signs of a self-stabilization here. The picture gets more complex if one takes into account development of the multiple modes growing from initially random perturbations. The shorter wavelengths grow faster and reach their strongly non-linear stage earlier than the longer ones. The mode that has the

strongest effect on the distortion of the shell is the mode with the scale-length comparable to the shell thickness. There exist a possibility that, because of the presence of some numerical factors, in the scaling problem, this mode will reach an amplitude several times greater than the instantaneous shell thickness.

We conclude this discussion on the note that, for shells that are not very thin (thickness of order of 0.1 of the initial radius), reaching a convergence ~10-20 seems feasible (Fig. 20). The thinner the shell, the faster do instabilities reach their non-linear phase. Whether the instability at this non-linear stage will cause a gradual broadening of the sheath and its mix with the magnetic field or cause more coherent structures of the type shown in Fig. 21 to develop (causing disruptions of the current and violent destruction of well-defined shell) is an open question. The numerical simulations and theoretical analyses (e.g., Peterson et al, 1996, 1997; Thornhill et al., 1997) seem to point in the direction of more violent scenarios (Fig. 22).

H. More on the relationship between flute and non-flute modes

We will present the corresponding analysis for the case where the thickness of the current-carrying transition region is comparable with the overall thickness of the shell, $h_l \sim h$. As we know, one should distinguish between the flute modes, for which the wave-number is perpendicular to the magnetic field (an axisymmetric mode in the cylindrical geometry), and non-flute modes. As a representative example of the latter, we consider the mode propagating at an angle of 45^0 with respect to the magnetic field. The qualitative plot of the growth rates vs the horizontal wave number k for these two modes is shown in Fig. 23. The curve for the flute mode lies above the curve for the non-flute mode. At small k's, one can make an exact prediction of the growth rate (Eq. (4.19)), which in this limit is independent of the specifics of the density and magnetic field distribution inside the shell. The reason for this has been discussed in Sections IV A, B.

At larger k's, the non-flute mode becomes stable. A specific value of the critical wave number k_0 is determined by the details of the density and magnetic field distribution within the shell thickness. Within an order of magnitude, $k_0 \sim 1/h$. For the flute mode the growth rate at large k's reaches a saturation determined, within an order of magnitude, by Eq. (4.22). In fact, the growth rate of the local modes ($k>>1/h$) is determined by the layer where the mode is localized. Note that the maximum growth rate of the local modes is a well defined quantity: it corresponds to the maximum value of the r.h.s. of Eq. (4.22) over the thickness of the sheath (roughly speaking, it corresponds to the maximum value of ρ'/ρ, assuming that this maximum does exist).

Figure 23 underlines the exceptional character played by the flute (axisymmetric) mode in the dynamics of imploding liners. The prevalence of the flute mode becomes even more visible at the nonlinear stage of the instability. When the shell becomes strongly distorted with respect to its unperturbed state (Fig. 21 a), the magnetic field at the tips of the fingers remains the same (or even increases, if one takes into account effects of the cylindrical geometry) as in the unperturbed state, while the mass density in the fingers decreases. This causes a catastrophic self-acceleration of the break-up process and may cause a total disruption of the pinch.

This scenario of developing axisymmetric modes at their non-linear stage, that can be traced back to Hussey, Roderick, & Kloc (1980), Baker & Freeman (1981), Kloc, Roderick, & Hussey (1982), and Roderick & Hussey (1986), has found confirmation in the modern simulations of the randomly distributed axisymmetric perturbations (Peterson et al, 1996, 1997, 1999; Matuska et al, 1996, Benattar et al., 1999). Fig. 22 depicts the isodensity contours with a clearly visible finger-like structure. The break-up of the shell was found also in the case where the initial perturbation was a single mode or a mixture of up to three single modes (Douglas, Deeney, & Roderick, 1998).

Nothing like this can happen for non-flute modes, at least for a thin-shell liner, $h<<r$. The reason is a very different reaction of the magnetic field to strongly non-linear,

non-axisymmetric perturbations of the type shown in Fig. 21 b: the magnetic field does not penetrate to the "fingertips" in this case and is, on the contrary, increasing at the lagging parts of the liner surface. Therefore, one can expect an early non-linear saturation of the non-axisymmetric modes and their much weaker effect on the liner implosion. As we shall see (Sec. VI E), one may even try to deliberately introduce non-axisymmetric perturbations to destroy too fast a growth of axisymmetric fingers.

The dominance of axisymmetric modes seems to be in agreement with experimental data. Fig. 20 shows an X-ray pinhole image of the pinch near the point of a maximum compression in the Z accelerator. The features perpendicular to the pinch axis are most pronounced - as one should expect in the case of axisymmetric perturbations. Note that in cylindrical implosions driven by an ablative force (Hsing et al, 1997) the high-m modes could be a dominant player in the dynamics of the implosion, reaching a non-linear stage and affecting the maximum convergence. This underlines once again the exceptional role of the magnetic drive in selecting the m=0 mode as the most dangerous one.

On the other hand, experiments on both gas-puff implosions (e.g., Shiloh, Fisher, & Bar-Avraham 1978, Burkhalter et al, 1979, Wong et al, 1998) and wire array implosions (e.g., Spielman et al, 1998, Deeney, et al., 1998a) show that the "final" imploded state always manifests significant deviations from a perfect axial symmetry. They can be attributed to low-m (m=1, 2) modes with k_z of the same order as for m=0 perturbations. According to the discussion at the end of Sec. IV H, development of low-m modes is not prohibited. The aforementioned experimental results show that they may reach a level comparable to m=0 mode. A quantitative analysis of a degree of non-axisymmetry late in the implosion may help in the understanding and control of the physics of the hydrodynamic stability.

V. EFFECTS OF DISSIPATIVE PROCESSES

A. Viscosity

Effects of plasma viscosity are among the ones whose influence on the Rayleigh-Taylor instability have been studied in the most detail, starting from Chandrasekhar's monograph (1961), where the stability of a boundary between the two semi-infinite viscous fluids was studied. A careful analysis of viscous effects in the case of a slab has been performed by Mikaelian (1996); see also references therein.

Viscous terms in the hydrodynamic equations are most important for small-scale motions. Therefore, it is reasonable to consider their effect on perturbations with a length-scale small compared to the characteristic scale of the density gradient, h (Fig. 11 a). If an element of the fluid is displaced by a small distance ξ in the vertical direction, it experiences the action of the buoyancy force produced by the difference of the densities inside this element and the surrounding substance, $\delta\rho \equiv \rho_i - \rho_e = -(\partial\rho/\partial x)\xi$. The force is equal to $\delta F = -\mathrm{V} g \delta\rho$, where V is the volume of the liquid element ($\sim 1/k^3$). The viscous force acting on an element of size $\sim 1/k$ moving in the resting fluid is (Landau and Lifshitz, 1987) $\delta F_{\mathrm{visc}} \approx -\rho\nu k^2 \dot{\xi}\mathrm{V}$ where ν is the kinematic viscosity. In this way one arrives at the following equation of motion:

$$\ddot{\xi} = \frac{g}{\rho}\frac{\partial\rho}{\partial x} - \nu k^2 \dot{\xi}. \tag{5.1}$$

From (5.1), one gets the following expression for the growth rate:

$$\Gamma = \sqrt{\frac{g}{h}}\left(\sqrt{1+\varepsilon_{visc}\frac{(kh)^4}{4}} - \sqrt{\varepsilon_{visc}}\frac{(kh)^2}{2}\right), \tag{5.2}$$

with $h^{-1} \equiv (1/\rho)\partial\rho/\partial x$, and

$$\varepsilon_{visc} \equiv \frac{\nu^2}{gh^3}. \tag{5.3}$$

The dimensionless parameter ε_{visc} characterizes the role of viscosity. For implosion of wire arrays, the parameter ε_{visc} is typically very small. Kinematic viscosity is related to

the mean free path ℓ_{ii} of the plasma ions by the relationship $\nu \sim \ell_{ii}\, v_{Ti}$. Then, using estimate (2.27), relating the thickness of the shell and the gravity acceleration, one finds that

$$\varepsilon_{visc} \sim \frac{A}{Z_{eff}+1}\left(\frac{\ell_{ii}}{h}\right)^2. \qquad (5.4)$$

We have taken into account a relationship: $\overline{m}/m_i = A/(Z_{eff}+1)$. In the implosions of metal liners, the ion-ion mean-free-path is orders of magnitude smaller than the liner thickness. Therefore, in this situation ε_{visc} is universally small. Only modes with very short wavelengths are affected by the viscosity in this case, $kh > \varepsilon_{visc}^{-1/4}$. Note that for these small-scale perturbations viscosity still does not provide a complete stabilization, it just reduces the growth-rate, which now becomes $\Gamma \approx \varepsilon_{visc}^{-1/2}(kh)^{-2}\sqrt{g/h}$.

In gas-puff systems, with lower densities and higher temperatures in the imploding plasma, one may reach conditions under which ε_{visc} becomes ~1. A transition to the case ε_{visc} ~1 may, in particular, occur in the implosion of two coaxial gaseous shells, where the outer shell hits the inner shell, causing a sudden increase of the temperature and, accordingly, of the viscosity (recall that the Coulomb collision cross section decreases with the temperature). At even higher temperatures one may find that the ion gyro-radius becomes less than the ion mean free path (see also Sec. VI I). This causes a reduction of the shear viscosity (Braginski, 1965) but the bulk viscosity remains high. The bulk viscosity appears in a way similar to the thermal conductivity which we will describe shortly.

B. Thermal conductivity and internal relaxation

Now we switch to a discussion of the effects of a thermal conductivity. The characteristic time for smoothing of temperature perturbations of a scale $1/k$ is $\tau \sim 1/k^2\chi$, where χ is thermal diffusivity. Usually, in the unmagnetized plasma, the thermal diffusivity is large compared to the kinematic viscosity (see Braginski, 1965; Huba, 1994).

may enter the problem of the Rayleigh-Taylor instability only via the finite compressibility of the matter. Therefore, we will base our discussion on Eq. (4.20) that takes compressibility effects into account. The thermal conductivity affects the dissipation of the mechanical motion by creating a phase shift between the perturbation of the density of a certain liquid element and the pressure perturbation introduced by this change of the density. Then, an irreversible part appears in the pdV work.

If thermal conductivity is very large, it maintains uniform temperature in the perturbations (isothermal perturbations). In particular, the sound speed that enters expression (4.20) for the growth rate becomes an isothermal sound speed. However, Eq. (4.20) still has unstable roots with the growth rates not much different from the adiabatic case. For short-wavelength perturbations, $k>1/h$, described by Eq.(4.22), the thermal diffusivity has a stabilizing effect (Catto, 1978). The characteristic time for the heat to diffuse over the scale-length $1/k$ of the perturbation is $\tau \sim 1/k^2\chi$. The growth rate significantly decreases if this time is less than a characteristic growth rate for adiabatic perturbations, $(g/h)^{1/2}$. There may exist other relaxation processes in the system, for example, establishing the ionization equilibrium (e.g., DeGroot et al, 1997a). They also affect the growth rate of perturbations by causing phase shift between δp and $\delta\rho$.

C. Resistivity

As has been pointed out by Hussey et al. (1995), Hammer et al. (1996), and Benattar et al. (1999), effects of magnetic field penetration through the imploding shell may influence the R-T instability of flute (axisymmetric) modes. An expectation is that it will add some dissipation and thereby decrease the growth rate. However, as was shown by Hammer et al (1996), there may exist modes that do not perturb the currents and therefore do not induce any additional dissipation. For a profile of the type of (2.28), such mode is localized near the surface $x=0$ and has the growth rate unaffected by the resistivity. The presence of this mode is related to the singularity of ρ'/ρ as x goes to zero.

As soon as the density profile near x=0 gets smoothed by the development of the instability, the short-wavelength perturbations become affected by the finite resistivity. The expression for the growth rate of these mode reads as (Hammer et al, 1996):

$$\Gamma = \sqrt{g\frac{\rho'}{\rho} + \left(\frac{D_M k^2}{2}\frac{s^2}{a^2}\right)^2} - \frac{D_M k^2}{2}\frac{s^2}{a^2}, \qquad (5.5)$$

where D_M is a magnetic diffusivity, $D_M=\eta/\mu$, s and a are the sound velocity and Alfven velocity, respectively. Note that in a strongly radiating plasma, where the magnetic pressure is much greater than the plasma pressure (see discussion related to Eq. (2.28), (2.29) in Sec. II G) and where, accordingly, $s<<a$, the stabilizing effect of resistive losses contains a small parameter s^2/a^2 and is relatively insignificant.

So far, we have been discussing the instability of the purely flute mode, i.e., the only mode that remains unstable at large wave-numbers in the case of a perfectly conducting plasma (see Sections IV A-C). The short-wavelength modes that have a cross-field (azimuthal) component of the wave vector are stabilized in such a plasma by virtue of the restoring force produced by a curved magnetic field which is frozen into the plasma and follows its displacements. It is clear that the high plasma resistivity decouples the plasma displacement and the magnetic field. A complete analysis of this problem goes beyond the scope of our survey. Here we restrict ourselves to the notion that in the case of plasma pressure comparable to the magnetic pressure and the skin-depth comparable to the whole thickness of the layer (Alfven velocity comparable to the sound velocity), the resistive uncoupling becomes significant at $D_M>sh$ where s is the sound velocity. In other words, the finite resistivity may lead not only to stabilizing but also to destabilizing effects.

VI. POSSIBLE WAYS OF MITIGATING THE RAYLEIGH-TAYLOR INSTABILITY

A. General comments

In the previous two sections we discussed in some depth the physics of the Rayleigh-Taylor instability. One important (and already mentioned) difference between the stability of an imploding liner and the stability of a steady-state object (like a plasma in devices with magnetic confinement) is that implosion takes a finite time, while a steady-state plasma configuration is supposed to last essentially forever. Therefore, if some instability is present in the steady-state system, the perturbations certainly reach a nonlinear stage, which is independent of the initial perturbations. A saturated turbulence then exists as long as the plasma formation (sustained by the external particle and energy sources). In imploding systems, on the other hand, the exponentiation factor G introduced by Eq. (4.38) is finite and sometimes not very large (in the range of 5). Under such circumstances, one can hope to reduce the deleterious role of instability by making more perfect initial states, with the relative root-mean-square perturbations less than 10^{-2}. Conversely, if the growth rate can be reduced by, say, 20% ($\Delta G/G \sim 0.2$) the requirements for the symmetry of the initial state could be reduced by a factor of 2.

Therefore, one possible line of defense is to create more perfect initial states (smaller initial perturbations) and look for the means to reduce the linear growth rate. If this approach fails and the instability reaches a nonlinear stage, one can try to prevent the most disastrous scenarios associated with a self-accelerating growth of the "bubbles" and gross violations of the cylindrical symmetry of the liner (Fig.21 a). In the further discussion, we mention various effects that may influence the linear and nonlinear stages of the problem. We emphasize that the original stability analyses that we are referring to were often not directly related to fast pinches.

Mitigation methods discussed below do not provide an ultimate solution in making the instability effect insignificant. Moreover, many of them introduce complications into the experimental setting. Still, we present a more-or-less complete set of existing suggestions with the hope that they may help in finding an efficient solution. One more general conclusion that can be drawn with respect to the mitigation problem is that very little can be done to affect the linear stability of long-wavelength perturbations of an "empty" thin shell ($\lambda >> h$, where h is the shell thickness): the linear behavior of these perturbations is described by Eq. (4.19) which does not contain any free external parameters.

B. Magnetic shear

As was mentioned in Secs. IV A and B, the most dangerous modes are axisymmetric modes that do not create any ripple in the magnetic field lines, maintaining their circular (straight in the planar geometry) shape. These modes remain unstable at high wave numbers $k \sim 1/h$ and have a large growth rate $\sim (g/h)^{1/2}$. Conversely, the modes with a finite azimuthal component of the wave number become stable if the wave number is high enough. It is well known from the theory of magnetically confined plasmas (see the original paper by Suydam, 1958, and general surveys by Bateman, 1980, and Freidberg, 1982) that one may reach reduction of the growth rate or even stabilization of flute modes by creating a magnetic shear, i.e., by creating a situation where the magnetic field vector, remaining normal to the gravity force, would change direction over the depth of the transition layer. In the Z-pinch geometry this would require introducing the axial magnetic field B_z, possibly, varying over the thickness of the shell.

From the outset, for the reasons discussed in the last two paragraphs of Sec. VI.B, one can conclude that the magnetic shear will have no effect on the stability of long-wavelength modes, $\lambda >> h$. One can, however, hope that the growth rate of the modes with $\lambda \sim h$ (and these are the most dangerous modes) will be reduced. Indeed, applying a general approach based on the energy principle (Suydam, 1958), Gratton, Gratton, and Gonzalez

(1988) have shown that, for the local modes ($\lambda << h$), the presence of the shear leads to the appearance of a stabilizing contribution to the expression (4.22) for the growth rate:

$$\Gamma^2 = \frac{g^2}{a^2 + s^2} + \frac{g\rho'}{\rho} - \frac{a^2\varsigma^2}{4}. \qquad (6.1)$$

The parameter ζ is the z derivative of the angle formed by the magnetic field with the direction of the wave vector at the point where the magnetic field is normal to the wave vector. If the z component of the magnetic field is zero, then shear is also zero. If the z component of the magnetic field is comparable to the azimuthal component, then $\zeta \sim 1/h$. In this case the magnetic shear can considerably reduce the growth rate of the local modes and can even completely stabilize them. In other words, the magnetic shear stabilization has some promise for local modes.

As we have already mentioned, the shear does not stabilize the large-scale modes with $\lambda >> h$. Still, the presence of the axial magnetic field enclosed by the liner may have some effect on the stability. Using the approach similar to that developed by Harris (1962), one can show that, if the magnetic field on the outer side of the shell has components B_{ye} and B_{ze} and on the inner side of the shell B_{zi} (there is no y component of the magnetic field inside the shell if there is no axial current inside the shell), the dispersion relation for the $\lambda >> h$ modes (an analog of Eq. (4.19)) becomes (Cf. Bud'ko et al., 1990):

$$\omega^4 - 2kg\omega^2 \frac{B_{ye}^2 \cos^2\alpha + \left(B_{ze}^2 + B_{zi}^2\right)\sin^2\alpha}{B_{ye}^2 + B_{ze}^2 - B_{zi}^2} - k^2 g^2 = 0, \qquad (6.2)$$

where α is defined according to Eq. (4.16), and the acceleration is $g = (B_{ye}^2 + B_{ze}^2 - B_{ze}^2)/\mu\sigma$. Dispersion relation (6.2) universally has an unstable root that scales as $\sqrt{kg}$ (we assume that the acceleration is directed inward, i.e. $B_{ye}^2 + B_{ze}^2 - B_{zi}^2 > 0$). On the other hand, if $B_{zi} > B_{ze}$, the growth rate for the α=0 mode is reduced compared to (4.19).

One should remember that it is undesirable to have an axial magnetic field enclosed by the shell, because then part of the energy of the imploding liner would be spent on the compression of this magnetic field. The other difficulty with imposing the axial magnetic field is that, in the time-frame of the implosion, the axial magnetic field remains frozen into the conducting electrodes. Therefore, strong distortions of the cylindrical symmetry of the type shown in Fig. 7 are inevitable. One could reduce this effect by introducing radial cuts, but, as the skin-depth is very small, the axial magnetic field would remain frozen into the segments of the electrode between two neighboring cuts.

C. Rotation

The possibility of using rotation of the shell for stabilization purposes (see Book, Winsor, 1974; Barcilon, Book, Cooper, 1974; Turchi et al., 1976). The stabilizing effect comes from the centrifugal force that is directed oppositely to the effective gravity force near the stagnation point. In the early works, it was supposed that rotation will be set in by mechanical means. The concept of centrifugal stabilization has been recently reconsidered by Rostoker, Peterson, and Tashiri (1995), who suggested using a cusp magnetic field to create an azimuthal torque that would appear because of the interaction of the z component of the current and the r component of the magnetic field. Hammer and Ryutov (1996) suggested using an ablative torque by producing a left-right asymmetric structure at the surface of the shell. Ryutov (1996), One can also use left-right asymmetric coatings on the surfaces of wires (Fig. 24): an ablation of the coating early in the pulse would produce a torque acting on the wires and imparting an angular momentum to them.

To have an appreciable effect on the instability, the rotation should change the radial acceleration by an order of 1. This, in turn, means that, near the point of maximum compression, the rotation energy should be comparable to the total implosion energy (see Sec. II.D). This is the energy penalty associated with this method of stabilization.

Stability analysis of the imploding rotating liner compressing the axial magnetic field was carried out by Barcillon, Book, and Cooper (1974). The critical point in this system is the turning point of the radial motion of the rotating liner. They concluded that it is difficult to reach a strong stabilizing effect, especially in the case of a thin liner. Velikovich and Davis (1995) studied stability of a steady-state configuration, r=const, where the centrifugal force is exactly balanced by the magnetic pressure (in the Z-pinch geometry). The stabilizing effect in this case was relatively modest. Although these results are somewhat discouraging, it is probably worth considering the stability of the Z pinch under realistic assumptions with regard to the time-history of the pinch radius $r(t)$. Although it is not very probable that rotation will entirely stabilize the system, it may reduce the growth rates to an admissible level.

D. Velocity shear

In principle, one can introduce an azimuthal shear flow instead of a solid-body rotation. The possible stabilizing effect of shear flow on the Rayleigh-Taylor instability was mentioned as early as 1961 by Chandrasekhar; in conjunction with fast Z pinches it was discussed by Hammer and Ryutov (1996) and Shumlak & Roderick (1998). To qualitatively understand the role of the shear, consider a slab geometry, with the slab of an incompressible fluid supported from below by a massless fluid. Let the unperturbed flow velocity be directed along the y axis and be linearly dependent on x: $v_y=u(x/h)$. The shear flow will have the strongest effect on perturbations with their wave vector directed along the direction of flow. For such perturbations, the shear flow will lead to their stretching in the y direction and thereby to strongly changing their eigenfunction. One can hope that stretching of the "fingers" typical for the Rayleigh-Taylor instability will reduce their growth. The time of the stretching of the perturbation is of the order of h/u, independent of the scale of the perturbation, while the growth rate of the gravity-driven perturbations is of the order $(kg)^{1/2}$. Obviously, the shear flow can have a significant effect on development of

the perturbations if condition $(h/u)(kg)^{1/2}<1$ holds. For the most dangerous perturbations with $k\sim 1/h$, one can rewrite this condition in terms of a so-called Froude number,

$$Fr \equiv \frac{u^2}{gh} > 1 \qquad (6.3)$$

Taking as an example h=0.1 cm, and $g=3\cdot 10^{15}$ cm/s^2, one finds that the velocity of the shear flow should be rather high, greater than 10^7 cm/s. It is difficult to produce such a velocity directly. One can, however, expect an enhancement of the azimuthal velocity during the implosion because of the conservation of the angular momentum of every cylindrical shell. (For the "canonical" wire array implosions, the viscous damping of the shear flow is insignificant). If the initial velocity of shear flow is 10^6 cm/s, the desired value will be reached at a convergence equal to 10. One can also speculate that the actual time required for the perturbations to grow from the initial small level to a nonlinear phase constitutes at least several e-folding times $(kg)^{-1/2}$. Accordingly, one could hope that, in the r.h.s. of inequality (6.3), one should write, instead of 1, some small number. Numerical analysis by Shumlak and Roderick (1998) seems to point in this direction.

Unfortunately, the shear flow does not have any effect on perturbations with the wave vector perpendicular to the direction of the flow. In other words, if the shear flow is in the azimuthal direction (the differential rotation), it does not affect azimuthally-symmetric perturbations (m=0). To stabilize these perurbations, one has to generate an axial shear flow, with v_z varying with x. This type of shear motion cannot be enhanced by the angular momentum conservation; therefore, requirements stemming from inequality (6.3), become more stringent.

To generate the shear flow, one can use a target consisting of two nested liners (Hammer, Ryutov, 1996). If the left-right asymmetric features are embedded into one of these liners, then the ablation will cause its rotation; when the two liners collide, a differential rotation emerges. If up-down asymmetric features are created, then the axial

shear flow is formed. Shumlak and Roderick (1998) discussed the use of a conical gas-puff to generate the axial shear.

The axial shear flow may have a stabilizing influence on quasi-equilibrium Z pinches that can be formed near the stagnation point. This stabilization mechanism for equilibrium Z pinches was discussed by Shumlak and Hartman (1995). Their conclusion was that, if the initial profile is not very far from the marginally stable "Kadomtsev profile," then even a weak velocity shear can produce considerable stabilization. On the other hand, Arber et al. (1995) have not found significant stabilization by the shear.

E. Hourglass effect

Douglas, Deeney, and Roderick (1997) have discovered in numerical simulations that, by making the initial surface of a uniform-fill Z pinch concave (Fig. 25), one can suppress the growth of Rayleigh-Taylor perturbations. Because of the characteristic shape of the sheath, one can call this effect an "hourglass effect." Douglas, Deeney, and Roderick considered implosions of high-Z (strongly radiating) gas-puffs (Ne, Xe), where the transition layer between the magnetic piston and the shock front is thin (Cf. Sec.II B). For a sufficiently large initial curvature, the stabilizing effect is quite strong. The authors attribute this effect to either the advection of perturbations to the electrodes (there is tangential flow along the curved surface, in the direction of electrodes) or the presence of the axial shear flow. In principle, one could discriminate between these two possibilities by changing the sign of the curvature (making the surface convex instead of concave): the flow would have changed its sign, and would advect perturbations to the equatorial plane, while the effect of shear should have remained the same as for the concave surface.

F. Deliberate violation of the azimuthal symmetry

As already mentioned in Sec. IV, the most dangerous small-m modes show a trend to strongly nonlinear development, with the finger-like structures penetrating deep to the

axis of the device (Fig. 22). Self-acceleration of the "fingertips" occurs because the mass density at the "fingertips" decreases, while the driving azimuthal magnetic field freely penetrates into this area through disk-like slots—a characteristic feature of axisymmetric perturbations. Derzon, Nash, & Ryutov (1997) suggested reducing the growth rate of the axisymmetric perturbations by deliberate introduction of a periodic azimuthal asymmetry, as shown in Fig. 26, with a large-enough amplitude and a large-enough mode number m. The idea is to destroy the azimuthal coherence of the finger-like structure and to create conditions for short-circuiting (crow-barring) the disk-like slots in many (m) points over the azimuth.

For this closure of the slots to occur at a moderately nonlinear stage of the growth of axisymmetric perturbations, when the peak-to-valley distance becomes of the order of their axial period λ, one has to produce the azimuthal perturbations for which amplitude, ξ, satisfies, roughly speaking, a condition: $\xi > \lambda/2$. One can conceive of several ways of creating azimuthal perturbations in a controlled way. One way is by assembling the wire array with wires of azimuthally varying thickness (i.e., of varying mass), similar to what has been shown in Fig. 26b: the heavier wires will lag behind the lighter ones, thereby creating a corrugated structure. Another possibility is to use wires of different materials (and, accordingly, of different mass). Still one more possibility is to use a kind of "imprinting" produced by the discrete structure of the return current structure (which typically consists of ~10 separate posts; the gaps between the posts provide a necessary diagnostic access). At the early stage of the discharge, when the separation of the current sheath from the posts is comparable to the inter-post distance, the radial driving force is varying over the azimuth, giving rise to formation of the corrugated structure. Such a structure has been observed experimentally Derzon, Nash, and Ryutov (1997).

In wire array implosions, the axial period of the most dangerous modes is in the range of 1-1.5 mm. Therefore, according to condition $\xi > \lambda/2$a, relatively modest amplitude of corrugation (0.5-0.75 mm) could be sufficient to produce considerable

stabilizing effect. The mode number of the corrugation should be made large enough to provide many short-circuit channels over the radius. This is limited from above by the constraint that, at a given amplitude, the high-mode-number perturbation become nonlinearly stabilized by the effect of expulsion of the magnetic field from the tips of azimuthal perturbations (Fig. 21b).The upper limit on the mode number set by this constraint is: $m < r/2\xi \sim r/\lambda$. For the typical set of parameters of a wire array implosion, the optimum mode number is ~15.

G. Accretion

As mentioned in Secs. II and IV, in implosions of gas-puff loads one can, in principle, create an initial density distribution such that the sheath will converge on axis without any acceleration (Fig. 5). In the clearest form, this idea was expressed by Hammer (1995) and, later, by Hammer et al. (1996), and Velikovich, Cochran, and Davis (1996). The energy penalty is associated with the radiative losses of the accreted material. The stabilizing effects are caused merely by the absence of acceleration. The interface between the magnetic field and the plasma remains stable with respect to exponentially growing modes, even for very short wavelengths (shorter than the distance between the shock and the interface). Another source of stabilization is related to the presence of a detached shock, as discussed by Gol'berg and Velikovich (1993): because the shock front itself is stable with respect to the ripple perturbations, it extends its stabilizing influence over the whole area between the shock and magnetic piston.

One can think of a discrete version of the scheme proposed by Hammer et al. (1996) where, instead of a continuous density distribution, one would create a set of nested wire arrays, with the masses approximately following the desired density distribution. This would mean that the lightest arrays would be on the outside and that their mass would gradually grow towards the inside. Whether the improved stability will outweigh the added complexity is a question that can eventually be answered only experimentally.

It has recently been discovered experimentally (Deeney, et al., 1998b) that a considerable improvement of the quality of the implosion can be reached by using a two-shell wire array, with the inner shell situated at a half-radius of the outer shell and having a mass *smaller* (not greater as in the aforementioned scheme) than the outer shell. The best result has been reached with the inner mass as small as a quarter of the outer mass. It is not clear yet what specific mechanism is responsible for this improvement. One can speculate that a strong heating during collision of the two shells causes a rapid viscous and thermal damping of perturbations developed in the outer shell by the time of their collision.

H. Enhanced thermal dissipation

Suggestions have been made (Ryutov, 1996; Ryutov, Toor, 1998) to increase the rate of viscous and thermal dissipation by replacing a uniform medium with a finely structured medium, with a scale ℓ of pre-existing nonuniformities that is small compared to the scale λ of the most dangerous perturbations. In the case of wire arrays, this could be done by replacing uniform wires with bundles of interwoven finer wires, or by alternating the composition of the wires in the array. The hope is that the presence of the fine structures will introduce small-scale motions (and temperature variations) overlaid on the "averaged" motions (and temperature variations) on the larger scale of the most dangerous perturbations. Because the dissipation rate by both viscosity and thermal conductivity scales as $1/\ell^2$, one could expect that the growth rate of the instability will be substantially reduced. The effect of enhanced dissipation is certainly present, but in the examples studied so far it causes only a relatively small decrease of the linear growth rate (see also Sec. V B). A new element that emerges in the picture is the appearance of the modes of oscillatory damping (in addition to the "standard" Rayleigh-Taylor modes). One can expect that the presence of these modes may favorably affect the nonlinear stage of the instability. However, this issue hasn't been studied thus far.

I. Finite Larmor radius (FLR) effects

The ion gyroradius is small compared to the typical sheath thickness during the run-in phase. At this stage, the ion component can be well described by fluid equations. The situation changes dramatically after the stagnation, when the ion thermal energy increases by orders of magnitude. Arber et al. (1995) studied the stability of an equilibrium pinch with the ion Larmor radius comparable to the pinch radius. They conclude that even if the m=0 mode is almost stable by virtue of reaching the Kadomtsev profile, the m=1 mode still remains strongly unstable even with FLR effects taken into account. The growth rate is reduced by a factor of a few with respect to an ideal MHD, but this is insufficient to have a long-lasting steady-sate equilibrium. Scheffel et al. (1997) have shown that the effects of a finite electron temperature have a destabilizing effect on the finite Larmor radius plasma.

Isichenko, Kulyabin, and Yan'kov (1989) considered the pinch column with a skin-layer much thinner than the ion gyroradius (so that the ion motion in the pinch interior is unmagnetized). They have found that the growth of short-wavelength perturbations, with $\lambda << r$, reaches a saturation $\sim v_{Ti}/r$, i.e., becomes slower than in the MHD approximation (where it is $\sim (v_{Ti}/r)(r/\lambda)^{1/2}$). However, the most disruptive mode with $\lambda \sim r$ remains essentially as unstable as in the MHD approximation. Therefore, the effects of a large Larmor radius do not provide sufficient stabilization in the stagnation phase. Velikovich (1991) has come to a similar conclusion.

VII. NON-MHD PHENOMENA

A. Microturbulence and anomalous resistivity

A potential source of microinstabilities is the relative motion of electrons and ions. The velocity u of this motion is directly related to the current density, $j = enu$ where n is the electron density. In the case of implosions of thin shells (like the ones formed in wire

array implosions), assuming that the current occupies the whole shell thickness, one can express u in terms of the total pinch current I:

$$u(cm/s) \sim 10^4 \frac{AI(MA)}{Z_{eff}\hat{m}(mg/cm)}. \qquad (7.1)$$

The assumption that the current flows through the whole thickness of the shell is quite plausible for the run-in phase of strongly radiating liners (Sec. II G).

In Z pinches, the current is directed across the magnetic field; the electron temperature is comparable to or lower than the ion temperature. Under such circumstances, the most probable instability that can lead to the appearance of anomalous resistivity is the lower hybrid instability, described by Krall and Liewer (1971), and Davidson and Gladd (1975). The early studies of this instability have been summarized in the survey by Davidson and Krall (1977). More recent results, specifically addressing the issues of nonlinear stabilization, can be found in analytical studies by Drake, Huba, and Gladd (1983) and by Drake, Guzdar, and Huba (1983) and in numerical analysis by Brackbill et al. (1990). Possible effects of this instability on the Pease-Braginski current in a fiber pinch was studied by Robson (1991) and Chittenden (1995).

The "natural" frequency of the lower-hybrid oscillations is (see, for example, Davidson and Krall, 1977):

$$\omega_{LH} = \omega_{ce}\sqrt{\frac{Z_{eff}m_e}{Am_p}} \qquad (7.2)$$

where m_p is the proton mass. Expression (7.2) for the lower-hybrid frequency pertains to the situation $\omega_{pe} > \omega_{ce}$, which is typical for Z pinches (ω_{pe} and ω_{ce} are electron plasma and electron cyclotron frequencies, respectively).

In the analysis of the lower-hybrid instability, usually only perturbations with $k_{\|}=0$ are considered. In order for such perturbations to cause electron scattering and contribute to the anomalous resistivity, their transverse scale-length should be comparable to or shorter than the electron gyroradius ρ_e. Otherwise, because the perturbations are slow, $\omega_{LH} << \omega_{ce}$, the electron magnetic moment will be conserved, and the electrons will experience only

adiabatic (reversible) variations of their velocity thereby making impossible the appearance of anomalous resistivity.

The other current-driven microinstability is the ion acoustic instability, which typically has a higher threshold in terms of the relative velocity of electrons and ions. Exstensive studies of this instability are summarized in the surveys by Vedenov and Ryutov (1975) and Galeev and Sagdeev (1979). In a singly charged plasma this instability can be present only if the electron temperature is much higher than the ion temperature, $T_e >> T_i$: at $T_e \sim T_i$ the ion sound speed is comparable to the thermal velocity of the ions, and acoustic waves experience a strong ion Landau damping. However, in a plasma with $Z_{eff} >> 1$, this instability can be excited even at $T_i > T_e$. Indeed, the sound speed in a plasma with high-Z ions is equal to

$$\sqrt{\frac{Z_{eff} T_e + T_i}{m_i}}, \tag{7.3}$$

while the ion thermal speed is $\sqrt{2T_i / m_i}$. Imposing a constraint that the sound speed exceed the ion thermal speed by a factor of 2, one finds the condition of weakly damped ion acoustic waves in a high-Z plasma:

$$T_e > 7T_i / Z_{eff}. \tag{7.4}$$

One sees that, at $Z_{eff} >> 1$, the weakly damped ion acoustic modes can exist even at $T_i > T_e$. The critical current velocity for the onset of the ion acoustic instability under such conditions is several ion thermal velocities,

$$u_{crit} = \zeta v_{Ti}, \tag{7.5}$$

with ζ equal to 2-4. In the case of hydrogen-containing substances (for example, agar), the hydrogen ions, because of their high thermal velocities, can considerably increase the Landau damping and push the critical velocity to higher levels.

If the condition (7.4) is violated with a large-enough margin (so that the ion-acoustic instability does not exist), the relative electron-ion velocity u may reach an electron thermal velocity, and a modified two-stream (or Buneman) instability may develop. Its

growth rate is higher than that of the ion acoustic instability. However, reaching so high u's for the typical parameters of the dense pinches is not very probable (see Sec. IX).

The effect of microinstabilities on plasma resistivity is traditionally described in terms of the effective electron scattering frequency ν_{eff} that should be added to the electron-ion collision frequency $1/\tau_{ei}$ in the expression for the plasma resistivity,

$$\eta = \frac{m_e(\nu_{eff} + 1/\tau_{ei})}{ne^2}. \tag{7.6}$$

An estimate that is commonly used for the effective collision frequency produced by the lower- hybrid instability is (Davidson and Gladd, 1975; Drake et al., 1984):

$$\nu_{eff} = \varsigma_1 \omega_{LH} \left(\frac{u}{v_{Ti}}\right)^2, \tag{7.7}$$

where ζ_1 is a numerical factor of the order of 1.

At low plasma density and high pinch currents, when u reaches the threshold of the ion-acoustic instability, this latter instability becomes dominant because it usually results in a higher effective collision frequency approaching the ion plasma frequency. Under condition $\omega_{pe}>\omega_{ce}$, typical for Z-pinch environment, the ion plasma frequency is much higher than the lower hybrid frequency. Therefore, if the threshold for the excitation of the ion acoustic perturbations is reached at all, this instability takes over in establishing the anomalous resistivity. Upon reaching the instability threshold, $u=u_{crit}$, the effective scattering turns on so sharply that, in most cases of interest for Z pinches, it just keeps the relative velocity at the threshold level, so that the current density is

$$j = enu_{crit} \tag{7.8}$$

with u_{crit} as in (7.5); if the threshold for the Buneman inastability is reached, then one has $u_{crit} \sim v_{Te}$. Equations (7.6)-(7.8) can serve as a basis for the analysis of the effect of anomalous resistivity on the properties of Z pinches.

Microfluctuations produced by the plasma current, in addition to the anomalous resistivity, may cause acceleration of a part of the plasma ions to suprathermal energies (see Sec. VII.B). The anomalous resistivity, if present, affects the skin depth and, therefore, the

Rayleigh-Taylor instability. The heating rate of the electrons during the implosion phase may grow considerably and therefore lead to enhancement of the radiation losses compared to classical estimates. In the case of quasiequilibrium pinches, the anomalous resistivity affects the Pease-Braginski current (Robson, 1991). We will not try here to consider a completely self-consistent picture. Our discussion provides only a general framework for the analysis of the corresponding processes. As we shall see, in the fast Z-pinch environment the velocity$u$ is typically smaller than or comparable to the ion thermal velocity. Therefore, we concentrate our attention on the lower hybrid instability.

1. Run-in phase

To be specific, we begin this subsection with a discussion of wire array; later in this subsection we also mention gas-puffs. The velocity u of the relative motion of the electron and ion fluids is typically comparable to the ion thermal velocity. For a set of characteristic parameters of the run-in phase of tungsten wire array implosions (A~*180*, T~ 40 eV, Z_{eff}~7, I=*10* MA, $\hat{m}$~*3* mg/cm), one finds that u~10^6 cm/s, roughly equal to v_{Ti}. For the "canonical" lower- hybrid instability, according to the paper by Davidson and Gladd (1975), the growth rate at $u<v_{Ti}$ scales as

$$(u/v_{Ti})^2\omega_{LH}. \qquad (7.9)$$

In the aforementioned numerical example, it is of the order of ω_{LH}~$1.5\cdot10^{11}$ s^{-1}, i.e., the e-folding time for this instability is orders of magnitude shorter than the duration of the run-in phase. Accordingly, the instability reaches its nonlinear saturation.

There is a subtlety here: for the set of parameters chosen above, and n_i~10^{19} cm^{-3}, one finds that both the products $\omega_{LH}\tau_{ei}$ and $\omega_{LH}\tau_{ii}$ are considerably less than 1. In other words, with respect to the lower-hybrid modes, the plasma is strongly collisional. By itself, this does not necessarily mean that the instability is totally impossible. Instead, this means that the theory presented in the aforementioned references should be reworked to include a hydrodynamic description of both electrons and ions, where the distribution

functions would be nearly Maxwellian, with the deviations from Maxwellian determined by the classical resistivity theory (e.g., Braginski, 1965). It also makes it very difficult for the instability to affect the classical estimate for the plasma resistivity (because the anomalous collision frequency has to compete with classical collision frequency, which is very high).

In gas-puff implosions with a smaller particle density, the role of the lower-hybrid instability can be more important. However, the classical electron-ion collision time remains shorter than the expected anomalous collision time. Therefore, again, the current penetration should be determined by a classical resistivity and/or by gross hydrodynamic instabilities. The anomalous resistivity can possibly play some role in the behavior of a very low-density halo plasma that may surround the main discharge.

The effect of anomalous resistivity can, in principle, be used to reduce the current rise time in a wire array. The idea is to surround it by another, lower-density shell where the current would be sharply terminated by development of the anomalous resistivity as in Branitskii et al., 1996a. Experimentally, these authors studied implosions of gas-puffs on a thin agar cylinder in the Angara-5 facility; Xe, Ar, and C_3H_8 (propane) were used as working gases. The annular jet had a radius of r_0=1.6 cm and a mass of 0.07 mg/cm; the maximum current was ~3 MA and the half-width of the current pulse was ~100 ns. The inner cylinder was made of agar, with a radius of r_i=0.5-1 mm, and a mass of 0.05-0.07 mg/cm. The switching of the current indeed occurred, but it didn't have a sharp front. The authors concluded that the current disruption in the outer shell is probably caused by the Rayleigh-Taylor instability, although other factors may have also contributed.

Baksht et al. (1997) also studied a multiwire array surrounded by an outer gas shell. The dimensions were larger than in the previous work: the diameter of the gas jet was 8 cm and the diameter of the wire array was 3 cm, with wires 20 μm in diameter (68 μg/cm). Reproducibility of the current switching was not very good. To improve the symmetry of implosions, the authors are going to introduce preliminary ionization of the gaseous shell (Cf. Sec. III of this paper). Note that another way of switching the current

(not based on the phenomenon of anomalous resistance) is to use a light external wire array imploding on a smaller-diameter heavier wire array: the current through the inner array will be small until the outer array reaches it (Davis, Gondarenko, Velikovich, 1997).

2. The stagnation phase.

In the stagnation phase, the temperatures of both plasma species are much higher, with the ion temperature considerably exceeding the electron temperature. On the other hand, the relative velocity u, according to (7.1), only decreases because of the increased Z_{eff}. Therefore, the ratio u/v_{Ti} should drop by a factor ~100 compared to the run-in phase. This decrease more than compensates for the growth of the magnetic field caused by a reduced pinch radius, so that the growth rate (7.5) decreases to, roughly speaking, 10^8 s^{-1}. The corresponding e-folding time is long compared to the duration of the stagnation phase, and this instability can hardly have a significant effect on the plasma resistivity during this phase.

It is interesting to note that, for the stagnation phase, the ratios of the relative velocity u to the ion thermal velocity is equal to the ratio of the ion gyroradius to the pinch radius and can be expressed in terms of very few input parameters. One can show that, assuming that the current flows uniformly over the cross-section of the stagnated plasma,

$$\frac{\rho_i}{r_{\min}} \sim \frac{u}{v_{Ti}} \sim \frac{A}{Z_{eff}\sqrt{\ln C}}\sqrt{\frac{m_p}{r_{op}\hat{m}}} \sim 10^{-3}\frac{A}{Z_{eff}\sqrt{\hat{m}(mg/cm)}}, \quad (7.11)$$

where ρ_i is the ion gyroradius, $r_{0p}=1.6\cdot10^{-16}$ cm is a classical radius of the proton, and C is the convergence (1.1). The estimate (7.11) corresponds to the ion temperature before the equilibration with electrons began, i.e., to the ion thermal velocity approximately equal to the liner velocity just before the on-axis stagnation.

Of course, if the current is concentrated in a thin shell, or flows through the low-density plasma halo, the role of microinstabilities may become more important. The other place where anomalous resistivity may become important is the neck (Fig. 21 a) formed as

a result of the development of a sausage mode (we discuss this latter situation in Sec. VII B). A discussion of the effects of anomalous resistance of the neck and some further references on this issue can be found in Sasorov (1992).

The study of the effects produced by anomalous resistivity in the equilibrium pinch can be found in Chittenden (1995). In the equilibrium Z pinches, where plasma density is typically lower than in fast Z pinches, the instability can become quite important because of a higher ratio u/v_{Ti} and much lower frequency of the Coulomb collisions.

B. Generation of suprathermal particles and particle beams

As mentioned in section IV, development of the Rayleigh-Taylor instability may lead to a situation where one or several constrictions of the type shown in Fig. 21a will be formed. Most commonly, the formation of high-energy particles in Z pinches is related to formation of m=0 constrictions. Various versions of theories are discussed in Haines (1983), Trubnikov (1986), Vikhrev (1986), and Deutsch & Kies (1988). These papers contain also an extensive further bibliography. Experimental results from fast z pinches are essentially unavailable. For experiments pertaining to generation of high-energy particles in fiber pinches see Mitchell et al (1998) and references therein.

One can distinguish three mechanisms that lead to the formation of high-energy particles in the constrictions. First, there is a direct acceleration mechanism related to the generation of a high inductive voltage during the current break-up after the neck formation. This mechanism was the first to be suggested to explain the generation of the neutrons in the experiments of early 1950s (see Vikhrev, 1986, and Deutsch & Kies, 1988, for references to experimental works). Second, there is a mechanism related to compressional heating of the substance situated in the neck, accompanied by ejection of the hot material from the ends of the constriction. Third, if a microturbulence is excited in the constriction (because of a high current density), there may occur a stochastic acceleration of the tails of the ion distribution function leading to generation of the high-energy ions. It is quite

conceivable that all three mechanisms for the formation of fast ions may act simultaneously. This is what makes the analysis of experiments on the generation of fast ions so difficult.

The chain of events that leads to inductive acceleration is as follows. After constriction develops, its impedance grows, and the current through the neck diminishes, causing the generation of a large inductive voltage. Spatial and temporal evolution of electric fields that can be generated in such an event have been analyzed in great detail by Trubnikov (see a summary of these results in Trubnikov, 1986).

Some qualitative conclusions that can be drawn from Trubnikov's analysis are as follows. Consider the motion of an individual ion in the time-varying electric field perpendicular to the azimuthal magnetic field. If the ion gyroradius is small compared to the neck radius a, and the electric field varies with a time scale exceeding ω^{-1}_{Ci}, the electric field does not accelerate ions but rather causes their drift motion, with the velocity proportional to the electric field strength E. This is an adiabatic process in the sense that the drift velocity grows when electric field (in the location of the ion) grows and decreases when electric field decreases (either because of the temporal variation of the electric field, or because the ions leave the zone of a strong electric field near the neck). Therefore, to ensure an efficient nonadiabatic energy transfer to the ions, one has to assume that the electric field varies on a time-scale short compared to the ion gyro-period. Another possibility is the ion acceleration near the axis of the discharge where the magnetic field is small. (An interesting question is what sets the lower limit for the pinch radius in the constriction. One can think that this is the ion gyroradius, see the trajectory analysis in Haines, 1983). To sustain the current through the neck with a rapidly growing resistance, an inductive electric field is generated directed along the pinch current. Accordingly, the ions should be accelerated predominantly in the direction of the pinch current at the time just before disruption. Collisions between the beam and plasma ions would cause scattering of the beam. To reach the electrode, the beam should be formed at a distance not greater than a couple of mean-free paths. The drag against plasma electrons in a cold plasma may also be substantial. An

analysis of the experimental measurements at the Angara-5 from the viewpoint of their compatibility with the beam source of the neutrons is presented by Imshennik (1992).

One can note in passing that it is conceivable that the currents possibly present on the galactic scales, form pinch-like structures, and development of the sausage instability gives rise to the generation of high-energy cosmic rays. This viewpoint was presented by Haines (1983) and Trubnikov (1990) (see also further references in the latter paper). The arguments pointing out the presence of currents up to 10^{19} A in the galactic environment were presented by Peratt (1986, 1990). Fig. 27 (Yusef-Zadeh, Morris, and Chance, 1984) depicts an object near the center of our galaxy where the presence of filaments may be a reflection of the pinch-effect.

The second mechanism, most completely presented in the paper by Vikhrev (1986), attributes the generation of fast particles to an adiabatic compression of the plasma in the neck. This process is conceived as a gradual compression of a plasma along the sequence of Bennett equilibria, with a gradual decrease of the linear particle density N (the number of particles per the unit length of the pinch) in the constriction by virtue of the axial ion losses through the ends; the hot ions escape in both directions. The Bennett equilibrium condition,

$$T = \frac{\mu I^2}{4\pi \mathcal{N}}, \tag{7.12}$$

shows then that the plasma temperature in the constriction grows. If the constriction is short, with a radius r comparable with its length ℓ, the hot plasma would escape very rapidly through the ends, and no significant amount of hot particles would be formed. However, if the length of the constriction is large, $\ell >> r$, then the number of hot particles would increase, and conditions for generation of a considerable number of neutrons (in the case of a deuterium or a deuterium-tritium plasma) would be reached.

If the ion-ion collision frequency is high enough, then the ion distribution is almost isotropic, and therefore the neutron radiation generated in the constriction would also be isotropic. Still, if some hot ions do escape along the axis, an asymmetry in the number of

the ions reaching the anode and the cathode may appear (leading to the asymmetry of the neutron generation on the electrodes). The situation is illustrated by Fig. 28, which depicts two ion trajectories originating on the axis. If the initial ion velocity is slightly tilted to the axis and directed towards the cathode, the magnetic field produces a focusing force, and the ion rapidly moves along the axis towards the cathode. On the other hand, if the initial velocity is directed toward the anode, the magnetic force is defocusing, and the ion gets involved in a gyromotion with a slow drift towards the anode (Cf. Haines, 1983). A collisionless version of the ion acceleration by pinch "walls" converging on axis was discussed by Deutsch and Kies (1988).

The third mechanism can be efficient in a plasma of a relatively low density, where the plasma resistance is dominated by microfluctuations (Sec. VII. A). The ion scattering on microfluctuations usually leads to formation of a high-energy tail of the ion distribution function (see surveys by Vedenov and Ryutov (1975) and Galeev and Sagdeev (1979)). The evolution of the high-energy tail of the ion distribution function is governed by a Fokker-Planck-type equation,

$$\frac{\partial f}{\partial t} = \frac{1}{\mathrm{v}^2}\frac{\partial}{\partial \mathrm{v}}\mathrm{v}^2 D(\mathrm{v})\frac{\partial f}{\partial \mathrm{v}}\,, \qquad (7.13)$$

with the diffusion coefficient proportional to the energy density of fluctuations. The distribution function in (7.13) is normalized according to the relationship $dn = 4\pi f(\mathrm{v})\mathrm{v}^2 d\mathrm{v}$, where dn is the number of ions per interval $d\mathrm{v}$ of the ion velocities. For simplicity, we present Eq. (7.13) for the case of an isotropic spectrum of the fluctuations. Equation (7.13) describes the diffusive broadening of the high-energy tail of the ion distribution. The majority of the ions remain in the ion core dominated by Coulomb collisions. Despite the small number of ions in the tail, they may be responsible for nuclear reactions with a high energy threshold and may thereby be used for diagnostics purposes (to identify regimes where suprathermal particles are present).

Consider in more detail the ion acceleration in the ion acoustic turbulence in a high-Z plasma. Assuming approximately equal temperatures of the electrons and ions, one finds that the oscillations excited by this instability near its threshold (7.5) have the wave-number

$$k \sim \sqrt{Z_{eff}}\frac{\omega_{pe}}{v_{Te}}. \qquad (7.14)$$

Based on the standard equations of the quasilinear theory, one finds that the diffusion coefficient in (7.13) is directly related to the effective electron collision frequency ν_{eff} that enters the expression for anomalous resistivity:

$$D \sim v^2 \nu_{eff} Z_{eff}^2 \sqrt{\frac{m_e}{m_i}}\left(\frac{T}{m_i v^2}\right)^{5/2}. \qquad (7.15)$$

The characteristic energy W^* of the tail ions at the time t after the onset of the anomalous resistivity will be

$$W^* \sim T\left(Z_{eff}^2 \nu_{eff} t\right)^{2/5}\left(m_e/m_i\right)^{1/5}. \qquad (7.16)$$

Equation (7.16) directly links the ion energy with the anomalous resistivity (7.6) and provides thereby a phenomenolgical link between the two phenomena: the anomalous resistivity and the formation of the ion tail.

The maximum energy is limited by the duration of the turbulent state or by the residence time of the ion within the neck. An absolute upper limit is set by the condition that the ion gyroradius becomes comparable to the neck size. This yields the following estimate for the maximum ion velocity v_i: $v_i m_i / Z_{eff} eB \sim a$, where a is the neck radius. As $B \sim \mu I/2\pi a$, one finds that

$$\frac{v_i}{c} \sim \frac{Z_{eff}}{A}\frac{I(MA)}{30}. \qquad (7.17)$$

At a current ~ 20 MA, the protons, in principle, can be accelerated to subrelativistic energies (Eq. (7.17) corresponds to nonrelativistic energies; at higher currents it breaks down). Of course, this is an estimate from above. Still, it shows the significance of the pinch current in providing conditions for generating high-energy particles.

So far we have been discussing the generation of fast ions. Fast Z pinch discharges often are accompanied by bursts of hard x rays, pointing to the presence of high-energy electrons. As a curiosity, one can mention the generation of multi-MeV electrons in high-altitude lightning (Fishman et al., 1984). Formation of electron beams is strongly suppressed by the presence of the transverse magnetic field of the pinch. It is hard to expect formation of an electric field exceeding *cB,* as this would require a complete current breakup within the time of the order of *r/c.* At $E<cB$, on the other hand, electrons cannot accelerate; they experience a slow nonrelativistic drift motion, with a velocity $E/B<<c$. For this reason, the models that attribute the formation of high-energy electrons to the mechanism of a local adiabatic compression are of some interest. They predict the formation of hot (possibly relativistic) electrons near the necks (Vikhrev, 1986). These areas then could serve as sources of hard x rays. It is interesting to note that electron beams were detected in so called X pinches (a discharge through two or more crossed wires), where they were generated near the intersection point (Ivanenkov et al., 1996).

Formation of beams of runaway electrons is possible near the pinch axis where the magnetic field is weak and the condition $E>cB$ can be satisfied. At a given density and a given electric field strength, there exists a group of electrons experiencing runaway. To be involved in a runaway process, the electron should have high-enough initial energy so that, before the first scattering, it doubles its energy. This condition, if expressed in terms of the effective collision frequency, reads as

$$\frac{eE\mathrm{v}}{\nu_{\mathrm{eff}}(\mathrm{v})} > \frac{m_e \mathrm{v}^2}{2}. \qquad (7.18)$$

We have explicitly included the dependence of effective collision frequency on the electron velocity. Electrostatic fluctuations of the lower-hybrid or ion acoustic type give rise to a dependence of $1/\mathrm{v}^3$ in ν_{eff}, very much like for classical Coulomb collisions. If the classical collisions are important, ν_{eff} should include them too. From Ohm's law, one finds that

$$u = \frac{eE}{m_e \nu_{eff}(v_{Te})} . \qquad (7.19)$$

Because the current is carried by the main body of electron distribution, the collision frequency that enters this equation corresponds to "thermal" electrons. For the $1/v^3$ dependence of the collision frequency, one finds from (7.18) and (7.19) that the critical energy above which the runaway process begins is (Benford, 1978): $w_{crit} = T v_{Te}/u$..The drift velocity u usually does not exceed a few ion thermal velocities. Therefore, only a small fraction of the total electron population can be involved in a runaway process. The spectrum of the runaway electrons can be found in Benford (1978).

Phenomena discussed in this section can be strongly affected by the presence of even a weak axial magnetic field. In particular, the neck formation can be stopped because the axial field would grow inversely proportional to the square of the neck radius, while the azimuthal field would grow inversely proportional to the first power of the radius. On the other hand, an axial magnetic field considerably broadens the zone where the runaway electrons can be accelerated.

In the implosions of hollow shells (e.g., the wire arrays), favorable conditions for runaway formation may be met inside the shell, where there is no magnetic field and the plasma density is low. An axial electric field may be present inside the shell if the skin depth exceeds the thickness of the shell (see Sec. II. G). The beam of accelerated electrons will be formed then much earlier than the on-axis stagnation occurs. An early appearance of the beam (detected by the x-ray radiation from the anode) can serve as an indicator of a great skin depth. At high enough beam-to-plasma density ratio, the beam may experience a two-stream instability. A survey of the effects caused by this instability can be found in Breizman and Ryutov (1974).

In addition to acceleration mechanisms related to the neck formation, the mechanisms based on the ion acceleration through the sheaths near the electrodes have also been studied (see Haines, 1983, and Trubnikov, 1986, for further references).

C. The Hall effect

When the electron gyrofrequency becomes greater than the electron collision frequency, the Lorenz force in the electron momentum equation becomes dominant over the electron-ion friction term. In a uniform plasma, the electron momentum equation should be written as:

$$m_e \nu_{ei} \mathbf{u} = -e\mathbf{E} - e(\mathbf{u}+\mathbf{v})\times\mathbf{B} \ . \qquad (7.20)$$

Here the electron-ion collision frequency includes, generally speaking, both the Coulomb collisions and anomalous scattering; **v** is the ion velocity (which almost coincides with the velocity of the center of mass); **u** is a relative electron-ion velocity. If |**u**| is greater than the characteristic velocity of the ion motion, then equation (7.20) shows that the magnetic field is convected together with electron fluid (not with a plasma as a whole). In the limit of a low collision frequency, the magnetic field is frozen into the electron fluid. The possibility appears then that the magnetic field will be redistributed at a time-scale that is short compared to the time-scale of the ion motion. Because the ion density within this short time-scale remains constant, only those electron displacements are allowed that do not perturb the electron density. This type of motion is described by so-called "electron magnetohydrodynamics" (EMHD), or "Hall magnetohydrodynamics". The latter name is related to the analogy of the last term in (7.20) to a Hall term in the theory of current flow in solid conductors. A general survey of EMHD has been published by Gordeev, Kingsep, and Rudakov (1994). A set of criteria defining the parameter domain where the effects of EMHD are important has been summarized in a more recent paper by Kingsep and Rudakov (1995). Dissipative phenomena in EMHD were discussed by Sevast'yanov (1993). Roughly speaking, the effects of EMHD become important if the following two conditions are satisfied: $\omega_{Ce} > \nu_{ei}$; $u > s, a$, where s and a are the sound and the Alfven velocities, respectively.

The motions of an electron fluid become particularly interesting when the plasma density is nonuniform. If the plasma density varies in the z direction, the skin-effect

becomes dependent on the direction of the current (see Gordeev, Kingsep, & Rudakov, 1994). Fast axisymmetric striations can be self-generated (Rudakov, Sevast'yanov, 1996). The streamlines of the current become wavy, with the axial wavelength of the order of the shell thickness. This happens within a time that is short compared to the time within which the ions would react to the firld perturbation (the ion background is assumed to be steady).

An interesting and so far unsolved issue is that of the influence of these fast phenomena on the quality of the shell implosion and the development of slower instabilities involving the ion motion (in particular, the Rayleigh-Taylor instability). In this respect, one should note that the current perturbations discussed by Rudakov and Sevast'yanov propagate along the axis with a velocity approximately equal to u; therefore, although the instantaneous force acting on the ions is strongly z-dependent, an averaging that occurs because of the travelling nature of these perturbations should make the average force z-independent and the possible seed for m=0 hydrodynamic instability decreases.

For the flute-type mode, with the wave vector orthogonal to the magnetic field, even the presence of a strong Hall effect does not change the $k^{1/2}$ scaling of the growth rate (Gordeev, 1999 a,b).

An important issue is the electron flow at the boundary between the electrode and the plasma: at the electrode surface the tangential component of the electric field vanishes, and the electron flow becomes almost parallel to the wall. Weak collisions gradually shift the electrons in the direction of the wall. Because this (axial) motion is slow (at weak collisions) the resistivity of the transition layer becomes anomalously high. More details on these issues can be found in the aforementioned survey by Gordeev, Kingsep, and Rudakov. A 2-D effect in electron magnetohydrodynamics may lead to increased plasma resistance (Esaulov, Sasorov, 1997).

D. Spontaneous generation of the magnetic field

In implosions of uniform gas loads, where a shock wave propagates in front of the magnetic piston, there exists a zone of highly ionized plasma behind the shock but before the piston where the magnetic field is zero, at least in the ideal case where no stray early-time breakdowns occurred at the beginning of the shot. It turns out that, if the system does not possess a perfect symmetry, high magnetic field can be spontaneously generated in this zone. The mechanism we are referring to was identified a long time ago in conjunction with experiments on laser plasma heating and is associated with non-collinearity of gradients of electron temperature and density (Stamper at al., 1971). When ∇n and ∇T aren't parallel, an electromotive force is generated in a plasma that drives the current and produces magnetic field. This term should be added to the standard induction equation, which acquires the form (Stamper at al., 1971):

$$\frac{\partial \mathbf{B}}{\partial t} = \nabla \times \mathbf{v} \times \mathbf{B} - \nabla \times (D_m \nabla \times \mathbf{B}) + \frac{\nabla n \times \nabla T}{en} . \qquad (7.22)$$

The first term in the r.h.s. describes the convection of the magnetic field with a plasma flow (line-tying), the second term describes joule dissipation (in the case of a uniform magnetic diffusivity it reduces to a diffusion term $D_M \nabla^2 \mathbf{B}$), and the last term is the thermo-electromotive force. Non-collinearity of ∇n and ∇T in the problem under consideration may emerge from the waviness of the piston caused, in turn, by the Rayleigh-Taylor instability.

Let us for a while neglect the ohmic losses (this is equivalent to a statement that the skin-depth is much smaller than the spatial scale of the perturbations). Then the maximum magnetic field is determined from the balancing of the first and the third terms in the r.h.s. of Eq. (7.22). Estimating the velocity of a plasma flow as a sound velocity s, we find that, within an order of magnitude, $B \sim T/es\lambda$, where λ is a spatial scale of nonuniformities. The magnetic field will vary (randomly, if the perturbations are random) at the scale λ. Assuming that one deals with an Ar plasma with a temperature of 100 eV and $Z_{eff} \sim 10$, one

finds that for λ~ 0.5 mm, the magnetic field is B~10 T. Under typical Z-pinch conditions, this magnetic field does not lead to magnetization of electrons, $\omega_{Be}\tau_{ei}$ remains less than 1. However, this field will be compressed at later stages of the implosion, when the shock wave has already converged on axis. This happens if the resistive dissipation time is longer than the compression time. In the opposite case, the magnitude of the magnetic field will be considerably decreased. The estimates for the conditions of a particular experiment can be made on the basis of Eq. (7.22). This mechanism of the magnetic field generation was possibly observed by Afonin and Murugov (1998).

Although this random field is usually small compared to the pinch magnetic field, it may play a significant role after the quasiequilibrium configuration is formed (Sec. II) and necks develop. In particular, this random field may prevent the runaway electrons from being freely accelerated along the axis of the column (Sec. VII. B).

The other situation where this mechanism for magnetic field generation may play a role is a blow-off plasma filling the interior of the imploding shell. One can expect that this plasma will be strongly nonuniform, and that the conditions for the appearance of the thermal electromotive force will be thereby satisfied. The presence of the random magnetic field will affect transport properties of the blow-off plasma.

VIII. APPLICATIONS OF FAST Z PINCHES

A. Radiation sources

1. Hard x rays

One of the traditional applications of fast Z pinches lies in generating short pulses of intense kiloelectron-volt radiation, with the energy of the quanta in the range up to 10 keV. For such applications, one can use a wire array made of some high-Z material (say, nickel), or an annular gas-puff of gases like Ar or Kr. If the parameters of the pinch are properly chosen, a plasma with an electron temperature of several hundred electron-volts to

over 1 keV can be formed, and the excitation of the L or K shells becomes feasible. A survey of the studies in this area prior to 1988 was published by Pereira and Davis (1988).

A rough optimization of the Z-pinch parameters for the highest yield in the desired K or L transition can be made based on the following arguments. The efficiency of converting the magnetic energy into the kinetic energy of the imploding shell is determined by the condition $\Pi=\Pi_{opt}$, where Π is a dimensionless parameter defined by Eq. (2.4). As is clear from Eq. (2.4), for a given pulse-power generator, i.e., for given values of I_{max} and τ, the product $\hat{m}r_0^2$ must be kept constant. This means that the pinch mass $\hat{m}$ and the initial pinch radius r_0 can be varied only subject to the constraint

$$\hat{m}r_0^2=const. \tag{8.1}$$

The kinetic energy per ion scales as the implosion velocity square, i.e., as $(r_0/\tau)^2$. The electrons acquire their energy from the ions, and the electron temperature therefore correlates with $(r_0/\tau)^2$. According to Eq. (8.1), the heavier liners have smaller initial radii, i.e., the electron temperature at stagnation decreases with increased mass of the liner. Eventually the electron temperature becomes insufficient to excite a certain K or L transition. Conversely, for the liners with less mass (larger initial radii), the kinetic energy per ion grows. At first sight, this means that the lighter liners are better as the sources of kilo-electronvolt x rays. However, if one goes too far in this direction, the radiation yield starts to decrease because the radiation power per unit volume scales as the density squared and, at small masses, decreases. Because of this, the pinch plasma begins to expand and cool down before any substantial fraction of the thermal energy gets converted into the radiation. The slower energy exchange between electrons and ions at higher temperatures also acts in this same direction. These two opposite trends — decrease of the electron temperature at high masses, and decrease of the radiation power at low masses — determine the optimum mass of the imploding liner. At higher masses, a self-absorption may reduce the K-shell radiation yield (Apruzese et al, 1998). More detailed discussion of these issues, together with supporting experimental information, can be found in Pereira

and Davis (1988), Thornhill, Whitney, and Davis (1990), Deeney et al. (1993, 1994) Deeney et al (1997a), Deeney et al., 1998a) , and Whitney et al. (1990, 1994).

In the recent experiments at the Z facility (Deeney et al., 1997b), the energy radiated in the K-shell transitions of Ti was well over a hundred kilojoules (Fig. 29). In Deeney,et al. (1998c) , it was shown that reducing the height of the pinch from 2 to 0.75 cm did not change the total radiation power or radiation energy. As the shortening of the pinch resulted in the decrease of the pinch inductance and some increase of the pinch current, the authors increased the mass per unit length to keep the load match in terms of keeping the parameter (Eq. (2.4)) more or less constant.

In real life, although a considerable fraction of the kinetic energy can be converted to radiation upon stagnation, the plasma column still has sufficient pressure to somewhat expand and to be compressed again by the magnetic pressure. This process may explain the presence of a longer, lower-amplitude, and longer-wavelength radiation pulse that follows the main peak (Peterson et al., 1997, 1999). Another phenomenon that may effect the final radiation yield is a short-circuiting of the transmission lines later in the pulse (Giuiliani et al, 1990).

The stability of the Z-pinch implosion is important for efficient x-ray generation; it sets the minimum effective size to which the pinch can be compressed. A more stable implosion would allow one to increase the initial pinch radius and to reduce the mass while still having high density at stagnation (sufficient to radiate the thermal energy before the pinch rebounds).

To obtain harder x rays, in the range of tens of kiloelectronvolts, one could use an alternative approach based on the adiabatic compression of a hydrogen plasma seeded with heavy impurities; the plasma temperature could possibly be made as high as 10 keV, allowing excitation of the K-lines of such elements as Xe. We discuss this possibility in some more detail at the end of Sec. VIII D.1.

2. Black-body radiation

Fast Z pinches with high atomic number materials are also used as a source of a thermal radiation with a temperature from tens of electronvolts to ~200 eV (and, in future, over 300 eV). If the implosion occurs in the center of a closed cavity (sometimes called a "hohlraum"), the radiation from the pinch, after several reflections from the walls, becomes almost black-body radiation (Matzen, 1997). The wall (and the radiation) temperature can be roughly evaluated from the equation: $P_{rad} = (1-\alpha)A\sigma T^4$, where P_{rad} is the power radiated by the pinch, A is the surface area of the cavity, and α is the albedo of its walls. In the experiments at the Saturn facility at Sandia, the radiation temperatures were in the range of 80-90 eV (Matzen, 1997; Matzen, 1999). In the experiments at the Z facility, temperatures in the range of 120-140 eV (Porter, 1997) and, more recently, 155±10 eV (Matzen et al, 1999) have been obtained.

B. Studies of material properties under extreme conditions

Thermal radiation generated by the just-described method can be used to drive shock waves in various materials. By studying the shock velocity, one can gain information about the equations of state of the materials under study. A typical geometry of such an experiment is shown in Fig. 30. Thermal radiation causes ablation of the material from the inner side of the sample, and the ablation pressure drives a shock whose velocity can be measured by measuring the time of the shock arrival at the outer side of the sample. To be sure that the radiation spectrum is indeed close to the black-body spectrum (and, therefore, that the drive can be characterized by a single function $T(t)$), small cavities can be attached to the main one in such a way (Fig. 31) that the samples are protected from direct irradiation by the pinch, and only the radiation from the walls of the cavity hits the surface of the sample (Matzen, 1997). Several configurations have been proposed that increase the uniformity of the radiation on the sample under study.

The hohlraum technique has been successfully used to study propagation of shocks in the materials that will be used in ICF capsules (Olson et al., 1997) and to study equations of state (EOS) of metals in the pressure range of ~3 Mbar (Branitskii, Fortov et al., 1996). The same technique is broadly used in physics research with laser-driven hohlraums where it has reached a high degree of sophistication. A general survey of this approach can be found in Rosen (1996). It has been successfully used for studies of the structure of shock-compressed materials (Kalantar, Chandler, et al., 1999), of hydrodynamic Rayleigh-Taylor and Richtmyer-Meshkov instabilities with controlled initial perturbations (Remington, Budil, et al, 1997), of the effects of a material strength on hydrodynamic phenomena (Kalantar, Remington et al., 1997, Remington, Budil et al., 1997a), and for astrophysical simulations (Remington et al., 1997b). An advantage of Z-pinch-driven hohlraums is a larger size and considerably higher total radiation output (centimeters vs. millimeters, and hundreds of kilojoules vs. tens of kilojoules). This, for example, allows one to use thicker hydrodynamic packages, minimizing problems with radiation preheat. Larger sizes of the samples and longer times would also lead to better accuracy of the EOS measurements. Gasilov et al (1995) suggested generating multimegabar shocks in a central rod (~ 1 cm long) hit by an imploding liner. For yet larger experimental volumes, other techniques, based on magnetic compression driven by chemical explosives, are feasible (Hawke et al., 1972).

C. Generation of high magnetic fields

The use of an imploding cylindrical shell for generating high magnetic fields had been suggested many years ago (Fowler et al., 1960; Sakharov et al., 1965). High fields are generated by compressing an initial modest axial field by an imploding, conducting cylindrical shell. Experiments with explosively driven systems have been reported in the 1960s (Fowler et al., 1960; Sakharov et al., 1965), reaching magnetic fields as high as 20 MG. Implosions of metal shells in the Z-pinch geometry were studied by Alikhanov et al.

(1981); a maximum magnetic field of 3.5 MG was obtained in a volume of a few tens of cubic centimeters.

We present a qualitative consideration of the magnetic field compression in the Z-pinch setting, assuming that the thickness of the shell is negligibly small and that the shell has a high conductivity. The condition of the conservation of the axial magnetic flux enclosed by this plasma shell is:

$$B_z r^2 = B_{z0} r^2_0 , \tag{8.2}$$

where B_{z0} is the initial axial magnetic field. When the convergence ratio is high enough, the final axial magnetic field can be considerably greater than the initial one. Here we neglect the edge effects of the type discussed in Sec. II F. This is correct if the length of the pinch is greater than its radius.

The compression of the axial magnetic field can be analyzed in a particularly straightforward fashion in the reference case of a constant pinch current. Then, the energy conservation law shows that at the point of the maximum compression, where the liner is at rest and its kinetic energy is zero, the following relationship holds:

$$\pi r^2 \frac{B_z^2}{2\mu} - \pi r_0^2 \frac{B_{z0}^2}{2\mu} = \pi r^2 \frac{B_\varphi^2}{2\mu}\left(2\ln\frac{r_0}{r}\right), \tag{8.3}$$

where B_φ is the azimuthal magnetic field at the surface of the liner. At a convergence $C>>1$, one can neglect the second term in the l.h.s. of this equation. One then finds that, at the stagnation point, the (axial) magnetic field inside the liner is related to the (azimuthal) magnetic field of the pinch current by the equation

$$B_z = B_\varphi \sqrt{2\ln C} . \tag{8.4}$$

Taking C=20, one finds that the magnetic field inside the liner can be made approximately 2.5 times higher than the azimuthal Z-pinch field at the point of the maximum compression. In other words, this scheme leads to relatively modest enhancement of the internal field compared to the external field that would be reached at the same convergence ratio. Still, this factor is non-negligible, especially because it is topologically more

convenient to use the magnetic field inside the shell for the studies of interaction of super-high fields with matter.

From Eqs. (8.2) and (8.4) one can see that the initial axial magnetic field required to reach this state is: $B_{z0} = B_{\varphi 0}\sqrt{2\ln C}/C$, where $B_{\varphi 0}$ is the initial azimuthal magnetic field. Taking, as an example, $B_{\varphi 0}$=0.5 MG, and a modest convergence C=20, one finds that the initial axial magnetic field should be ~60 kG, and the final axial magnetic field will be 25 MG. Accounting for the finite thickness of the imploding shell leads to somewhat smaller enhancement factors, because part of the implosion energy is spent on the plasma heating and compression. These and other pertinent effects have been discussed, e.g., by Felber, Liberman, and Velikovich (1985).

In experiments carried out during the last decade, annular gas-puffs have been used to produce conducting imploding shells (Wessel et al., 1986; Baksht et al., 1987; Felber, et al., 1988 a,b). Magnetic fields in the range of 40 MG were reported in Felber, et al. (1988). In summary, an axial implosion of the seed magnetic field is a proven way of reaching an axial magnetic field a few times higher than the azimuthal magnetic field at the stagnation point.

D. Controlled thermonuclear fusion (CTF)

There are two significantly different ways for using fast Z pinches for reaching CTF. The first is based on the direct shock and/or adiabatic heating of an imploding DT plasma (possibly nested inside a liner made of a heavier material). The second is based on generating high-temperature black-body radiation by colliding the liner with some inner shell; the black-body radiation then drives a spherical pellet in very much the same fashion as in the indirectly driven laser fusion systems (for a survey of those see Lindl, 1995). We discuss these two schemes in the next two sub-sections.

As was mentioned in the Introduction, quasi-equilibrium pinches (not the fast pinches that are the subject of this survey) have also been considered as a potential

candidate for fusion reactors, but we will not discuss that approach here. Surveys of quasistatic pinches in conjunction with fusion applications have been published by Haines (1982), Dangor (1986), and Robson (1989, 1993).

A well-known difficulty with using fast Z pinches in a future commercial fusion reactor is related to the considerable neutron and thermomechanical damage that would be suffered by the pulsed power generator if the pinch is not separated from the generator by a large-enough distance. A possible solution to this problem was suggested by Robson (1989), who envisaged using two long liquid lithium jets that would serve as electrodes for the Z-pinch. Drake et al. (1996) considered another technique that could possibly be used if the energy to be delivered to the Z pinch is less than ~1 MJ per pulse. For this case one could conceive of dropping miniature diode assemblies, consisting of fusion targets and the necessary circuitry, to the reactor chamber and energizing them by a charged particle beam or even by a fast projectile (in this latter case, the assembly would have to carry a seed magnetic field that would be compressed by a fast projectile and drive the Z-pinch circuit).

The whole issue of stand-off energy sources has not been explored in any detail. It would therefore be premature to write off the Z pinches as a prototype of a fusion reactor solely on the basis of the absence of proven solutions for the power supply problem. In addition, even if such solutions are not found, the fast Z pinches can still be very useful for the fusion program; they could provide a relatively inexpensive demonstration of fusion ignition in a variety of pulsed power fusion concepts.

1. Plasma heating by implosion

First consider implosions of thin shells made of a DT mixture (e.g., Nedoseev, 1991). Cryogenic DT fiber arrays can serve as such shells. The lifetime τ of the hot plasma column formed at the stagnation point will be of the order of r_{min}/v_{Ti} where r_{min} is the radius of the column (related to the initial radius of the shell by Eq. (1.1)), and v_{Ti} is the ion

thermal velocity corresponding to the temperature ~10 keV (i.e., v_{Ti}~10^8 cm/s). The Lawson criterion reads as

$$n(\mathrm{cm}^{-3})\tau\,(\mathrm{s}) > Q\cdot 10^{14} \tag{8.5}$$

where n is the DT plasma density and Q is the ratio of the fusion energy to the thermal energy of the imploded plasma (the gain factor). This condition can be rewritten as $W(\mathrm{J/cm}) > 10^{31} Q^2/\mathrm{n}(1/\mathrm{cm}^3)$, where W is the energy per unit length of the plasma column. Even with a relatively modest assumption with regard to the required gain, Q~10, this condition means that one has to reach a density level of ~10^{25} cm^{-3} to keep the energy of the plasma below 10^8 J/cm. According to Eq. (2.9), to reach this energy, one would have to generate unrealistically high pinch currents, ~10^9 A. On the other hand, increasing the density in the imploded state above 10^{25} cm^{-3} would require attaining unrealistically high convergences. A possibility of improving the implosion stability and, thereby, the axial convergence was analyzed by Golberg, Liberman and Velikovich (1990), with a conclusion that a break-even requires a radial convergence ~ 30, with the energy release in the range of hundreds of megajoules/cm.

These observations point out the desirability of using a heavier shell to confine the DT plasma near the stagnation point. In this case, however, another difficulty surfaces: high electron thermal conductivity in the fusion plasma. Because the thermal capacity of the heavy shell is much greater than that of a fusion plasma it confines, there will be heat losses from the DT plasma to the confining shell. It turns out that this heat-loss mechanism leads to the approximately same energy limitations as discussed above and, for this reason, does not make this fusion concept more realistic.

Potentially, very high densities can be achieved in 3-D implosions with a linear convergence of ~30 (typical for laser-driven fusion). The whole concept then becomes similar to that of laser fusion, with the only difference being that the implosion of the capsule is driven by magnetic pressure. In principle, almost spherically symmetric implosions are feasible in the magnetic compression scheme, despite the fact that the

magnetic pressure cannot be made spherically symmetric. This had been demonstrated in a multi-megajoule explosively driven experiment by Mokhov et al. (1979). More recently, quasispherical implosions in the Z-pinch geometry have been experimentally studied by Degnan et al. (1995). A linear convergence ratio of ~6-7 has been reached. It remains, however, unclear whether the very fast, high-convergence implosions needed to ignite the fuel in the center of the capsule are actually feasible. This issue requires further analysis.

One more school of thought (e.g., Yan'kov, 1991) pursues the detonation wave approach, in which the nuclear burn wave would be ignited in some point of a cylindrical column and would propagate along the axis. The detonation could be ignited in a "neck" that could be deliberately produced at a certain axial location. Linhart et al. (1993) consider even the possibility of detonating a column of pure deuterium (not a DT mixture) by imploding a short section filled with DT. These schemes would give rise to very large energy release per pulse, in the range of 1 GJ (approximately equivalent to 250 kg of high explosives). A strong heating of a CH fiber plasma in the zone of a deliberately created constriction was observed by Aranchuk et al. (1997). Numerical simulations by Lindemuth (1990) have shown a spontaneous formation of hot spots as a result of the development of a sausage instability in cryogenic deuterium fibers. Alikhanov et al. (1984) observed a spontaneous formation of 10 μm diameter necks in gas-puff pinches with the initial radius of a few centimeters.

Very high densities of DT fuel can be reached in the so-called staged pinch (Rahman et al., 1995), where a liner would implode onto a DT fiber situated near the liner axis and carrying an initial axial current. Compression of the azimuthal magnetic field has an interesting feature; the rate of its growth becomes very high when the outer liner comes close to the inner fiber. This is a result of the fact that, when the gap between the fiber and the liner is much greater than the fiber radius, the fiber inductance depends on the gap only logarithmically, whereas with gaps smaller than the fiber radius, this dependence changes to linear. Therefore, the current in the fiber experiences a very sharp rise, compresses the

fiber and ignites the fusion fuel. Numerical examples presented in Rahman et al. (1995), show that the fiber density may reach the values ~10^{25} cm^{-3} even at a relatively modest current of 2 MA, in the imploding liner with an initial radius of 2 cm. However, this optimistic conclusion is based on the assumption that the inner surface of the liner remains cylindrical within an accuracy of a few micrometers at the time of the maximum compression. This does not seem easily achievable.

Probably, the most straightforward approach, if not to ignition then to break-even, could be based on adiabatic compression of a magnetized plasma. It has been understood for many years that, to suppress heat losses from the fusion plasma to the walls of the imploding liner, one can use a relatively weak magnetic field, such that its pressure is small compared to the plasma pressure, i.e., the condition

$$\beta \equiv \frac{2\mu p}{B^2} >> 1 \qquad (8.6)$$

is satisfied. This condition is, in fact, almost mandatory because, if the inequality (8.6) reverses its sign, the liner implosion becomes inefficient: the liner works predominantly against the magnetic pressure, and the liner energy is converted predominantly to the energy of the compressed magnetic field (not the thermal energy of a plasma).

As was pointed out by Drake et al. (1996), a 3-D implosion of the liner is preferable to a purely cylindrical implosion. This can be understood in the following way: the z-component of the magnetic field inside the shell scales as the square instantaneous convergence C^2; in other words, the magnetic pressure scales as C^4:

$$p_M = p_{M0} C^4, \qquad (8.7)$$

where p_{M0} is the magnetic pressure of the axial magnetic field at the beginning of the implosion. The pressure p of a fully ionized hydrogen plasma scales as a volume to the power (-5/3), or $p = p_0 C^{10/3}$ for a purely cylindrical implosion. Clearly, the magnetic pressure grows faster than the plasma pressure, and, at the high convergence ratios that are of interest in this problem, becomes greater than the plasma pressure. On the other hand,

for a 3-D implosion, the scaling for the magnetic pressure remains unchanged (Eq. (8.7)), while the plasma pressure now scales as C^5 and grows faster than the magnetic pressure.

Plasma confinement under condition (8.6) was discussed many years ago by Budker and his coworkers (see Alikhanov et al, 1967; Budker, 1973). In the context of a laser heated plasma it was discussed by Pashinin and Prokhorov (1971). Since then, it has been studied in a lot of detail theoretically and numerically (e.g., Vekshtein, 1987). The general conclusion was that, because the plasma pressure is almost constant over the radius, the plasma density becomes very high near the cold walls. Magnetic field gets convected to this high-density region from the plasma core, and a "cushion" of a very high magnetic field is formed near the walls. At moderate plasma betas (see Eq. (8.6) for the definition of beta), below 10-20, the resulting confinement of the hot plasma core proves to be quite satisfactory: the confinement time exceeds tens of the Bohm confinement time. At high densities typical of the system under consideration, this confinement time does not substantially limit the plasma gain (see Drake et al., 1996, for more details). This concept is sometimes referred to as magnetized target fusion (MTF), Lindemuth and Kirkpatrick, 1983. A high-energy (many tens of megajoules) variant of this system is the MAGO device under study at Los Alamos National Laboratory and the All-Russian Scientific Research Institute of Experimental Physics (Lindemuth et al., 1996).

Among magnetic configurations that could be imploded are the field-reversed configuration (FRC), the spheromak, and the diffuse Z-pinch. Figure 32 shows an FRC nested inside the liner. To make the implosion 3-dimensional, it was suggested that the liner mass density vary over the length, with a maximum density near the equatorial plane (Cf. Alikhanov et al, 1977). The liner would be then squeezed near the ends faster than near the equator, and the FRC would be compressed both axially and radially. What is yet to be proven in this approach is the formation of a FRC suitable for the subsequent compression. The experience here is limited to relatively large (tens of centimeters in diameter) FRCs with a plasma with a density $\sim 10^{15}$ cm^{-3}. Preliminary scaling analysis

(Ryutov, 1997) shows that creation of a much smaller (1-2 cm diameter) FRC with a plasma density ~10^{18} cm^{-3} and temperature ~100 eV is feasible.

In Drake et al. (1996) this scheme has been analyzed for relatively slow (1-2 μs) implosions of heavy (at least a few grams) liners that could be driven by relatively simple condenser banks. The conclusion was drawn that a 10-keV DT plasma under break-even conditions can be formed at as low a plasma energy content as ~100 kJ. No analyses have been made with regard to potentialities of this scheme with much lighter liners and faster drivers, such as the ones used in the Z facility.

Note that, if seeded with heavier impurities, this plasma could serve as a high-power source of hard x rays. If the atomic number of the impurities is chosen in such a way that they are completely stripped at 10 keV, one can generate a smooth bremsstrahlung spectrum, corresponding to a temperature ~10 keV. If the impurities are heavy (like Xe), then a considerable fraction of energy could be radiated in K-shell lines with energies ~20 keV and higher (Toor, Ryutov, 1997).

2. Generation of a black-body radiation to drive a fusion capsule

A very different way of using Z-pinches for fusion (Smirnov, 1991; Matzen, 1997; and also earlier unpublished reports from both Sandia and Troitsk) is based on the scheme resembling indirect-drive laser inertial confinement fusion (ICF); a nice qualitative discussion of this application of fast Z pinches has been recently published by G. Yonas (1998). When an imploding liner collides with an inner shell situated near the axis, the impact energy is converted into thermal energy in both shells. If the imploding plasma shell is sufficiently thick, it will trap the radiation produced by the stagnation (Fig. 33). In analogy with the terminology used in laser fusion, the interior of the shell filled with (almost) black-body radiation is called a "hohlraum." To emphasize the fact that the walls of the hohlraum continue to implode after the impact between the two shells, a term "flying radiation case" or "dynamic hohlraum" is often used (Matzen, 1997; Brownell et al, 1998,

Matzen et al., 1999). A spherically symmetric capsule filled with DT fuel is situated in the center of the dynamic hohlraum. The thermal radiation causes the ablation and implosion of the surface layers of the capsule. We will not discuss here issues of capsule design and its implosion physics (see Olson et al, 1999, and Hammer et al., 1999, for capsule designs), but focus on some issues related to Z-pinch-driven hohlraums.

The radiation temperatures required for ignition of an indirect-drive DT capsule are in the range of 250 eV for designs similar to ICF capsules driven by lasers (Lindl, 1995) The temperatures presently reached in the Z-pinch experiments are in the range of 130-180 eV (e.g., Nash et al, 1997b, 1999; Leeper et al, 1998). These ICF ignition and high yield capsules also require precise pulse shaping and a high degree of radiation symmetry.

The temporal dependence of the radiation flux can be controlled by adjusting the shape of the inner and/or the outer shells. For example, the configuration shown in Fig. 34a will produce a long "pedestal" caused by the interaction of the ends of the two shells, followed by a sharp pulse produced during the impact of the central, almost parallel, parts of the shell. The minimum attainable duration of the impact (and, accordingly, the maximum possible radiation flux) is determined by the thickness of two shells at the time of their impact. In the overall context of pulse shaping and radiation symmetry, the importance of eliminating gross hydrodynamic instabilities becomes quite clear.

For these ICF capsules to reach ignition, the radiation field at the location of the capsule ablating surface should be spherically symmetric to within an accuracy of ~ 1% in the lower azimuthal modes. Because the Z-pinch geometry does not possess this symmetry, the size of the capsule should be a small fraction of the size of the radius of the dynamic hohlraum. One method of isolating the radiation source from the capsule is to fill the dynamic hohlraum with a low atomic number, low density material that creates a large plasma pressure but is relatively thin to the radiation produced by the stagnation of the imploding plasma. A more radical solution of this problem is an overall spherical symmetrization of the implosion, as shown in Fig. 34b. Although the problem of the

irradiation symmetry is difficult, it does not look insurmountable. Detailed studies of laser-driven hohlraums have shown that one can reach quite satisfactory results by a proper shaping of the hohlraum, by using optimally placed passive screens, and by reducing the pellet diameter to approximately one-third of the diameter of the hohlraum.

An attractive feature of Z-pinch-driven dynamic hohlraums is the relatively low cost of the pulsed-power generator and the high total impact energies (in the range of a few hundred kilojoules to a few megajoules) available in the existing devices like Z, Saturn, or Angara-5.

In addition to radiation temperature, pulse shaping, and symmetry, several other issues should be considered in the design of dynamic hohlraums. We mention some of them here without attempting serious analysis. (1) The ablation surface of the capsule must be isolated from the imploding liners and the shocks that they generate. For example, if the hohlraum is filled with a foam, the shock wave excited in the foam by the impact with the liner must not interact with the ablation surface of the capsule before the capsule implodes. In the case of an empty hohlraum, the low-density ejecta can be of some concern if they reach the capsule before the ablation process is well established. (2) Some low-density blow-off plasma will almost certainly be present inside of an empty hohlraum during the early phase of the Z-pinch implosion (its source can be the radiation preheat during the run-in phase or inductive splitting of the drive current). By itself, because of its low density, it will probably have no significant effect on the pellet. However, if the axial electric field penetrates through the liner, it could generate particle beams in this low-density plasma, which might then cause considerable preheat of the pellet and violate its spherical symmetry. (3) A magnetic field may be generated inside the plasma filling the hohlraum that may affect pellet performance.

All these issues are in a relatively early stage of assessment. On the other hand, none of them seems to pose insurmountable problems for the dynamic hohlraum concept in general. In particular, one could eliminate most of them altogether by using geometries of

the type shown in Fig. 35, where the Z-pinch implosions occurs at the ends of the main hohlraum.

E. Other possible applications

In some modes of operation, especially if the neck formation could be triggered in a controlled way, Z pinches could serve as sources of high-energy, high-intensity beams of charged particles, in particular protons and deuterons. Such beams could then be used for the generation of short-lived isotopes. The proton-rich isotopes required for positron emission tomography for medical purposes could possibly be produced (see Dawson, 1993, for a discussion of a different method of producing these isotopes). The beam could also be used for measuring the nuclear cross-sections for very short-lived isotopes.

Rudakov et al. (1991) and Kingsep et al. (1997) discussed the possibility of creating a very-high-power flux to the electrodes by an adiabatic compression of a plasma by an imploding liner. The heat losses to the liner would be suppressed by an axial magnetic field. The amplification of the flux to the electrodes would occur because of a very strong dependence of the electron thermal diffusivity on the electron temperature ($\chi_e \propto T_e^{5/2}$, see Huba, 1994).

The fact that a Z pinch produces high-intensity radiation with a spectrum that is at least crudely controllable can be used for generating population inversion in various active media. Porter et al. (1992 a,b) have successfully used the radiation of a sodium wire array to pump a Ne gas cell and create a population inversion for the transitions with wavelengths near 11 Å.

Z pinches have already been used for collecting information that could be of interest in astrophysics. Very encouraging results have been achieved in the studies of the opacities of the iron plasma (Springer et al, 1997). Interesting possibilities exist for simulating various high-energy-density astrophysical phenomena — for example, the formation of high-energy intergalactic jets. For this purpose, deliberate creation of jets of the type shown

in Fig. 8 could be made, and their propagation could be detected through the gas or plasma filling the space beyond the anode surface.

IX. SUMMARY AND A GLANCE TO THE FUTURE

The fast Z pinch is a fascinating object, whose behavior is determined by a variety of processes of magnetohydrodynamics, radiative transport, atomic physics, plasma microinstabilities, and beam physics. A particular "shot" is formed by a chain of inseparable stages, from the current initiation and fast early-time instabilities, through the run-in phase where hydrodynamic instabilities distort and broaden the imploding shell, to a final on-axis stagnation, accompanied by a burst of intense radiation, by the possible formation of a transitional quasi-equilibrium configuration, and, sometimes, by disruption of the plasma column and the generation of fast particles. The Z pinch is to a high degree a self-organized object, where a change of a single input parameter may trigger a long chain of tightly interwoven processes occuring on various temporal and spatial scales and leading to an outcome very different from simple "mechanistic" predictions.

We believe that all pieces of physics that are important for the Z-pinch performance have been identified in this survey. Theory and simulations correctly describe many sides of these phenomena. In particular, the gross dynamics of implosions of wire arrays is nicely predicted by 1-D hydrodynamic simulations, which provide a correct value of the time of a pinch collapse on axis (or on the inner cylinder). On the other hand, it is still difficult to predict, based on first principles, the temporal evolution of the thickness of the shell and the experimentally observed shape of the radiation pulse (although, by playing with a few adjustable parameters, one can reach a reasonable agreement). In addition, experimental information on the development of hydrodynamic perturbations during the run-in phase is relatively sparse. More generally, one can say that, although the key

physics phenomena have probably already been identified, their sometimes subtle interplay still requires a much better understanding.

One area where experimental information is almost nonexistent is the direct detection of microturbulence that may be responsible for the anomalous resistance and other effects. Any measurements of this kind are particularly difficult at large facilities, where the huge energy release in the diode region requires heavy shielding and forces one to move the diagnostics equipment to large distances from the pinch area. In such a situation, indirect information can probably be used to detect anomalous plasma resistance. If it is actually present, then one can expect a considerable axial electric field to exist inside the empty imploding shell, leading to generation of electron beams early in the pulse. The other way of making indirect measurements is related to the possibility of changing the composition of the pinch material. For instance, varying the relative amount of a light (say, deuterium) component may considerably affect microturbulence and may interfere with the phenomena of electron magnetohydrodynamics. Effects of electron magnetohydrodynamics can be controlled to certain extent by a weak axial magnetic field that would lift the restriction associated with the current flow across the field lines in the outer part of the pinch. The present survey contains some information and references necessary for the planning of such dedicated experiments, which seem to be quite important. They would allow one to define the parameter domain where fast Z pinches are governed by standard MHD equations, and would establish the significance (or insignificance) of the anomalies outside that domain. Smaller university-scale facilities (of the type described in Haines, 1997 and Bauer et al., 1997) where one can study specific phenomena in a more benign environment can also be of great help.

Previous advances in fast-Z-pinch physics were reached in direct correlation with progress in pulsed power technology: the higher pinch current has always led to a considerable increase in the maximum kinetic energy of the imploding liner and maximum radiation power. A good recent example is the progress made in the transition from the

Saturn facility to the Z facility. The current pulsewidth was increased over a factor of 2 (from ~ 50 to ~ 110 ns) and the current was increased by a factor of ~2.5 (from approximately 7 to approximately 18 MA), resulting in an increase in the radiated energy of a factor of ~5 and an X-ray power increase of a factor of ~3 (see Matzen, 1997). Therefore, it is interesting to discuss what one can expect from a further increase of the pinch current if new facilities become available (as an example, one can refer to a discussion of a 60 MA generator X-1 by Leeper et al., 1998 and of a 50 MA-range facility based on the inductive energy storage by Azizov et al., 1998). In the discussion that follows, we assume that the current can be represented as

$$I=I_{max}f(t/\tau), \tag{9.1}$$

where f is some given bell-shaped function with a maximum equal to 1; in other words, we assume that the shape of the current waveform does not change, only scaling factors over the horizontal (τ) and vertical (I_{max}) axes change (τ has a meaning of pulse-width). For discharges with similar current waveforms, the optimum set of parameters is related by the equation (2.4):

$$\frac{\mu I_{\max}^2 \tau^2}{4\pi\hat{m} r_0^2} = \Pi = const \tag{9.2}$$

Provided the parameter Π is kept constant, the time-histories of the pinch radius are similar for similar current wave-forms (i.e., for the same function f in (9.1)). One can expect that, if the shell thickness h is determined by the hydrodynamic instability, then the thicknesses of two shells with the same value of the parameter Π will also have similar time-histories, i.e., the shell thickness will be proportional to r_0 times some function $g(t/\tau)$, identical for two systems with similar current wave-forms. This would also mean that, in two implosions with the same function f and the same Π, the attainable convergence C_{max} will be the same.

The velocity of the shell scales as r_0/τ,

$$v \sim r_0/\tau\ . \tag{9.3}$$

According to (9.2), this means that the kinetic energy of the shell (per unit length) at the instant of the on-axis collapse scales as I_{max}^2:

$$W_{kin} \propto I_{\max}^2 \tag{9.4}$$

Remarkably, the radius, mass, and implosion time do not enter this relationship. The maximum power Q (per unit length) that can be released in the stagnation is of the order of

$$Q \sim W_{kin}(\mathrm{v}/h) \tag{9.5}$$

where h in this equation is a shell thickness at the instant of the stagnation. For similar implosions, h scales as r_0. Therefore, according to (9.3),

$$Q \propto I_{\max}^2/\tau \tag{9.6}$$

The initial radius of the pinch and the mass $\hat{m}$ do not enter this equation (provided the parameter Π is kept constant). Equations (9.4) and (9.6) provide a rationale for increasing the current in the generators used to feed the pinch discharge; both the maximum attainable implosion energy and the maximum power scale as I^2_{max}. They also show that the maximum power is inversely proportional to the current pulse-width.

Some additional constraints on the parameters of the systems with a higher current may stem from the observation that, at higher currents, some of the applicability conditions of the hydrodynamic description of the system may break down. In particular, at higher currents one may enter the parameter domain where the relative velocity of the electrons and ions would considerably exceed the ion thermal velocity, triggering the onset of anomalous resistivity and increasing the Ohmic losses during the implosion phase. The relative velocity u of electrons and ions scales (for the liners made of the same material) as $I_0/\hat{m}$ (see Eq. (7.1)). The plasma temperature during the implosion of liners of heavy materials is not sensitive to the other parameters of the system and is in the range of 30-40 eV (i.e., the ion thermal speed is essentially constant). For a tungsten liner with T=40 eV and Z_{eff}=6, one finds that the constraint $u<4\mathrm{v}_{\mathrm{Ti}}$ (Eq. (7.5)) can be rewritten as:

$$\frac{I_{\max}(MA)}{\hat{m}(mg/cm)} < 10 \tag{9.7}$$

The electron magnetization parameter $\omega_{Ce}\tau_{ei}$ at a constant temperature (characteristic of the run-in phase), and for liners made of the same material, scales as $I_0 r_0 / \hat{m}$. As we have seen in Sec. VII.A, in implosions of tungsten wire arrays at the Z facility (I_{max}=20 MA, $\hat{m}$=2 mg/cm, r_0=2 cm), the magnetization parameter is ~0.5. Accordingly, the condition that this parameter remains less than 1 can be presented as:

$$\frac{I_{\max}(MA) r_0(cm)}{\hat{m}(mg/cm)} < 40 \qquad (9.8)$$

It is not obvious that violation of the conditions (9.7) and (9.8) should necessarily lead to any catastrophic consequences. Still, to remain in the domain where a relatively simple hydrodynamic description is valid and where successful experiments at the existing devices Z and Saturn have been carried out, it is probably reasonable, in the planning of the future experiments, to take into account constraints (9.7) (9.8). Figure 36 shows the split of the parameter domain by the constraints (9.7)-(9.8) for I_{max}=20 MA, τ=100 ns (Fig. 36a) and I_{max}=60 MA, τ=150 ns (Fig. 36b).

At higher currents, constraints on the dimensions of the diode assembly may become important. If the magnitude of the surface current in the magnetically insulated transmission line (MITL) is too high, an explosion of the skin layer in the MITL may occur within the pulse duration, resulting in a great increase of Joule heating losses in the line. The surface current in the MITL scales as the current divided by the diode radius. To keep this current below its critical value, one would have to increase the diode radius proportionally to the current. The increase of the radius of the return current conductor should be accompanied by a proportional increase of the initial pinch radius (to maintain the parasitic inductances at a low level). Therefore, one concludes that the parameter I_{max}/r_0 should remain below some critical level. Taking this value from the current experiment at the Z facility, we obtain one more constraint on the parameters of the experiment with a higher current:

$$\frac{I_{\max}(MA)}{r_0(cm)} < 15 \ . \qquad (9.9)$$

An inspection of Fig. 36b reveals that there is a broad area in the parameter space where a Z pinch with a current several times higher than the presently-reached level of 20 MA can operate with a high efficiency characteristic of the existing experiments. Taking as an example an operational point shown in Fig. 36b, one finds that, at a liner mass 10 mg/cm, the optimum radius is approximately 4 cm. With the assumed pulse-width of 150 ns, this would give an implosion velocity only 30% higher than in the current experiments. This is beneficial in the sense that collisional relaxation times will remain short, and no further deviations from local thermodynamic equilibrium than in current experiments will occur. At the same time, the total liner energy will increase by a factor of 9, and the power will increase by a factor of 6.

Reaching a higher current may be interesting not only for providing a means for generating higher radiation power or a higher temperature of the dynamic hohlraum but also for a range of problems of more general interest. In particular, it is worth noting that the presently achieved current is only several times less than the so-called proton Alfvén current,

$$I_{pA} \equiv \frac{2\pi m_p c}{e\mu} = 30MA \qquad (9.10)$$

At currents exceeding I_{pA}, the gyroradius of a subrelativistic proton becomes smaller than the radius of the current channel. The attainment of this current may bring about some new interesting phenomena in the generation of high-energy ion beams at the stagnation phase (Sec. VII.B). This may be of great value for the better understanding of the mechanism of the generation of cosmic rays.

In summary, during the past decade, the physics of fast Z pinches has made significant progress, both in terms of pinch parameters attained in experiments at large facilities and in the identification of key physics issues governing pinch phenomenon. In the coming years, one can expect further progress related to: (1) development of diagnostic instrumentation; (2) dedicated experiments at smaller, university-scale facilities; (3)

advances in computer simulations, and (4) development of schemes of mitigation of the most dangerous instabilities. Fast Z pinches will continue to play an important role as the sources of kilo-electronvolt radiation, as drivers for fusion-related experiments, and as sources of information on material properties at extreme conditions. With the development of better means of control of the neck formation at the point of a maximum compression, new possibilities can open for generating high-current beams of heavy ions. Fast Z pinches may also provide important insights into the mechanisms of astrophysical phenomena.

Acknowledgments

The authors are grateful to R. Spielman and M. Douglas for a careful reading of the manuscript and constructive comments. Discussions with our colleagues G. Allshouse (deceased), B. Bauer, R. Bowers, G. Chandler, C. Deeney, M. Haines, J. Hammer, R. Leeper, W. Matuska, D. McDaniel, T. Nash, D. Peterson, J. Porter, J. Quintenz, T. Sanford, J. Seamen, V. Smirnov, P. Springer, B. Stygar, and A. Toor helped us a lot in clarifying various physics issues touched upon in the survey.

This work was supported by the U. S. Department of Energy at Sandia National Laboratories under Contract No. DE-AC04-94AL85000 and at Lawrence Livermore National Laboratory under Contract No. W-7405-ENG-48. Sandia is a multiprogram laboratory operated by Sandia Corporation, a Lockheed Martin Company, for the U.S. Department of Energy.

Figure captions.

Fig. 1 Various types of fast z pinches: a) An annular gaseous jet (Stallings et al., 1979); the axis of the diode is horizontal; the nozzle is a cathode, and the mesh is an anode; the plot at the right shows the radial density distribution; b) A cylinder made of agar foam in a Z-pinch diode (Derzon et al, 1997). An anode in this experiment was a transparent wire mesh; the cylinder (1 cm diameter) is surrounded by eight return-current posts; c) a photograph of a 4-cm diameter tungsten wire aray used in the PBFA-Z facility (Spielman et al, 1997). The array had 240 wires; the mass per unit length of the array was 2 mg/cm; d) A high-Z liner imploding on a low-density foam (Matzen, 1997). An internal ICF capsule is situated in the center of the foam cylinder; e) A quasi-spherical liner implosion (Degnan et al, 1995). An aluminum liner slides along conical electrodes. The initial radius of the outer surface is 4 cm; the time-sequence is: t_1=0; t_2=12.7 μs; t_3=14 μs. The right column represents the results of 2D MHD computations.

Fig. 2 Schematic of the PBFA-Z facility (Spielman et al, 1996). The diameter of the facility is 30m. The outermost part is formed by Marx generators. They are connected to 36 transmission lines with water insulation which, in turn, feed magnetically insulated transmission lines converging at the diode. The diode is situated inside the central tank.

Fig. 3 Cross section view of the PBFA-Z diode with on-axis annular target. There are nine cutaway slots in the current return can for diagnostic access. The PBFA-Z machine is configured with the anode physically on the top of the target, other machines, such as Saturn, are configured with the anode down. The power from the magnetically insulating transmission lines flows to the diode through the gap in the lower part of the figure.

Fig. 4 Measured current (dots), current and wire radius calculated with Screamer code (dashes and solid line, respectively), and Kimfol-filtered (200-280 eV) x-ray diode signal, $\times 10^6$ for PBFA-Z shot 104. Courtesy of K. Struve, SNL. A long "latent period" during which the shell radius decreases very slowly is clearly visible.

Fig. 5 Density distributions for constant velocity implosions. Shown are the profiles with velocities $3 \cdot 10^7$ cm/s and $6 \cdot 10^7$ cm/s. The current waveform was determined self-consistently for the Saturn circuit equations (Hammer et al., 1996).

Fig. 6 Producing a quasi-spherical implosion with an initially cylindrical liner with varying thickness. The liner is thicker near the equatorial plane (Cf. Drake et al., 1996).

Fig. 7 Distortion of the axial magnetic field in the course of a liner implosion (δ is the skin-depth). Strong enhancement of the initial magnetic field occurs within a skin layer; as the perfectly conducting liner moves towards the axis, the magnetic flux initially enclosed by the liner has to be transferred through a thin skin layer. Thick lines depict a cylindrical liner, thin lines with arrows are magnetic field lines.

Fig. 8 Possible scenario of the implosion of a wire array in the case of a hollow anode. The picture is made deliberately asymmetric to emphasize statistical character of the bridge formation.

Fig. 9 Scale size rendition of target compared to time-integrated (TI) and gated x-ray images of the foam target. Plasma jetting along the axis outside of the pinch and near single mode structure between the electrodes is observed. The diameter of the anode ring is 1 cm.

Fig. 10 The slab geometry used in the stability analysis; $\mathbf{g} \equiv -\mathbf{e}_z g$ ($g>0$).

Fig. 11 Density distribution in the shell: a - the case where the density distribution can be characterized by a single length-scale h; b - thin skin-layer, $h_{skin} << h$; c - skin-layer much thicker than the shell thickness.

Fig. 12 Laser shadowgraphs of the Xe liner implosion at the Angara-5 facility (Branitski et al., 1991). The frames are separated by 30 ns; the current was 1.6 MA. The axis of the discharge is vertical. The cathode is at the bottom. The anode (a thick dark strip in the middle of the figure) was made of a mesh, so that the plasma penetrates beyond the anode and produces some perturbations there.

Fig.13 Growth rates for several values of the propagation angle α; the values of α are $\pi/2$, $\pi/4$, and 0 (from the top to the bottom curve).

Fig. 14 The Lagrange coordinates $\xi(z,t)\equiv(\xi_x(z,t); \xi_x(z,t))$ describing implosion of a thin shell.

Fig. 15 Surface density redistribution in the flute mode. The thickness of the solid line roughly corresponds to the density. The dashed line depicts the initial position of the shell.

Fig. 16 Density, pressure and velocity distribution in the plasma column in the case where strong shock is excited. The magnetic piston is situated at the surface 1, the shock wave at the surface 2.

Fig. 17 The plot of amplification factor vs the convergence for the load imploding on axis at the time of the current maximum for purely axisymmetric perturbations.

Fig. 18 Variation of the density distribution caused by the local displacement of the fluid element. The average gradient within the segment *ab* becomes zero.

Fig. 19 Development of a non-linear mode of a thin shell (Basko, 1994). The time is measured in units of the inverse growth rate. The time τ_* of the first appearance of the cusps is in these units equal to $-\ln(k\xi_{\xi 0})$ where $k\xi_{\xi 0}$ is the initial amplitude of the perturbation.

Fig. 20 View of 200-280 eV pinch radiation taken from 88° at Z. The radiation is created by the stagnation of a nested wire array on-axis. The diameter of the radiating zone is approximately 2 mm. Photo courtesy of C. Deeney at SNL.

Fig. 21 Nonlinear stage of the development of the R-T instability. a: flute (axisymmetric) mode (a vertical cross-section); b: non-axisymmetric mode (a horizontal cross-section).

Fig. 22 Numerical results showing the possibility of current disruption by the m=0 mode (a 40 mm diameter tungsten wire array on PBFA-Z after impacting a 2.5 mm radius foam). Courtesy of D. Peterson, LANL

Fig. 23 Overall sketch of the growth rate for the flute mode (upper curve) and the mode propagating at 45° to the magnetic field (lower curve) for a shell with a smooth density distribution that can be characterized by a single spatial scale h; k is a tangential wave number. Shown in the figure is a *maximum* growth rate over all the modes with a given k. This comment becomes significant at large k, where localized (in x) modes form essentially a continuous spectrum, occupying the whole range of Γ, from the maximum one (shown in the figure) to zero.

Fig. 24 Left-right asymmetric coating. Shown in thicker lines are the areas coated by the material with a lower sublimation energy, which will ablate early in the pulse. the direction of the ablation flow is shown by arrows. Diameters of the wires are grossly exaggerated. Only part of the array is shown. Current flows into the paper.

Fig. 25 An effect of a curved surface of a uniform-fill krypton Z pinch (from Douglas, Deeney, and Roderick, 1997). Shown are density isocontours at the same time into the implosion for (a) a straight cylinder; (b) a 1.0 mm circular arc, (c) a 2.5 mm circular arc, and (d) a 5.0 mm circular arc.

Fig. 26 A corrugated wire array. The azimuthal mode number in this case is m=6. The thickness of the line in the panel (a) corresponds to the local surface density of the liner material. The surface of a perfectly conducting liner coincides with one of the field lines. The adjacent field line is shown in dashed line. Panel (b) shows a part of the initial array that can produce a structure similar to the one shown in panel (a): the array is assembled of the wires of two different diameters, $d_1$and d_2.

Fig. 27 The image of filaments near the center of our Galaxy obtained at the wavelength 20 cm (Yusef-Zadeh et al., 1984). According to Trubnikov (1990), they may be pinches.

Fig. 28 Two ion trajectories originating in the same point "O" on the axis and forming initially the same small small angle with the axis. If the initial velocity is directed towards the cathode, the ion trajectory remains in a close vicinity of the axis; if the initial

velocity has an opposite direction, the ion trajectory acquires a peculiar character, with a much slower drift towards the anode.

Fig. 29 The measured currents and x-ray powers from shot Z302, a 40 mm diameter, 96 wire array with 20.3 μm-diameter titanium wires. The load (solid) and MITL (dashed) currents are shown, along with the total power (solid) and kilo-electron-volt (dashed) x-ray powers. From Deeney et al. (1999).

Fig. 30 Experimental arrangements used in the studies of the shock wave propagation (from Olson, 1997): a) the average shock velocity can be measured from comparing the shock breakout times at two steps; b) continuous measurements of the shock velocity can be made in a wedge sample.

Fig. 31 A side-on view (above) and an end-on view (below) of a configuraion with secondary hohlraums attached to the main one and eliminating the effect of a direct irradiation of the sample by the pinch plasma. From Matzen (1997).

Fig. 32 A field-reversed configuration nested inside the liner with axially varying thickness of the walls.

Fig. 33 A schematic of the dynamic hohlraum experiment.

Fig. 34 Various configurations of the dynamic hohlraum. a) A configuration with a shaped inner shell. A hyperboloid of revolution shape can be made from straight wires, by tilting them by the same angle with respect to the axis of revolution; b) A quasispherical implosion. This type of the implosion can be generated also with the initially cylindrical wire array with the axially varying linear mass density. The axial variation of the mass can be reached by a controlled surface deposition technique; the substrate will be an initially uniform wire array.

Fig. 35 A static hohlraum with two Z-pinch radiation sources situated at the ends.

Fig.36 Parameter space for fast Z-pinches: a) I_{max}=20 MA, τ=100 ns; b) I_{max}=60 MA, τ=150 ns. Shaded area represents the domain where conditions (9.7)-(9.9) are satisfied. The bold line corresponds to Eq. (9.2) with

$[I_{max}(MA)]^2[\tau(ns)]^2 / \hat{m}(mg/cm)[r_0(cm)]^2 = 5 \cdot 10^5$ (a typical value for the current experiments).

References

Afonin, V.I., 1995, Plasma Phys. Rep., **21**, 250.

Afonin, V.I., V.M. Murugov, 1998, Plasma Phys. Rep., **24**, 332.

Aivazov, I.K., V.D. Vikharev, G.S. Volkov, L.B. Nikandrov, V.P. Smirnov, V. Ya. Tsarfin. 1988, Sov. J. Plasma Phys., **14**, 110.

Aliaga-Rossel, R., et al., 1998, IEEE Trans. on Plasma Sci., **26**, 1101.

Alikhanov, S.G., et al., 1977, *Plasma Phys. and Contr. Nucl. Fusion Res.*, Proc.of the 6th Intern. Conf., Vienna, IAEA, 1977, v. 3, p. 517.

Alikhanov, S.G., et al., 1981, *Plasma Phys. and Contr. Nucl. Fusion Res.*, Proc.of the 8th Intern. Conf., Vienna, IAEA, 1981, v. 2, p. 699.

Alikhanov, S.G., V.G. Belan, G.I. Budker, A.I. Ivanchenko, G.N. Kichigin, 1967, Sov. J. At. Energy, **22**, 1307.

Alikhanov,S.G., et al., 1984, Sov. J. Plasma Phys.,**10**, 1051.

Al'bikov, V.A., et al., 1990, Soviet J. At. Energy, **68**, #1, 29.

Antolak, A.J., et al., 1997, Rev. Sci. Instrum. **68**, 858.

Apruzese, J.P., et al., 1998, Phys. Plasmas **5**, 4476.

Aranchuk, L.E., S.L. Bogolyubski, O.V. Tel'kovskaya, 1985, Sov. Phys. Techn. Phys., **30**, 1312.

Aranchuk, L.E., et al., 1986, Sov. J. Plasma Phys., **12**, 765.

Aranchuk, L.E., et al., 1997, Plasma Phys. Rep, **23**, 194.

Aranson, I., B. Meerson, P. Sasorov, 1993, Phys. Rev, **E47**, 4337.

Arber, T.D., P.G.F.Russel, M. Coppins, J. Scheffel, 1995, Phys. Rev. Lett., **74**, 2698.

Atchinson, W.L., R.J. Fael, V. Morgan, R.E. Reynovsky, 1997, Paper C204, Conf. on High-Density Z Pinches, Vancouver, Canada.

Averkiev, V.V., A.N. Dolgov, V.K. Lyapidevskii, A.S. Savelov, G. Kh. Shalakhutdinov, 1992, Sov. J. Plasma Phys., **18**, 374.

Azizov, E.A., et al., 1998, Paper CN-69/IF/2 presented at the 17th IAEA Fusion Energy Conference, Yokohama, Japan.

Bailey, J., Y. Ettinger, A. Fisher, N. Rostoker, 1982, Appl. Phys. Lett., **40**, 460.

Baker, W.L., et al., 1978, J. Appl. Phys., **49**, 4694.

Baker, L., J.R. Freeman, 1981, J. Appl. Phys., **52**.

Baksht, R.B., et al., 1987, Sov. Phys. Techn. Phys., **32**, 145.

Baksht, R.B., et al., 1995, Plasma Phys. Rep., **21**, 907.

Baksht, R.B., , et al., 1997, Plasma Phys. Rep., **23**, 135.

Baksht, R.B., A.G. Russkikh, A.A. Chagin, 1997, Plasma Phys. Rep., **23**, 175.

Baksht, R.B., A.G. Russkikh, A.V. Fedyunin, 1995, Tech. Phys., **40**, 1224.

Barak, G., N. Rostoker, 1982, Appl. Phys. Lett., **41**, 918.

Barcilon, A., D.L. Book, A.L. Cooper, 1974, Phys. Fluids, **17**, 1707.

Barnier, J-N., J-M. Chevalier, B.D. Dubroca, J. Rouch, 1998, IEEE Trans. on Plasma Sci., **26**, 1094.

Bartnik, A., G.V. Ivanenkov, L. Karpinski, S.A. Pikuz, T.A. Shelkovenko, 1990, Sov. J. Plasma Phys., **16**, 857.

Bartnik, A., et al., 1994, Quant. Electron., **24**, 169.

Bashilov, Yu. A., S.V. Pokrovskii, 1976, JETP Lett., **23**, 421.

Basko, M.M., 1994, Phys. Plasmas, **1**, 1270.

Bateman, G., 1980, *MHD instabilities* (MIT Press, Cambridge, MA).

Bauer, B., et al., 1997, In: *Dense Z-pinches* (AIP Conf. Proc., v.409), p. 153.

Beg, F.N., et al., 1997, Plasma Phys. Contr. Fusion. **39**, 1.

Benattar, R., et al., 1999, Phys. Plasmas, **6**, 175.

Benford, G., 1978, Appl. Phys. Lett, **33**, 983.

Bennett, W.H., 1934, Phys. Rev., **45**, 890.

Bernstein, I.B., D.L. Book, 1983, Phys. Fluids, **26**, 453.

Bishop, A., 1958, *Project Sherwood (The US Program in Controlled Fusion)* (Addison-Wesley Publishing Company, Inc., Reading, Massachusets, USA).

Bobrova, N.A., T.L. Razinkova, V.P. Sasorov, 1992, Sov. J. Plasma Phys., **18**, 269.

Book, D.L., 1996, Phys. Plasmas, **3**, 354.

Book, D.L., E. Ott, M. Lampe, 1976, Phys. Fluids, **19**, 1982.

Book, D.L., N.K. Winsor, 1974, Phys. Fluids, **17**, 662.

Brackbill, J.U., D.W. Forslund, K.B. Quest, D. Winske, 1990, Phys. Fluids, **27**, 2682.

Braginski, S.I., 1958, Sov. Phys. JETP, **6**, 494.

Braginski, S. I., 1965, In: *Reviews of Plasma Physics* edited by M.A. Leontovich (Consultants Bureau, NY), v.1 p.205.

Branitskii, A.V., et al., 1996, Plasma Phys. Rep., **22**, 277.

Branitski, A.V., et al., 1997, In *Proc. 11th Intern. Conf. on High Power Particle Beams*, Prague, Czech Rep., June 1996 (Czech Ac. Sci.), v.1, p.292.

Branitskii, A.V., et al., 1991, Sov. J. Plasma Phys., **17**, 311.

Branitskii, A.V., et al., 1992 a, Sov. J. Plasma Phys., **18**, 129.

Branitskii, A.V., et al., 1992 b, Sov. J. Plasma Phys., **18**, 588.

Breizman, B.N., D.D. Ryutov, 1974, Nucl. Fusion, **14**, 873.

Brownell, J.H., R.L. Bowers, K.D. McLenithan, D.L. Peterson, 1998, Phys. Plasmas, **5**, 2071.

Budker, G.I., 1973, In *Proc. 6th Europ. Conf. Contr. Fusion and Plasma Phys.*, Moscow, USSR, July 30—Aug. 4, 1973. v.2, p. 136.

Bud'ko, A.B., M.A. Liberman, 1992, Phys. Fluids, **B4** 3499.

Bud'ko, A.B., M.A. Liberman, F.F. Kamenets, 1990, Plasma Phys. Contr. Fusion, **32**, 309.

Bud'ko, A.B., M.A. Liberman, A.L. Velikovich, F.S. Felber, 1990, Phys. Fluids., **B2**, 1159.

Bud'ko, A.B., A.L. Velikovich, M.A. Liberman, F.S. Felber, 1989, Sov. Phys. JETP, **69**, 76.

Burkhalter P.G, J. Shiloh, A. Fisher, R.D. Cowan, 1979, J. Appl. Phys. 50, 4532.

Bychkov, V.V., M.A.Liberman, A.L. Velikovich, 1990, Phys. Rev. A, **42**, 5031.

Camarcat, N., J. Delvaux, B. Etlicher, et al., 1985, Laser and Particle Beams, **3**, 415.

Catto, P.J., 1978, Phys. Fluids, **21**, 30.

Chandrasekhar, S., 1961, *Hydrodynamic and hydromagnetic stability* (Clarendon Press).

Chen, C.J., P.S. Lykoudis, 1972, Solar Phys., **25**, 380.

Chittenden J.P., 1995, Phys. Plasmas, **2**, 1242.

Chittenden, J.P., M.G. Haines, 1990, Phys. Fluids, **B2**, 1889.

Chittenden, J.P., et al., 1997, Phys. Plasmas, **4**, 4309.

Choi, P., C. Dumitrescu-Zoita, 1997, In: *Dense Z-pinches*, (AIP Conf. Proc., v. 409) p. 51.

Chukbar, K.V., 1993 a, Plasma Physics Rep., **19**, 783.

Chukbar, K.V., 1993 b, Plasma Physics Rep., **19**, 785.

Clark, R.W., J.Davis, and F.L. Cochran, 1986, Phys. Fluids, **29**, 1971.

Clark, R.W., R. Richardson, J. Brannon, M. Wilkinson, and J. Katzenstein, 1982, J.Appl. Phys., **53**, 5552.

Cochran, F.L., J. Davis, and A.L. Velikovich, 1995, Phys.Plasmas, **2**, 1.

Coppins, M., I.D. Culverwell, and M.G. Haines, 1988, Phys. Fluids, **31**, 2688.

Dangor, A.E., 1986, Plasma Phys. Contr. Fusion, **28**, 1931.

Davidson, R.C., N.T. Gladd, 1975, Phys. Fluids, **18**, 1327.

Davidson, R.C., N.A. Krall, 1977, Nuclear Fusion, **17**, 1313.

Davis, J., N.A. Gondarenko, A.L. Velikovich, 1997, Appl. Phys. Lett., **70**, 170.

Dawson, J.M., 1993, In: *Proc. of the 2nd Wisconsin Symp. on ^{3}He and Fusion Power*, (University of Wisconsin, WSCAR-TR-AR3-9307-3, J. Santarius, compiler) p. 127.

Deeney, C., et al., 1993, Phys. Fluids, **B5**, 992.

Deeney, C., et al., 1994, J. Appl. Phys., **75**, 2781.

Deeney C., et al., 1997a, Rev. Sci. Instrum., **68**, 653.

Deeney, T. J. et al., 1997b, Phys. Rev. E **56**, 5945.

Deeney, C., et al., 1999, Phys. Plasmas, **6**, 2081.

Deeney, C., et al., 1998a, Phys. Plasmas **5**, 2431.

Deeney, C., et al., 1998b, Phys. Rev. Lett. **81**, 4883.

Deeney, C., D. L. Peterson, R. B. Spielman, K. W. Struve, and G. A. Chandler, 1998c, Phys. Plasmas **5**, 2605.

Degnan, J.H., et al., 1995, Phys. Rev. Lett., **74**, 98.

DeGroot, J.S., et al., 1997a, In: *Dense Z-pinches* (AIP Conf. Proc., v.409) p.157.

DeGroot, J.S., A.Toor, S.M. Goldberg, M.A. Liberman, 1997b, Phys. Plasmas, **4**, 737.

Derzon, M.S., et al., 1996, Phys. Rev. Lett., **76**, 435.

Derzon, M.S., et al., 1997a, Rev. Sci. Instr., **68**, 848.

Derzon, M.S., et al., 1997b, Bull. Am. Phys. Soc., **42**, 1994.

Derzon, M.S., T.J. Nash, D.D. Ryutov, 1997, Bull. Am. Phys. Soc., **42**, 2069.

Desjarlais, M., B. Marder, 1999, Physics of Plasmas, **6**, 2057

Douglas, M.R., C. Deeney, N.F. Roderick, 1997, Phys. Rev. Lett., **78**, 4577.

Douglas, M.R., C. Deeney, and N. Roderick, 1998, Phys. Plasmas 5, 4183.

Drake, J.F., P.N. Guzdar, J.D. Huba, 1983, Phys. Fluids, **26**, 601.

Drake, J.F., J.D. Huba, N.T. Gladd, 1983, Phys. Fluids, **26**, 2247.

Drake, J.F., P.N. Guzdar, A.B. Hassam, J.D. Huba, 1984, Phys. Fluids, **27**, 1148.

Drake, R.P., J.H. Hammer, C.W. Hartman, L.J. Perkins, D.D. Ryutov, 1996, Fusion Technology, **30**, 310.

Esaulov, A.A., P.V. Sasorov, 1997, Plasma Phys. Rep., **23**, 1997.

Felber, F.S., 1982, Phys. Fluids, **25**, 643.

Felber, F.S., et al., 1988a, Phys. Fluids, **31**, 2053.

Felber, F.S., et al., 1988b, J. Appl. Phys., **64**, 3831.

Felber, F.S., M.A. Liberman, and A.L. Velikovich, 1985, Appl. Phys. Lett., **46**, 1042.

Felber, F.S., N. Rostoker, 1981, Phys. Fluids, **24**, 1049.

Fishman, G.J., et al., 1984, Science, **264**, 1313.

Fowler, C.M., W.B. Garn, R.S. Caird, 1960, J. Appl. Phys., **31**, 588.

Freidberg, J.P., 1982, Rev. Mod. Phys., **54**, 801.

Galeev, A.A., R.Z. Sagdeev, 1979, In *Reviews of Plasma Physics*, edited by M.A. Leontovich (Consultants Bureau, N.-Y.), v.7, p.1.

Gasilov, V.A., S.V. Zakharov, A. Yu. Krukowskii, K.V. Skorovarov, 1995, Plasma Phys. Rep., **21**, 399.

Gasque, A.M., et al., 1996, In *Proc. of the 11th Intern. Conf. on High-Power Particle Beams*, Prague, Czech Rep., June 1996 (Czech Ac. Sci.), v.1, p.550.

Giuliani, J.L., Jr., et al., 1990, J. Quant. Spectrosc. Radiat. Tranfer, **44**, 471.

Golberg S.M., M.A.Liberman, A.L.Velikovich, 1990, Plasma Phys. Contr.Fus, **32**, 319.

Gol'berg, S.M., Velikovich, A.L., 1993, Phys. Fluids, **B5**, 1164.

Gonzalez A.G., J. Gratton, 1990, Plasma Phys. and Contr. Fus., **32**, 3.

Gordeev, A.V., 1987, Sov. J. Plasma Phys., **13**, 713.

Gordeev, A.V., A.S. Kingsep, L.I. Rudakov, 1994, Physics Rep., **243**, 215.

Gordeev, A.V., 1999a, Plasma Phys. Rep., 25, 70.

Gordeev, A.V., 1999b, Plasma Phys. Rep., 25, 227.

Gordeev, E.M., et al., 1998, Plasma Phys. Rep., 24, 916.

Gratton, J., F.T. Gratton, A.G. Gonzalez, 1988, Plasma Phys. Contr. Fus., **30**, 435.

Grigor'ev, S.F., Zakharov, S.V., 1987, Sov. Tech. Phys. Lett., **13**, 254.

Guderley, G., 1942, Luftfahrforschung, **19**, 301.

Haines, M.G., 1960, Proc. Roy. Soc., **77**, 643.

Haines, M.G., 1974, J. Plasma Phys., **12**, 1.

Haines, M.G., 1982, Physica Scripta, **T2/2**, 380.

Haines, M.G., 1983, Nucl. Instrum. Methods, **207**, 179.

Haines, M.G., 1989, Plasma Phys. Contr. Fus., **31**, 759.

Haines, M.G., M. Coppins, 1991, Phys. Rev. Lett., **66**, 1462.

Haines M.G., 1997, In *Dense Z-pinches* (AIP Conf. Proc.), v. 409, p. 27.

Haines, M.G., 1998, IEEE Trans. on Plasma Sci., 26, 1275 (1998).

Haines, M.G., et al., 1996, Laser Particle Beams, **14**, 261.

Hammel, B.A., et al., 1994, Phys Plasmas, **1**, 1662.

Hammel, J.E., 1989, In *Dense Z-pinches* (AIP Conf. Proc.), v. 195, p. 303.

Hammer, J.H., 1995, Bull. Am. Phys. Soc., **40**, 1863.

Hammer, J.H., et al., 1996, Phys. Plasmas, **3**, 2063.

Hammer, J.H., et al., 1999, Phys. Plasmas, **6**, 2129.

Hammer, J.H., D.D. Ryutov, 1996, In *Proc. of the 11th Intern. Conf. on High-Power Particle Beams*, Prague, Czech Rep., June 1996 (Czech Ac. Sci.), v.1, p. 178.

Hammer, J.H., D.D. Ryutov, 1999, Phys. Plasmas, **6**, #7.

Harris, E.G., 1962, Phys. Fluids, **5**, 1057.

Hawke, R.S., et al., 1972, Appl. Phys., **43**, 2734.

Hsing, W.W., C.W. Barnes, J.B. Beck, et al., 1997, Phys. Plasmas, **4**, 1832.

Huba, J.D., 1994, NRL Plasma Formulary, NRL/PU/6790-94-265.

Hussey, T.W., Roderick, N.F., 1981, Phys. Fluids, **24**, 1384.

Hussey, T.W., Roderick, N.F., Kloc, D.A., 1980, J. Appl. Phys., **51**, 1452.

Hussey, T.W., M.K. Matzen, N.F. Roderick, 1986, J. Appl. Phys., **59**, 2677.

Hussey, T.W., N.F. Roderick, U. Schumlak, R.B. Spielman, C. Deeney, 1995, Phys. Plasmas, **2**, 2055.

Imshennik, V.S., 1992, Sov. J. Plasma Phys., **18**, 349.

Imshennik, V.S., Neudachin V.V., 1987, Sov. J. Plasma Phys., **13**, 707.

Imshennik, V.S., Neudachin V.V., 1988, Sov. J. Plasma Phys., **14**, 393.

Inogamov, N.A., 1985, PMTF, **5**, 110.

Isichenko, M.B., K.L. Kulyabin, V.V. Yan'kov, 1989, Sov. J. Plasma Phys., **15**, 617.

Ivanenkov, G.V., A.R. Mingaleev, S.A. Pikuz, V.M. Romanova, and T.A. Shelkovenko, 1996, Plasma Phys. Rep., **22**, 363.

Kadomtsev, B.B., 1966, In: *Reviews of Plasma Physics* edited by M.A. Leontovich (Consultants Bureau, NY), v.2, p. 153.

Kalantar, D. H., et al., 1999, Rev. Sci. Instrum., **42**, 2068.

Kalantar, D., D. Hammer, 1993, Phys. Rev. Lett., **71**, 3806.

Kalantar, D.H., et al., 1997, Bull. Am. Phys. Soc., **42**, 1953.

Katzenstein, J., 1981, J.Appl. Phys., **52**, 676.

Kilkenny, J.D., et al., 1994, Phys. Plasmas, **1**, 1379.

Kingsep, A.S., V.I. Kosarev, A.I. Lobanov, A.A. Sevast'yanov, 1997, Plasma Phys. Rep., **23**, 953.

Kingsep, A.S., L.I. Rudakov, 1995, Plasma Phys. Rep., **21**, 576.

Kleev, A.I., A.L. Velikovich, 1990, Plasma Phys. Contr. Fus., **32**, 763.

Kloc, D., N.F. Roderick, T.W. Hussey, 1982, J. Appl. Phys., **53**, 6706.

Kolb, A.S., 1960, Rev. Mod. Phys., **32**, 74.

Krall, N.A., P.C. Liewer, 1971, Phys. Rev., **A4**, 2094.

Kull, H.J., 1991, Physics Rep., **206**, 197.

Landau, L.D., E.M.Lifshitz, 1987, *Fluid Mechanics* (Pergamon Press, New York).

Lazier, S.E., T.L. Barber, M.S. Derzon, J.W. Kellogg, 1997, Rev. Sci. Instr., **68**, 660.

Lebedev, S.V., et al., 1998a, Phys. Plasmas, **5**, 3366.

Lebedev, S.V., et al., 1998b, Phys. Rev. Lett., **81**, 4152.

Lebedev, S.V., et al., 1999, Phys. Plasmas, **6**, 2016.

Leeper, R.J., et al ., 1998, Paper CN-69/OV3/4 presented at the 17th IAEA Fusion Energy Conference, Yokohama, Japan.

Leeper, R.J., et al., 1997, Rev. Sci. Instr., **68**, 871.

Lezzi, A.M., A. Prosperetti, 1989, Phys Fluids, **A1**, 1784.

Lindemuth, I.R., 1990, Phys. Rev. Lett., **65**, 179.

Lindemuth, I.R., et al., 1996, *Plasma Physics and Controlled Nuclear Fusion Research* (Proc. of the 16th Intern. Conf., Vienna, IAEA), v.2, p.723.

Lindemuth, I.R., R.C. Kirkpatrick, 1983, Nucl. Fusion, **23**, 263.

Lindl, J., 1995, Phys. Plasmas, **2**, 3933.

Linhart, J.G., 1993, In *Dense Z-pinches* (AIP Conf. Proc.), v. 299, p. 664.

Lisitsyn, I.V., S. Katsuki, and H. Akiyama, 1999, Phys. Plasmas, **6**, 1389.

MacFarlane, J.J., et al., 1997, Rev. Sci. Instr., **68**, 1069.

Manheimer, W., D. Colombant, E. Ott., 1984, Phys. Fluids, **27**, 2164.

Matuska, W., et al., 1996, Phys. Plasmas, **3**, 1415.

Matzen, M.K., 1997, Phys. Plasmas, **4**, 1519.

Matzen, M.K., et al., 1999, Plasma Phys. Contr. Fus. **41**, A175.

Maxon, S., et al., 1996, Phys. Plasmas, **3**, 1737.

Meek, J.M., J.D. Craggs, 1978, *Electric breakdown of gases* (John Wiley & Sons, NY).

Meierovich, B.E., 1986, Sov. Phys. Usp. **29**, 506.

Meierovich, B.E., Sukhorukov, S.T., 1991, Sov. J. Plasma Phys., **17**, 598.

Mikaelian, K.O., 1996, Phys. Rev. **E 54**, 3676.

Mitchell, I.H., et al., 1998, IEEE Trans. on Plasma Sci., **26**, 1267.

Miyamoto, T., 1984, Nucl. Fusion, **24**, 337.

Mokhov,V.N., et al., 1979, Sov. Phys. Dokl.,**24**, 557.

Mosher, D., D. Colombant, 1992, Phys. Rev. Lett., **68**, 2600.

Mosher, D., et al., 1998, Bull. Am. Phys. Soc., **43**,

Munro, D.H., 1988, Phys. Rev. A, **38**, 1433.

Muron, D.J., M.J. Hurst, M.S. Derzon, 1997, Rev. Sci. Instrum., **68**, 656.

Nash, T.J., et al., 1997a, Rev. Sci. Instrum., **68**, 1083.

Nash, T.J., et al., 1997b, In *Dense Z-pinches* (AIP Conf. Proc.), v. 409, p. 175.

Nash, T.J., et al., 1999, Phys. Plasmas, **6**, 2023.

Nedoseev, S.L., 1991, In *Phys.of Alternative Magn. Conf. Schemes* (Proc. Intern. School of Plasma Phys. "Piero Caldirola", Editrici Compsitori, Bologna) p. 575.

Neudatchin, V.V., P.V. Sasorov, 1991, Nucl. Fusion, **31**, 1053.

Olson, R.E., et al., 1997, Phys. Plasmas, **4**, 1818.

Olson R.E., et al., 1999, Fusion Technology, **35**, 260.

Ott, E., 1972, Phys. Rev. Lett. **29**, 1429.

Pashinin, P.P., A.M. Prokhorov, 1971, Sov. Phys. JETP, **60**, 1630.

Parks, D.E., 1983, Phys. Fluids, **26**, 448.

Pease, R.S., 1956, Proc. Roy. Soc., **70**, 11.

Peratt, A.L., 1986, IEEE Trans. Plasma Sci., **PS-14**, 639.

Peratt, A.L., 1990, IEEE Trans. Plasma Sci., **PS-18**, 26.

Pereira, N.R., 1990, Phys. Fluids, **B2**, 677.

Pereira, N.R., J. Davis, 1988, J. Appl. Phys., **64**, R1.

Pereira, N.R., N. Rostoker, J.S. Pearlman, 1984, J. Appl. Phys., **55**, 704.

Peterson, D.L., et al., 1996, Phys. Plasmas, **3**, 368.

Peterson, D.L., et al., 1997, In *Dense Z-pinches* (AIP Conf. Proc.), v. 409. p. 201.

Peterson, D. L, et al., 1998, Phys. Plasmas **5**, 3302.

Peterson, D.L., et al., 1999, Phys. Plasmas, **6**, 2178.

Phillips, J.A., 1987, In *McGraw-Hill Encyclopedia of science and Technology*, (McGraw-Hill, New York), v.13, p. 521,

Pikuz S.A., et al., 1997, In *Dense Z-pinches* (AIP Conf. Proc.), v. 409, p. 429.

Porter, J.L., 1997, Bull. Am. Phys. Soc., **42**, 1948.

Porter, J. L., et al., 1992a, Phys. Rev. Lett., **68**, 796

Porter, J. L., R.B. Spielman, M.F. Vargas, M.K. Matzen, 1992b, Rev. Sci. Instrum., **63**, 5703.

Potter, D., 1978, Nuclear Fusion, **18**, 813.

Raizer, Yu.P., 1991, *Gas Discharge Physics* (Springer Verlag, Berlin-Heidelberg).

Rahman, H.U., P. Amendt, N. Rostoker, 1985, Phys. Fluids, **28**, 1528.

Rahman, H.U., F.J. Wessel, N. Rostoker, 1995, Phys. Rev. Lett., **74**, 714.

Remington, B.A., et al., 1997a, Bull. Am. Phys. Soc., **42**, 1840.

Remington, B.A., et al., 1997b, Phys. Plasmas, **4**, 1994.

Robson, A.E., 1989, In *Dense Z-pinches* (AIP Conf. Proc.), v. 195, p. 362.

Robson, A.E., 1991, Phys. Fluids, **B3**, 1461.

Robson, A.E., 1993, In *Dense Z-pinches* (AIP Conf. Proc.), v. 299, p. 707.

Roderick, N.F., 1986, J. Appl. Phys., **60**, 1269.

Roderick, N.F., T.W. Hussey, 1984, J. Appl. Phys., **56**, 1387.

Roderick, N.F., T.W. Hussey, 1986, J. Appl. Phys., **59**, 662.

Roderick, N. F., et al., 1998, Phys. Plasmas **5**, 1477.

Rosen, M.D., 1996, Phys. Plasmas, **3**, 1803.

Rosenau, P., R.A. Nebel, H.R. Lewis, 1988, Phys. Fluids, **B1**, 1233.

Rostoker, N., G.G. Peterson, H. Tahsiri, 1995, Comments on Plasma Phys. and Contr. Fus., **16**, 129.

Rudakov, L.I., K.A. Baigarin, Y.G. Kalinin, V.D. Korolev, M.A. Kumachov, 1991, Phys Fluids, **B3**, 2414.

Rudakov, L.I., A.A. Sevastyanov, 1996, Plasma Phys. Rep., **22**, 1095.

Ruden, E., H.U. Rahman, A. Fisher, N. Rostoker, 1987, J. Appl. Phys., **61**, 1311.

Ryutov, D.D., 1996, Phys. Plasmas, **4**, 4376.

Ryutov, D.D., 1997, 2nd Symp. *Current trends in international fusion research*, Wash. DC, March 1997, p.44.

Ryutov, D.D., A. Toor, 1998, Phys. Plasmas, **5**, 22.

Sakharov, A.D., et al., 1965, Sov. Phys. Doklady, **10**, 1045.

Samokhin, A.A., 1988, J. Appl. Mech. Techn. Phys., **29**, 243.

Sanford, T.W.L., et al., 1996, Phys. Rev. Lett., **77**, 5063.

Sanford, T.W.L., et al., 1997a, Phys Plasmas, **4**, 2188.

Sanford T.W.L., et al., 1997b, Rev. Sci. Instrum., **68**, 852.

Sanford, T. W. L., et al., 1998a, Phys. Plasmas **5**, 3737.

Sanford, T. W. L., et al., 1998b, Phys. Plasmas **5**, 3755.

Sanford, T.W.L., et al., 1999a, Phys Plasmas, **6**, 1270.

Sanford, T.W.L., et al., 1999b, Phys Plasmas, **6**, 2030.

Sarkisov, G.S., B. Etlicher, 1995, JETP Lett., **61**, 797.

Sarkisov, G.S., B. Etlicher, S. Attelan, C. Rouille, 1995a, JETP Lett., **61**, 555.

Sarkisov, G.S., et al., 1995b, JETP Lett., **61**, 484.

Sarkisov, G.S., et al., 1995c, JETP, **81**, 743.

Sasorov, P.V., 1991, Sov. J. Plasma Phys., **17**, 874.

Sasorov, P.V., 1992, Sov. J. Plasma Phys., **18**, 143.

Scheffel, J., T.D. Arber, M. Coppins, P.G.F. Russel, 1997, Plasma Phys. Contr. Fus., **39**, 559.

Sethian, J.D., A.E. Robson, K.A. Gerber, A.W. DeSilva, 1987, Phys. Rev. Lett., **59**, 892.

Sevast'yanov, A.A., 1993, Plasma Phys. Rep., **19**, 227.

Sharp, D.H., 1984, Physica, **12D**, 3.

Shiloh, J., A. Fisher, N. Rostoker, 1978, Phys. Rev. Lett., **40**, 515.

Shiloh J, A. Fisher, E. Bar-Avraham, 1979, Appl. Phys. Lett., **35**, 390.

Shumlak, U., Hartman, C., 1995, Phys. Rev. Lett., **75**, 3285.

Shumlak, U, and N.R. Roderick, 1998, Phys. Plasmas, **5**, 2384.

Skowronek, M., P. Romeas, 1985, J.App. Phys., **57**, 2519.

Smirnov, V.P., 1991, Plasma Phys. Contr. Fus., **33**, 1697.

Smith, R.S., W.O. Doggett, 1985, Appl. Phys. Lett., **46**, 1128.

Spielman, R.B., et al., 1985a, J. Appl. Phys., **57**, 830.

Spielman, R.B., et al., 1985b Appl. Phys. Lett., **47**, 229.

Spielman, R.B., et al., 1989, Proc. 7th IEEE Pulsed Power Conf., Monterey, p. 445.

Spielman, R.B., et al., 1996, In *Proc. of the 11th International Conf. on High-Power Particle Beams*, Prague, Czech Rep., 1996, (Ac. Sci. Czech Rep.), v. 1, p. 150.

Spielman R.B., et al., 1997, In *Dense Z-pinches* (AIP Conf. Proc.), v. 409, p. 101.

Spielman, R. B., et al., 1998, Phys. Plasmas **5**, 2105.

Springer, P. T., et al., 1997, J. Quant. Spectrosc. Radiat. Transfer, **58**, 927.

Stallings, C, K. Childers, I. Roth, R. Schneider, 1979, Appl. Phys. Lett., **35**, 524.

Stamper, J.A., K. Papadopoulos, R.N. Sudan, S.O. Dean, E.A. McLean, 1971, Phys. Rev. Lett, **26**, 1012.

Struve, K.W., et al., 1997, 11 IEEE Int. Pulsed Power Conf., Baltimore, MD, June 29-July 2, 1997.

Stygar, W.A., et al., 1997, 11 IEEE Int. Pulsed Power Conf., Baltimore, MD, June 29-July 2, 1997.

Suydam, B.R., 1958. *Proc. 2nd Intern. Conf. on the Peaceful Uses of Atomic Energy*, Geneva, Switzerland, v. 31, p. 157.

Thornhill J.W., K.G. Whitney, J. Davis, 1990, J. Quant. Spectrosc. Radiat. Transfer, **44**, 251.

Thornhill, J.W, J. Davis, J.P. Apruzese, K.G. Whitney, F.L. Cochran, 1997, *In Dense Z-pinches* (AIP Conf. Proc.), v. 409, p. 193.

Tonks, L., 1937, Trans. Electrochem. Soc., **72**, 167.

Tonks, L., 1939, Phys. Rev., **56**, 360.

Toor, A., D. Ryutov, 1997, Bull. Am. Phys. Soc., **42**, 2053.

Trubnikov, B.A., 1986, Sov. J. Plasma Phys., **12**, 271.

Trubnikov, B.A., 1990, Sov. Phys. Usp., **33**, 1061.

Turchi, P.J., W.L. Baker, 1973, J. Appl. Phys., **44**, 4936.

Turchi, P.J., A.L. Cooper, R. Ford, D.J. Jenkins , 1976, Phys. Rev. Lett., **36**, 1546.

Uman, M.A., 1986, *All about lightning* (Dover Publications).

Vedenov, A.A., D.D. Ryutov, 1975, In *Reviews of Plasma Physics* edited by M.A. Leontovich (Consultants Bureau, NY), v.6, p. 1.

Vekshtein, G.E., 1990, In *Reviews of Plasma Physics* edited by B.B. Kadomtsev (Consultants Bureau, NY), v.15, p. 1.

Velikhov, E.P., et al., 1972, Sov. Phys. Dokl., **17**, 772.

Velikovich, A.L., 1991, Sov. Phys. Techn. Phys., **36**, 210.

Velikovich, A.L., F.L. Cochran, J. Davis, 1996, Phys. Rev. Lett., **77**, 853.

Velikovich, A.L., Davis, J., 1995, Phys. Plasmas, **2**, 4513.

Veretennikov, V.A., et al., 1992, Sov. J. Plasma Phys., **18**, 131.

Vikhrev, V.V., 1986, Sov. J. Plasma Phys., **12**, 262.

Vikhrev, V.V., S.I. Braginski, 1986, In *Reviews of Plasma Physics* edited by M.A. Leontovich (Consultants Bureau, NY), v. 10, p. 425.

Volkov, G.S., Utyugov, E.G., Frolov, I.N., 1993, Plasma Phys. Rep., **19**, 579.

Volkov, G.S., et al., 1999, Plasma Phys. Rep., **25**, 34.

Wessel, F.J., et al., 1986, Appl. Phys. Lett., **48**, 1119.

Whitham, G.B., 1974, *Linear and Nonlinear Waves* (John Wiley & Sons, New York).

Whitney, K.G., J.W.Thornhill, J.P.Apruzeze, J. Davis, 1990, J. Appl. Phys.,**67**, 1725.

Whitney, K.G., et al., 1994, Phys Rev **E50**, 2166.

Wong, K.L., et al., 1998, Phys. Rev. Lett. **80**, 2334.

Yan'kov, V.V., 1991, Sov. J. Plasma Phys., **17**, 305.

Yonas, G., 1998, Sci. Am., **279**, 40.

Youngs, D.L., 1991, Phys. Fluids, **A3**, 1312.

Yusef-Zadeh, F., M. Morris, D. Chance, 1984, Nature, **310**, 557.

Zel'dovich, Ya.B., Yu.P. Raizer, 1967, *Physics of Shock Waves and High-Temperature Hydrodynamic Phenomena* (Academic Press, NY and London).

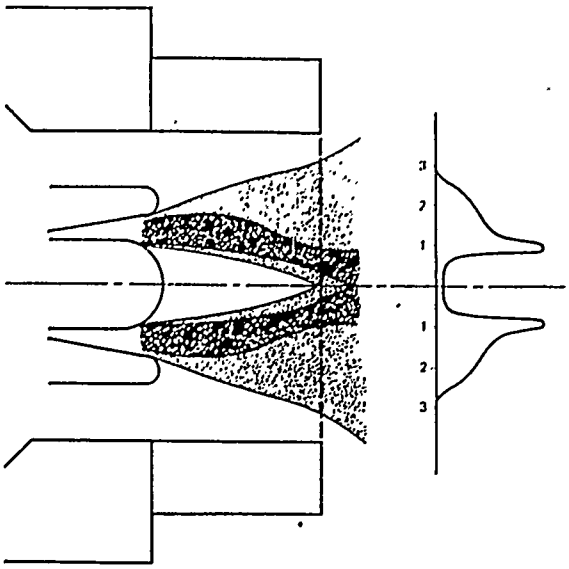
3
2
1
1
2
3

(a)

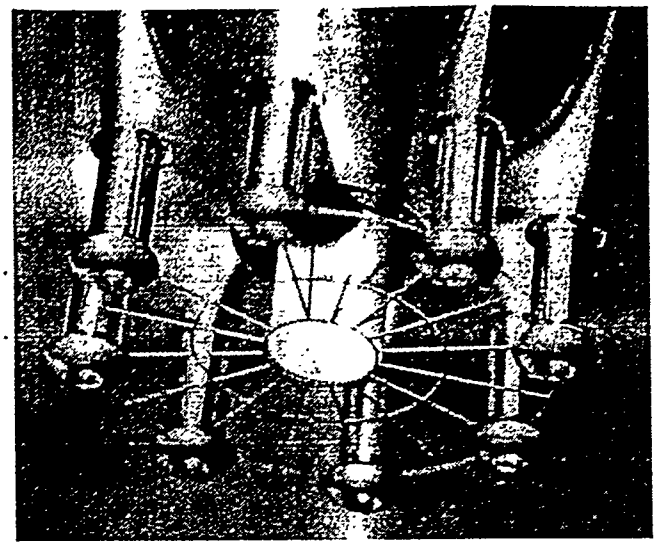

(b)

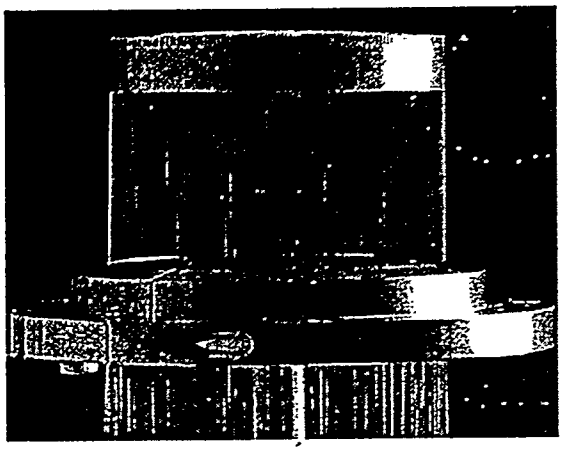

(c)

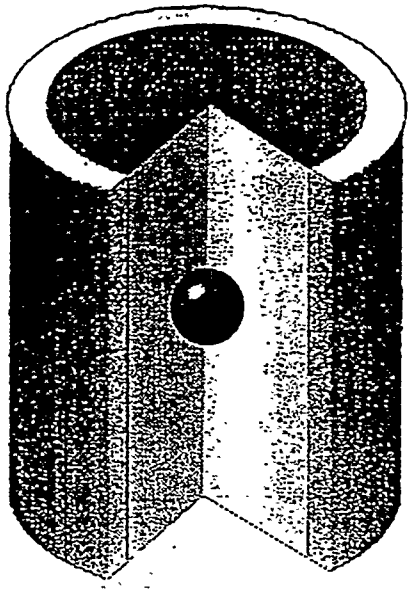

(d)

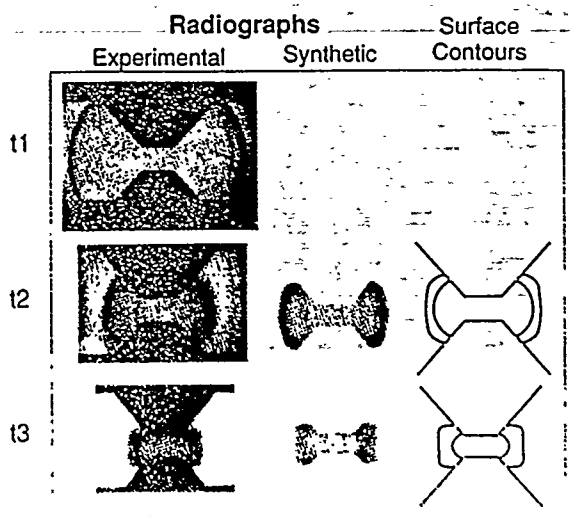
Radiographs
Surface
Experimental
Synthetic
Contours
t1
t2
t3

(e)

Fig. 1

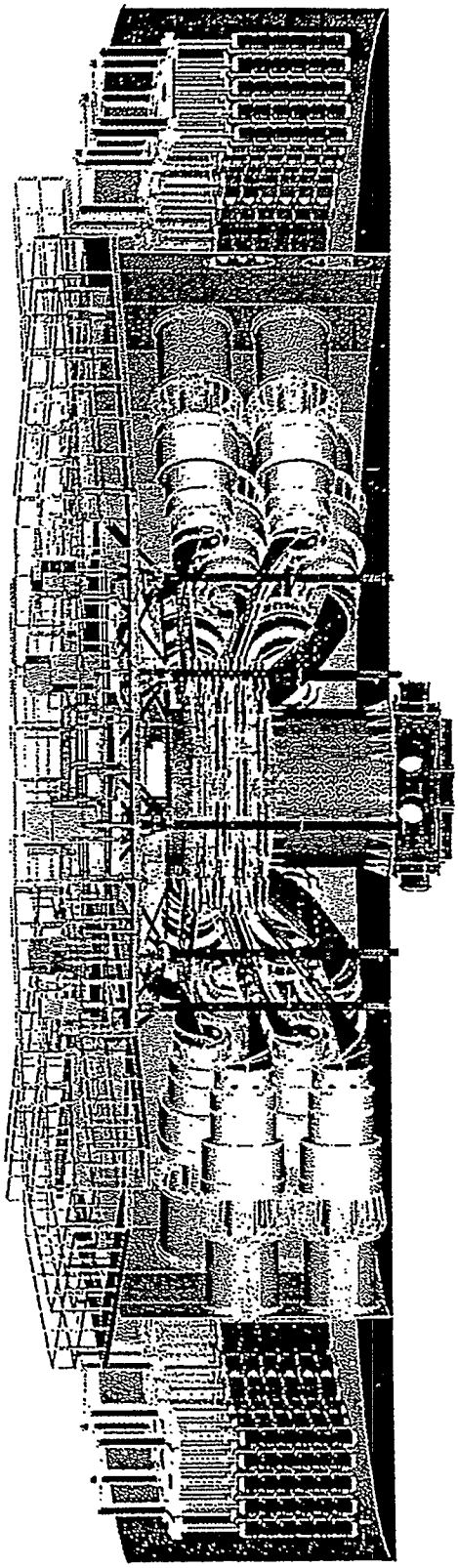

Fig 2

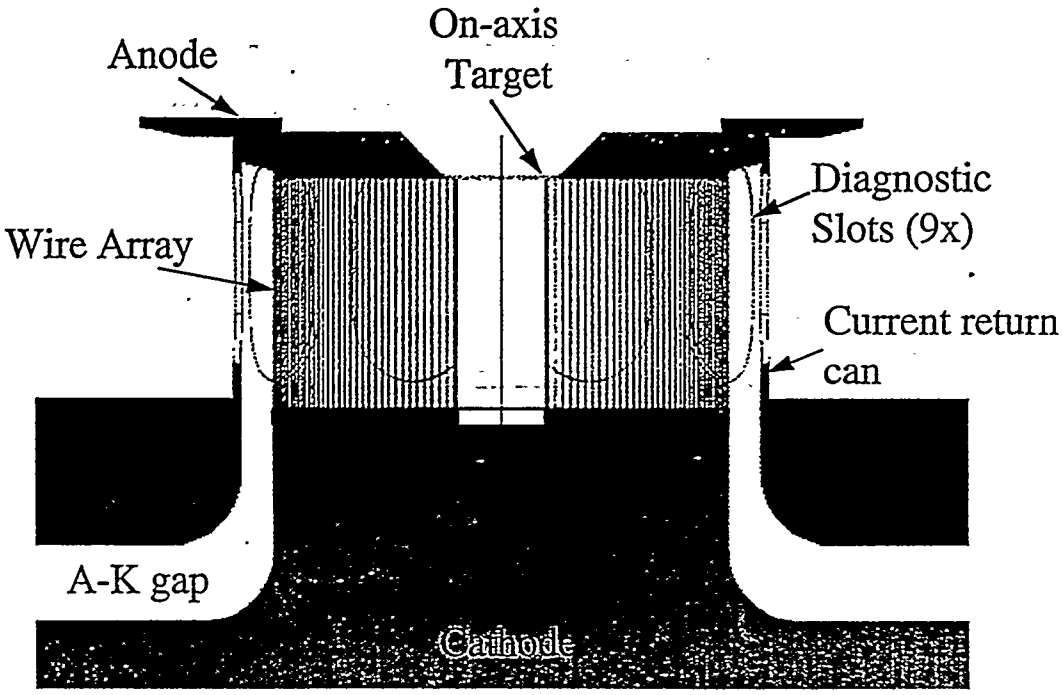
Anode
On-axis
Target
Diagnostic
Slots (9x)
Wire Array
Current return
can
A-K gap
Cathode

Fig. 3

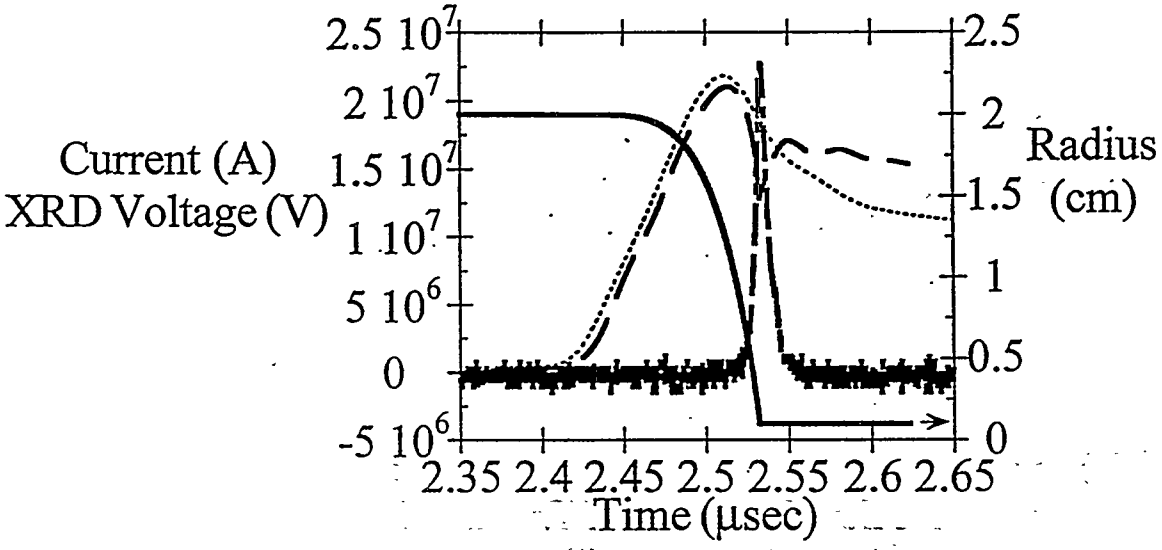
Current (A)
XRD Voltage (V)
2.5 10^7
2 10^7
1.5 10^7
1 10^7
5 10^6
0
-5 10^6
2.35 2.4 2.45 2.5 2.55 2.6 2.65
Time (μsec)
2.5
2
1.5
1
0.5
0
Radius
(cm)

Fig. 4

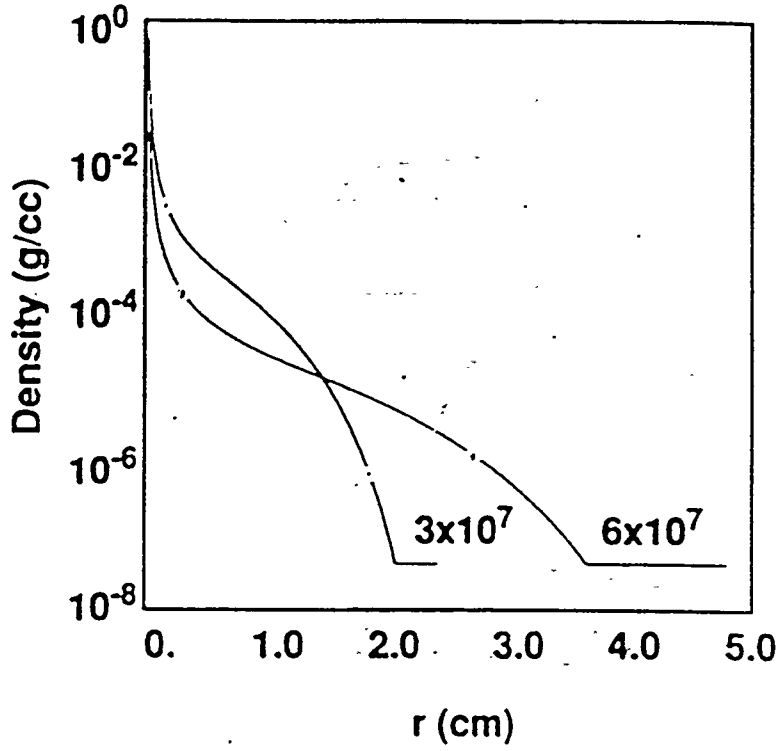

Fig. 5

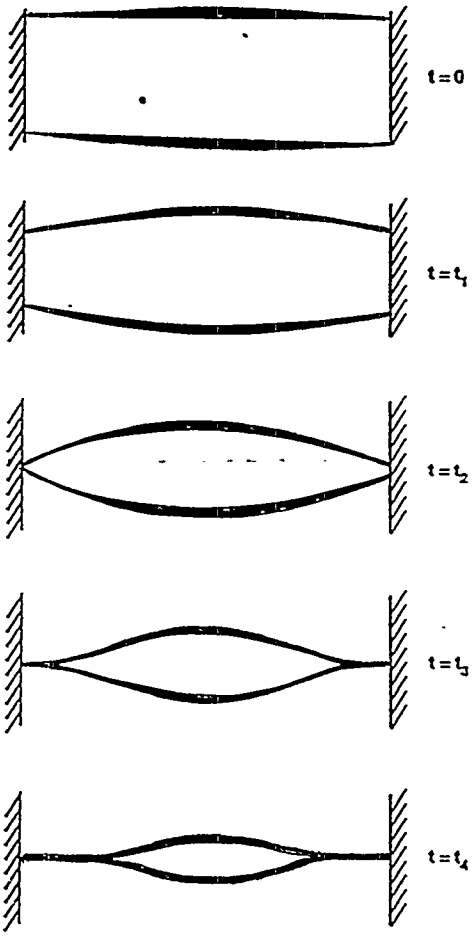
t=0
t=t1
t=t2
t=t3
t=t4

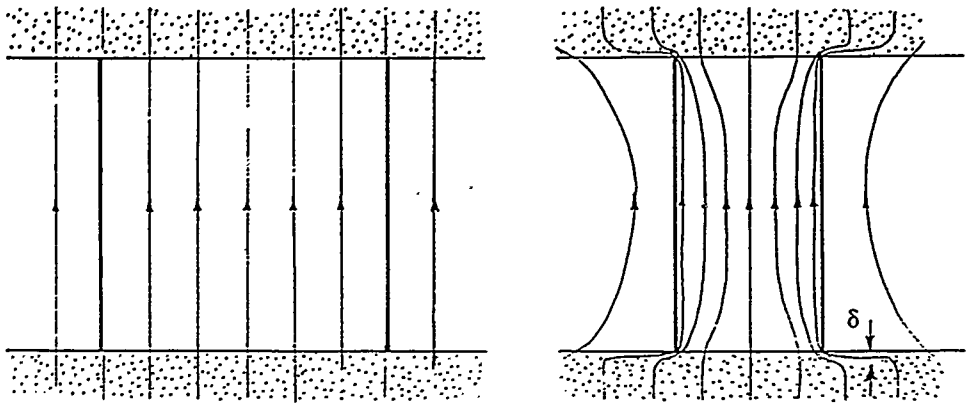

a *b*

Fig. 7

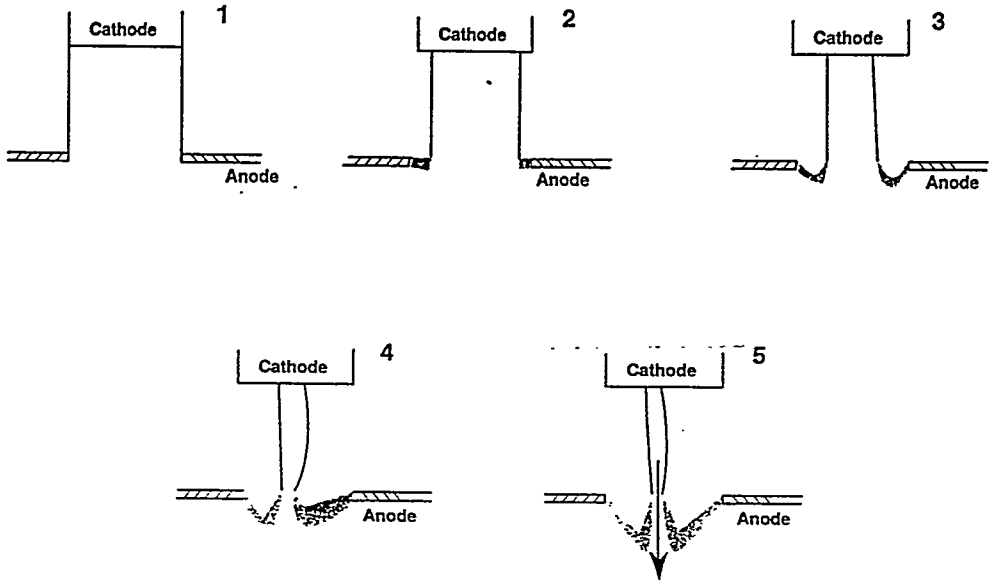
Cathode
1
Anode
Cathode
2
Anode
Cathode
3
Anode
Cathode
4
Anode
Cathode
5
Anode

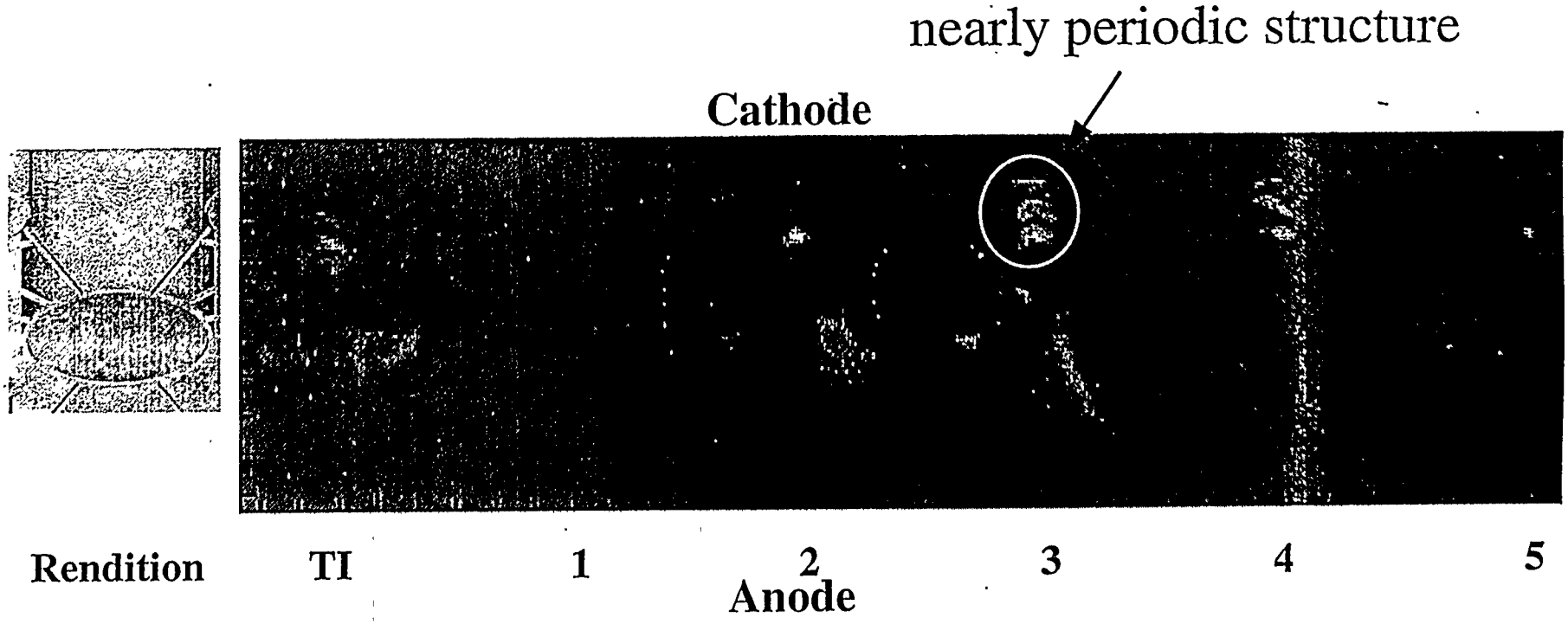
nearly periodic structure
Cathode
Rendition
TI
1
2
3
4
5
Anode

Fig. 9

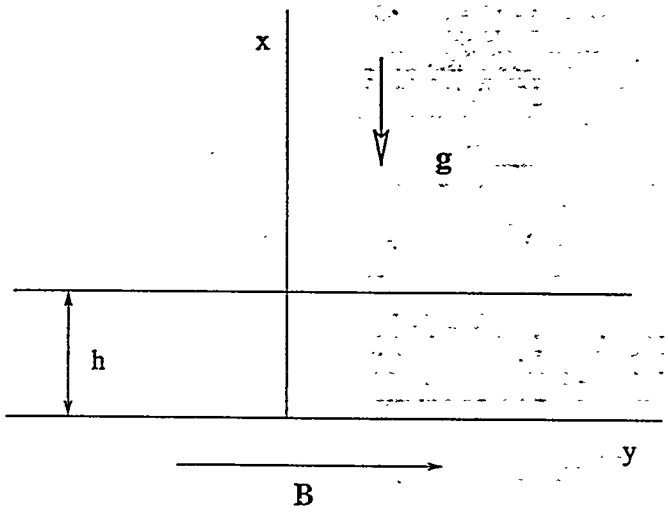

Fig. 10

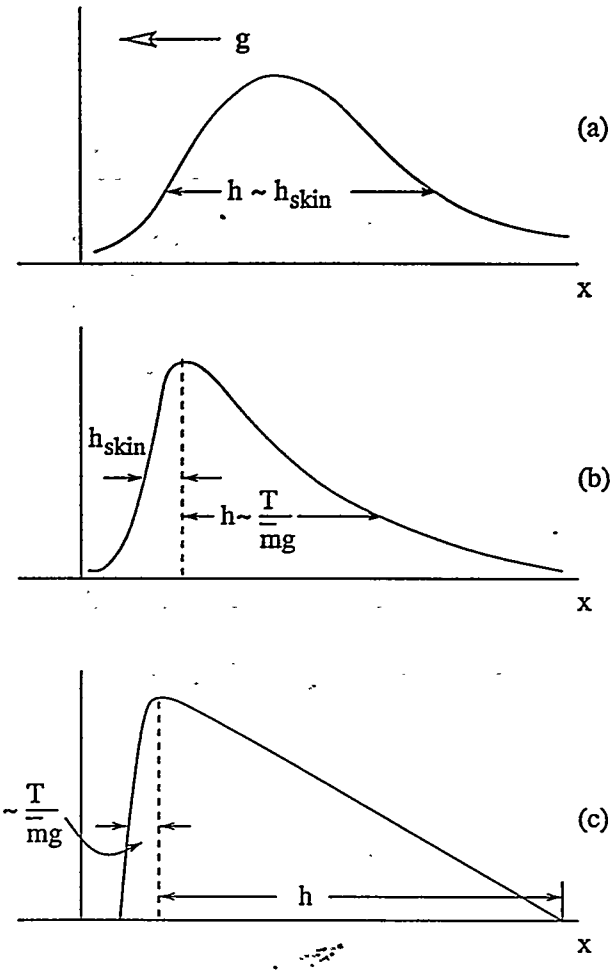
g
(a)
h ~ h_{skin}
x
h_{skin}
(b)
h~ $\frac{T}{mg}$
x
~ $\frac{T}{mg}$
(c)
h
x

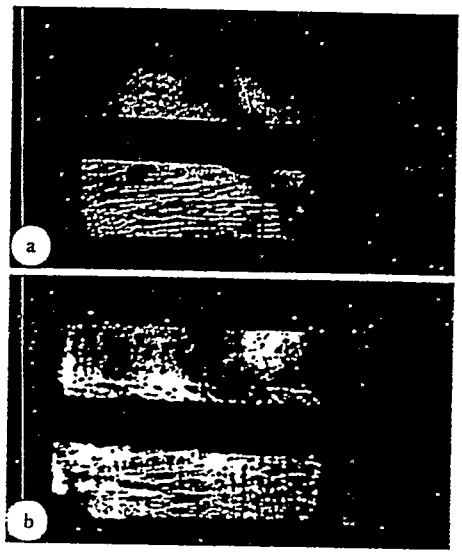

Fig. 12

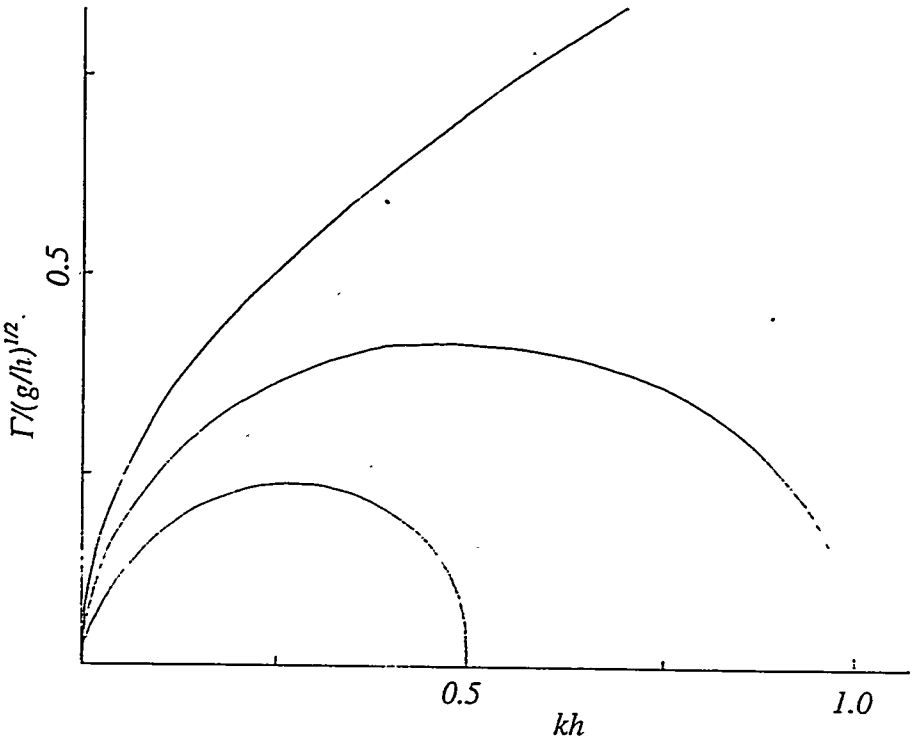
0.5
$\Gamma/(g/h)^{1/2}$
0.5
1.0
kh

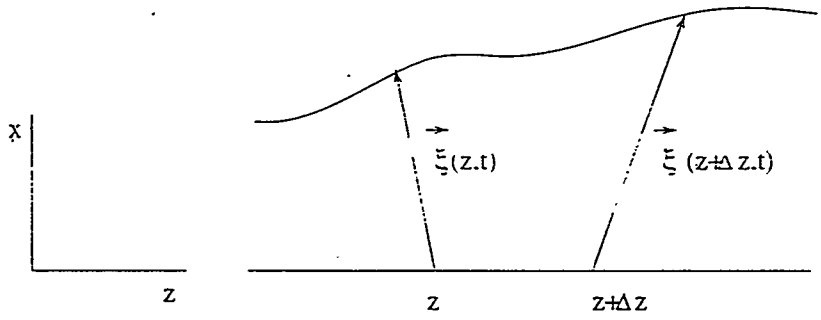
x
z
ξ(z.t)
ξ (z+Δ z.t)
z
z+Δz

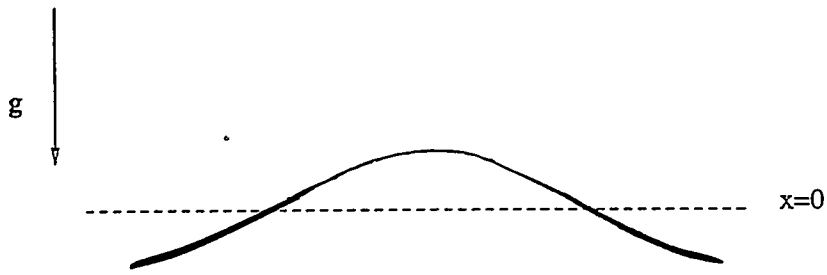
g
x=0

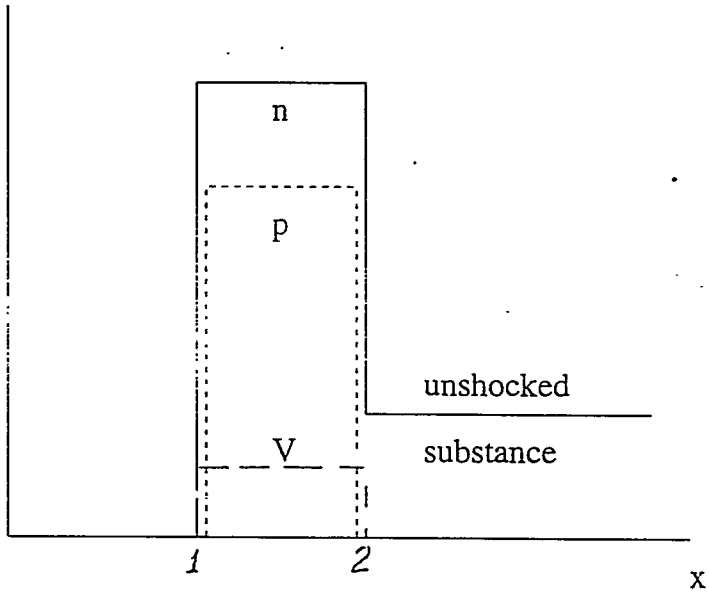
n
p
unshocked
substance
V
1
2
x

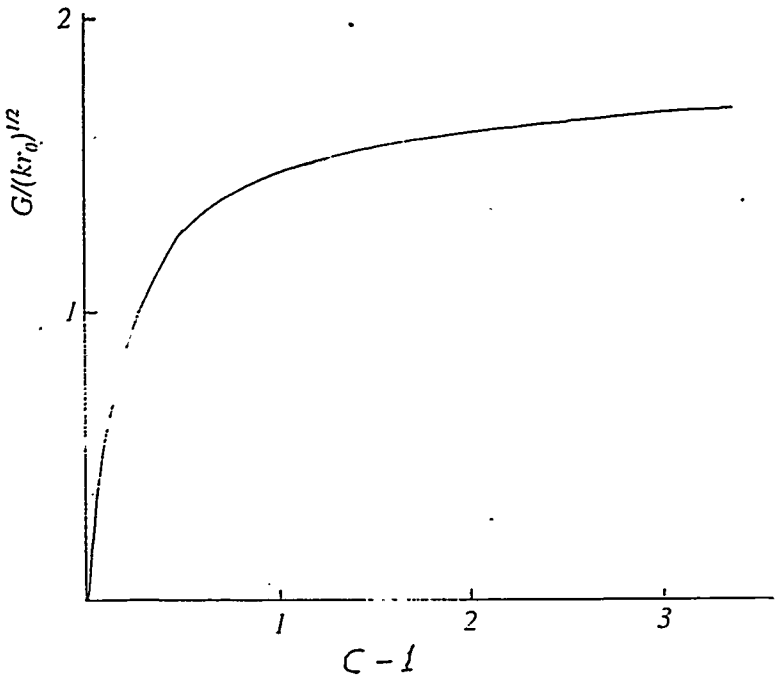
2
1
$G/(kr_0)^{1/2}$
1
2
3
C-1

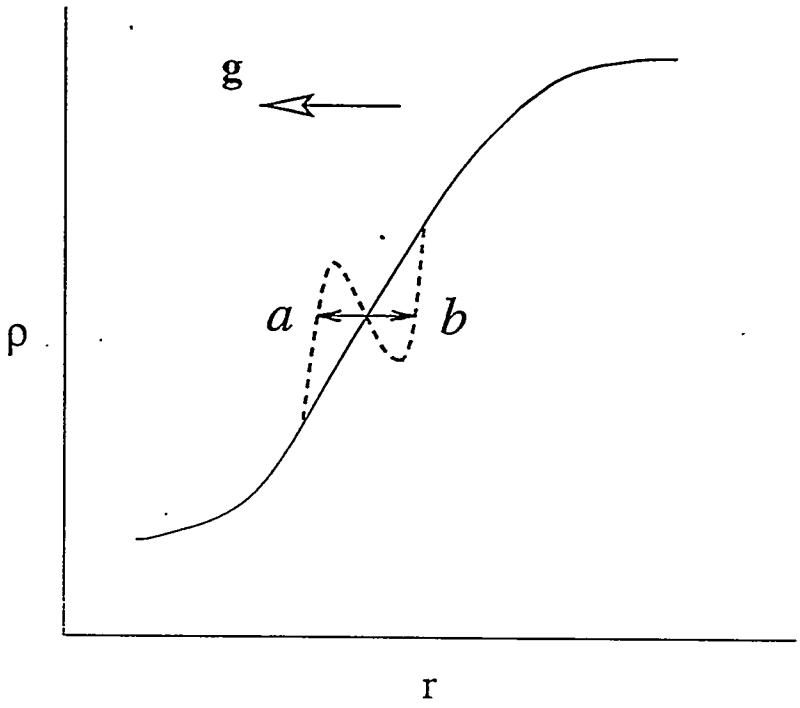
g
a
b
ρ
r

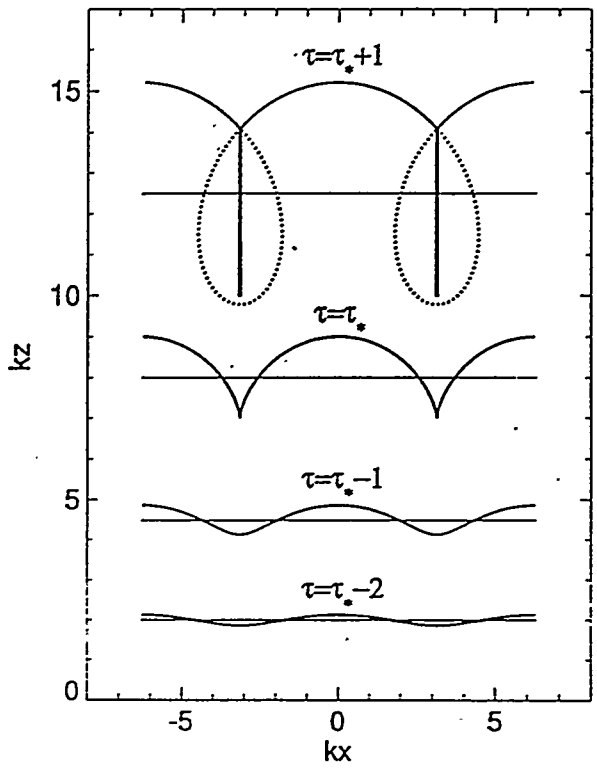
τ=τ*+1
τ=τ*
τ=τ*−1
τ=τ*−2
15
10
5
0
kz
-5
0
5
kx

[redacted]

20

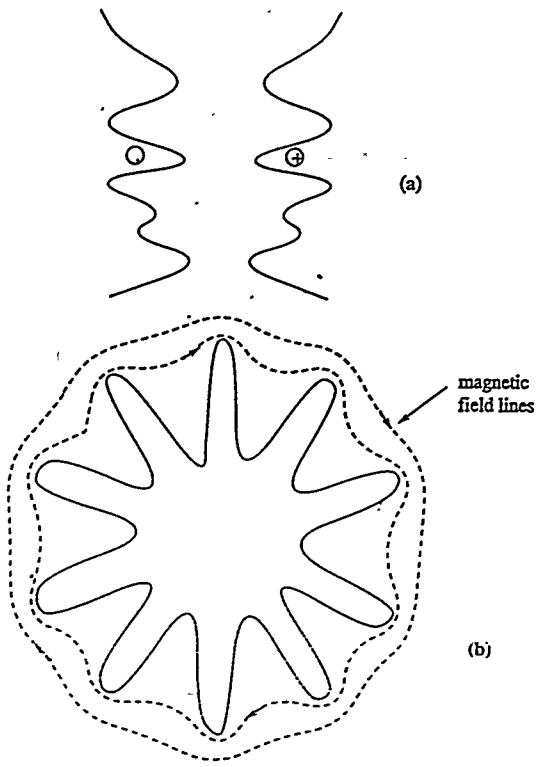

Fig. 21

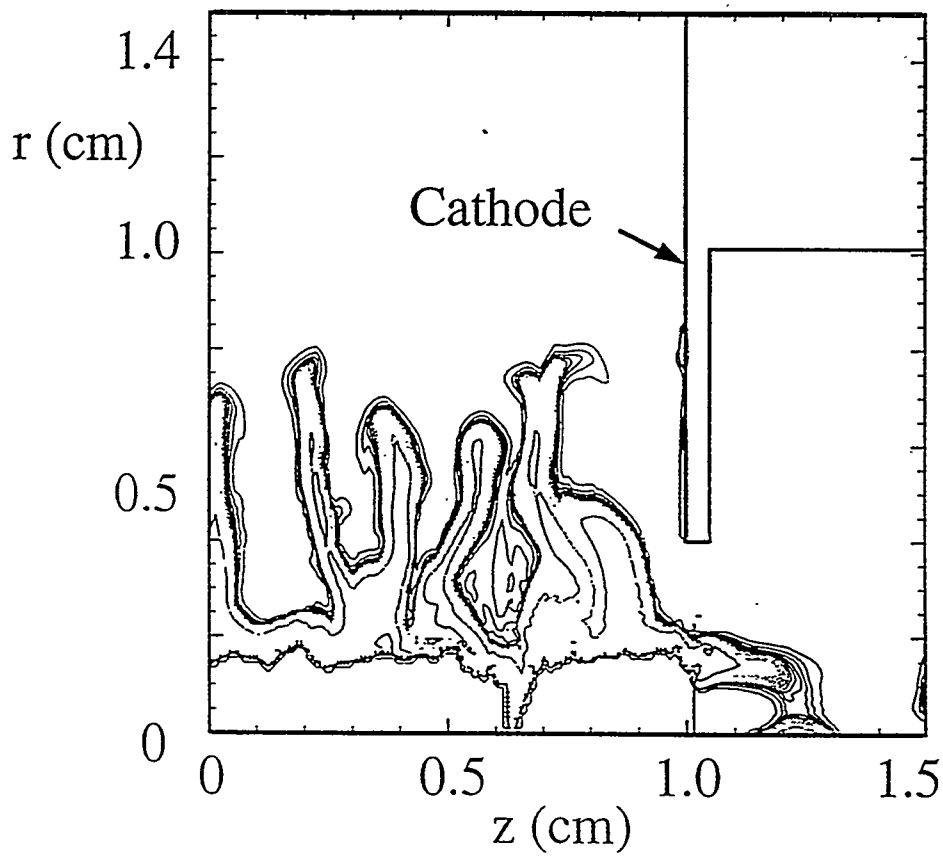
1.4
r (cm)
1.0
0.5
0
Cathode
0
0.5
1.0
1.5
z (cm)

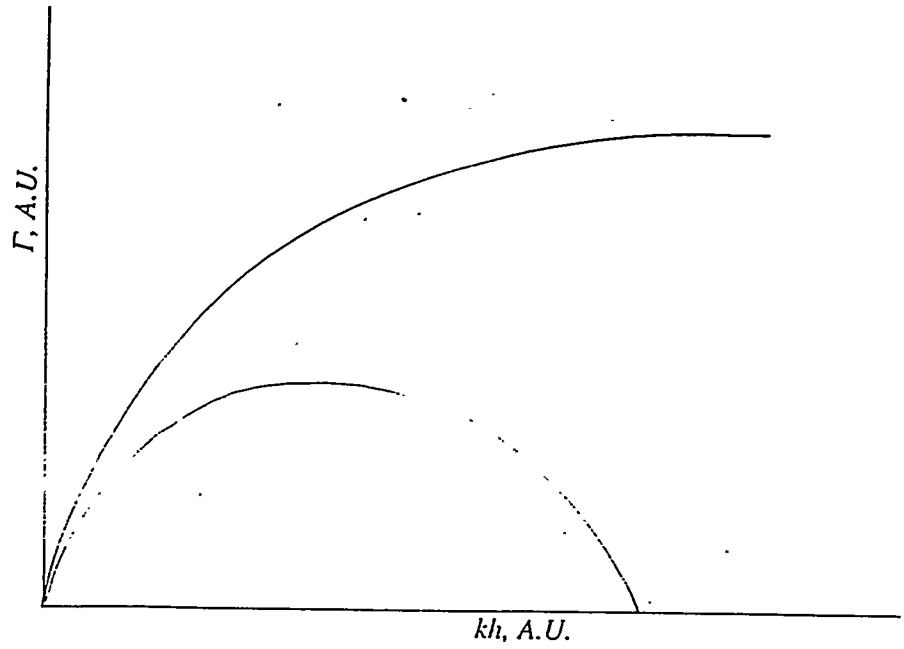

Fig. 23

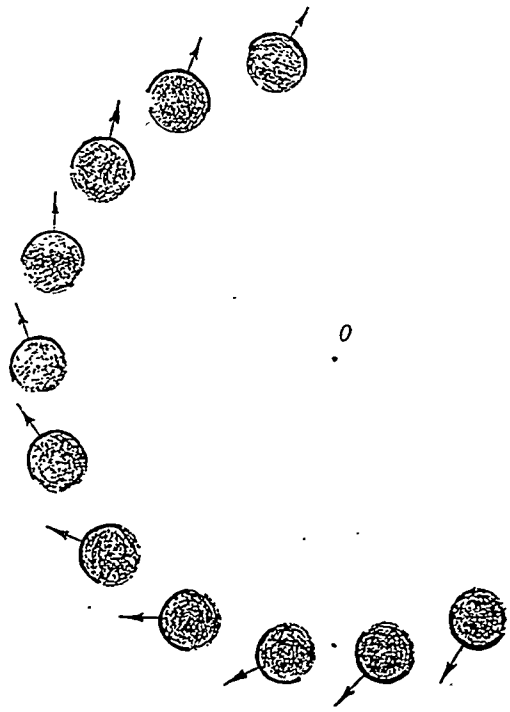
O

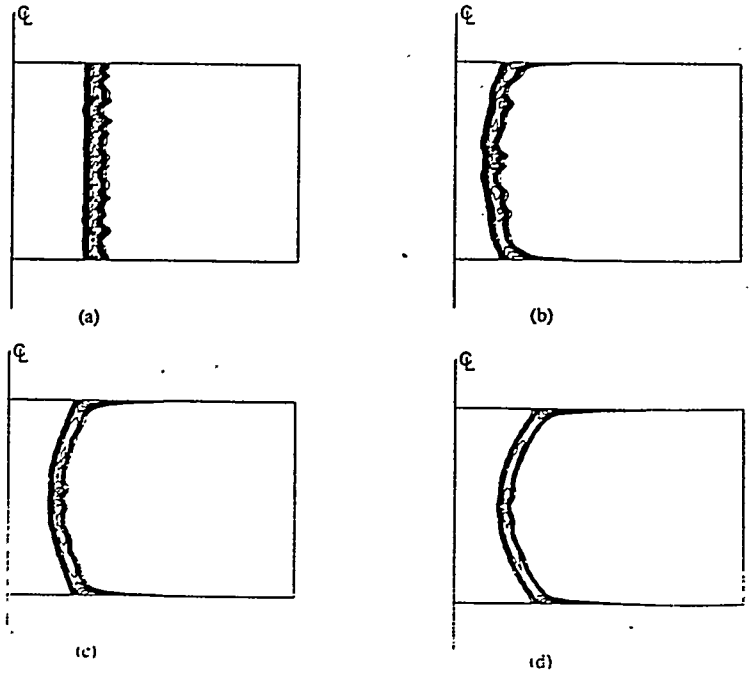

T: 25

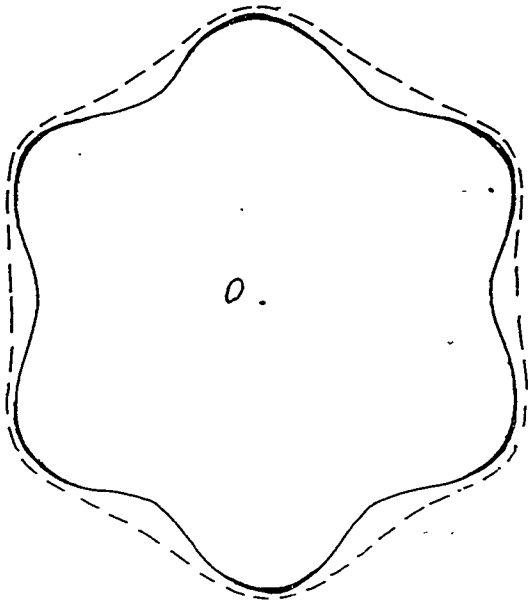

(a)

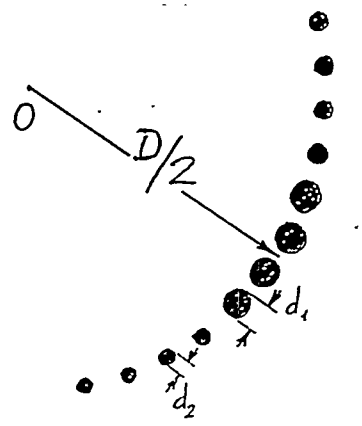

(b)

Fig. 26

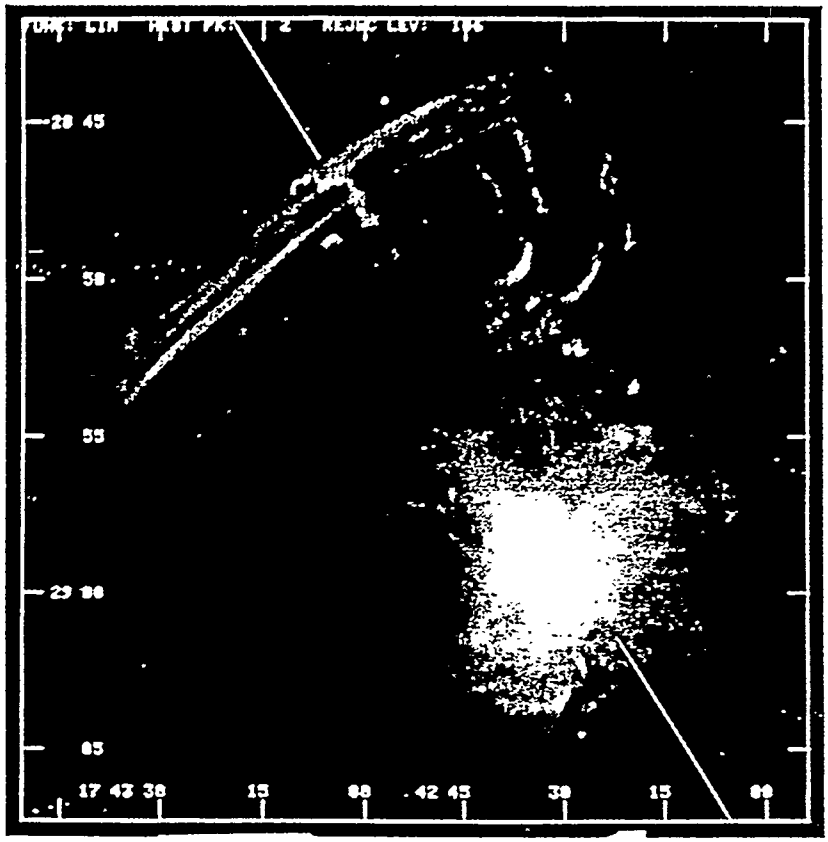

Fig 27

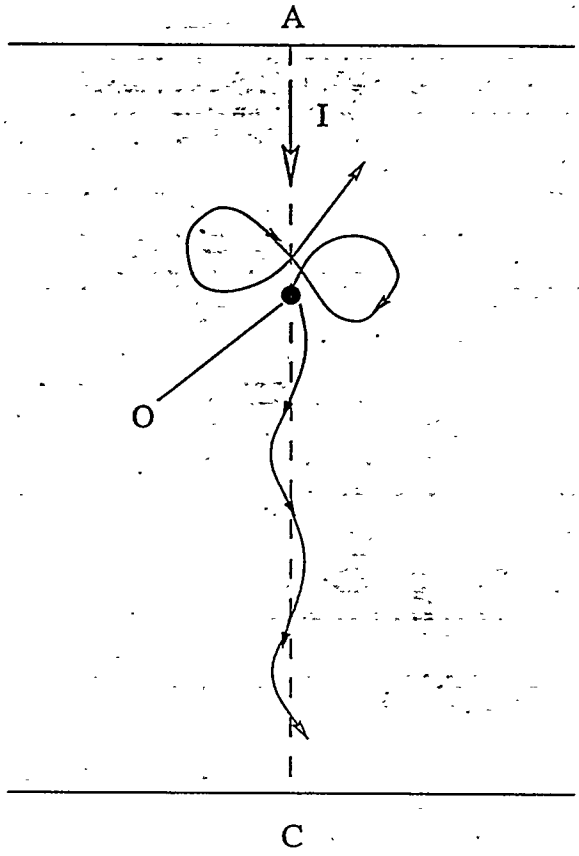
A
I
O
C

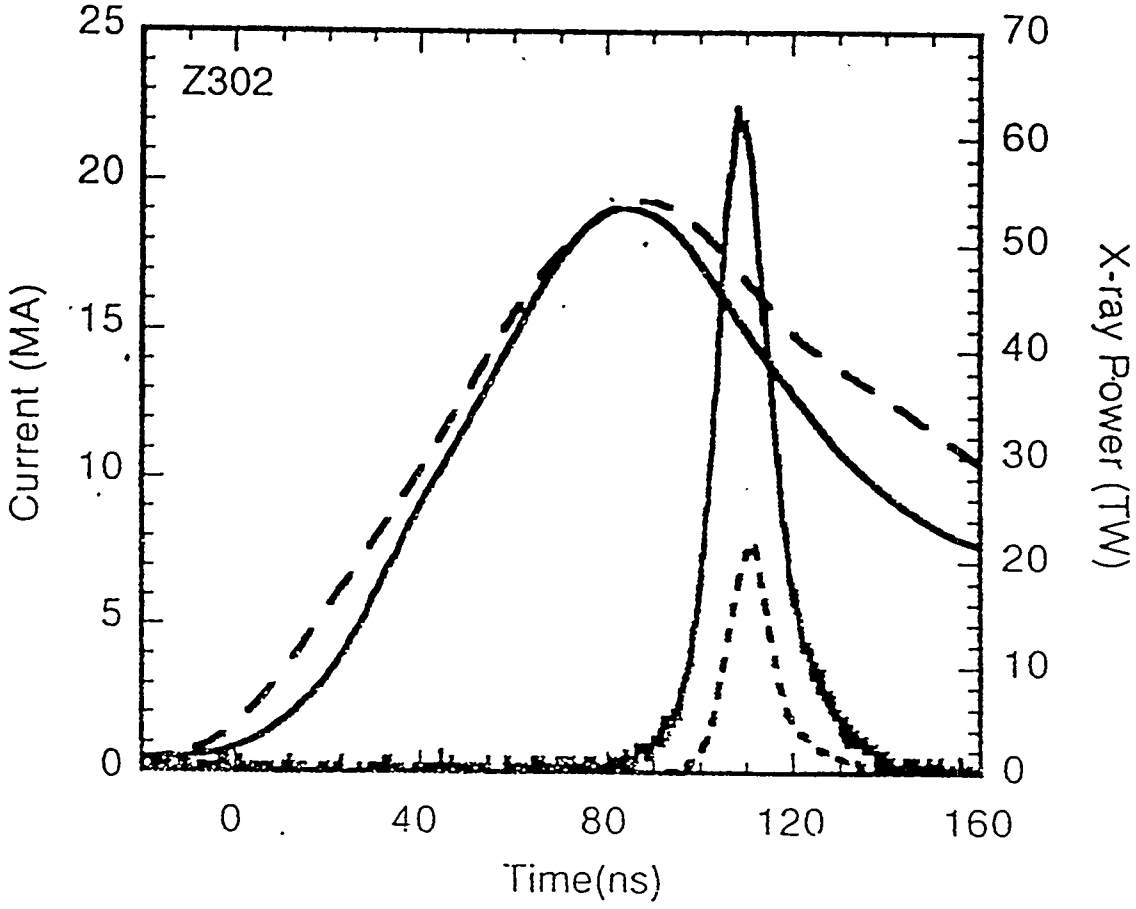
Z302
Current (MA)
X-ray Power (TW)
Time(ns)
0
5
10
15
20
25
0
10
20
30
40
50
60
70
0
40
80
120
160

F. 29

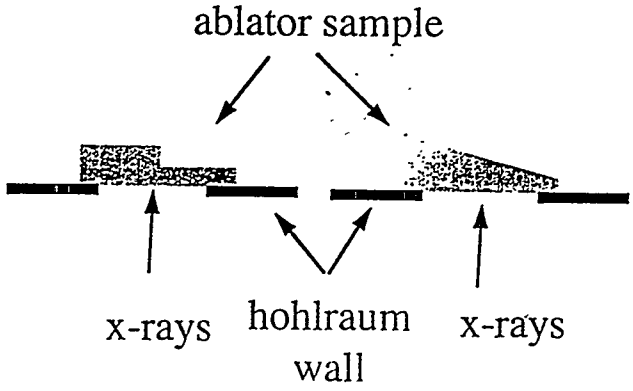
ablator sample
x-rays
hohlraum wall
x-rays

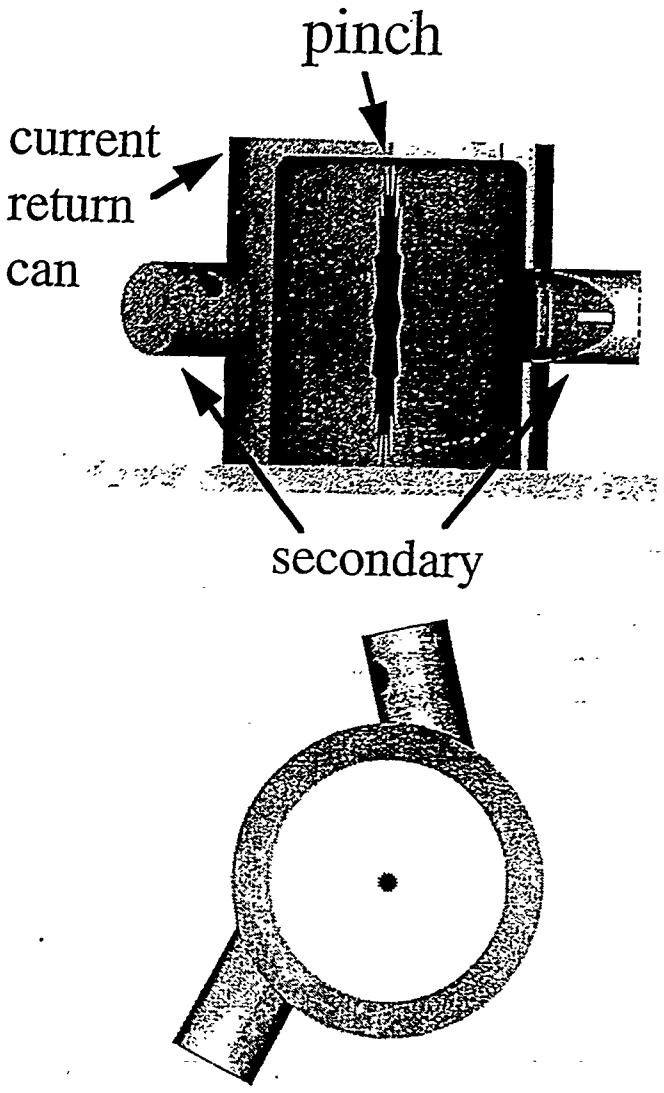

Fig. 31

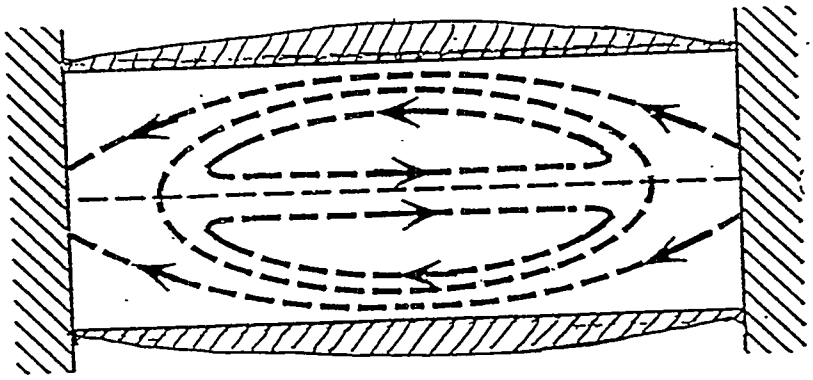

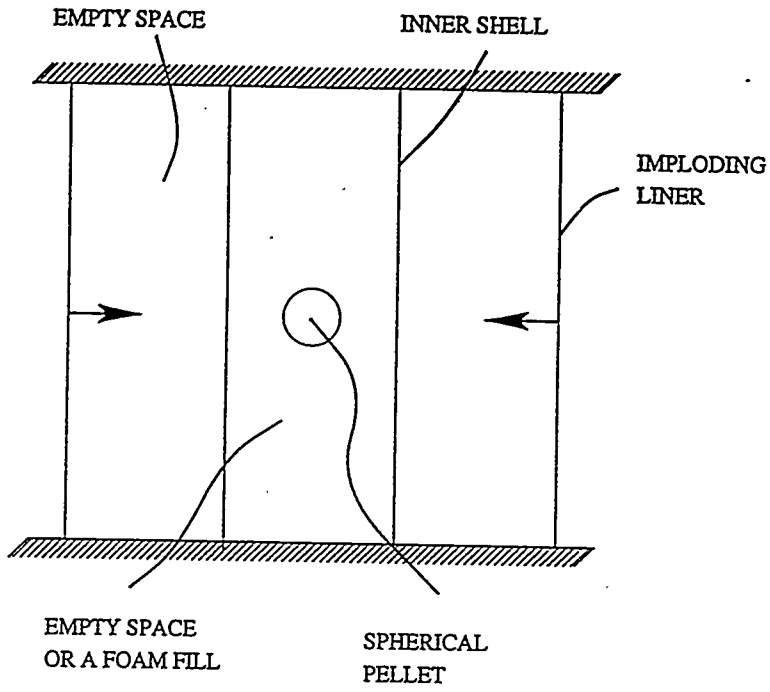
EMPTY SPACE
INNER SHELL
IMPLODING
LINER
EMPTY SPACE
OR A FOAM FILL
SPHERICAL
PELLET

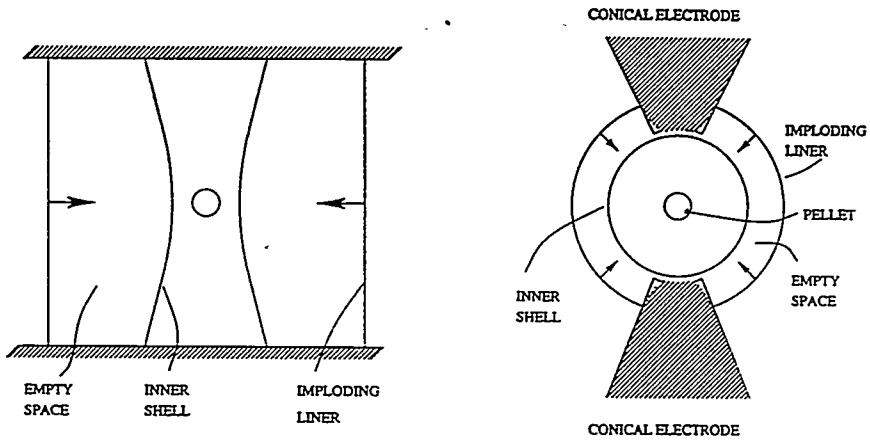
EMPTY SPACE
INNER SHELL
IMPLODING LINER
(a)
CONICAL ELECTRODE
IMPLODING LINER
PELLET
EMPTY SPACE
INNER SHELL
CONICAL ELECTRODE
(b)

Fig. 34

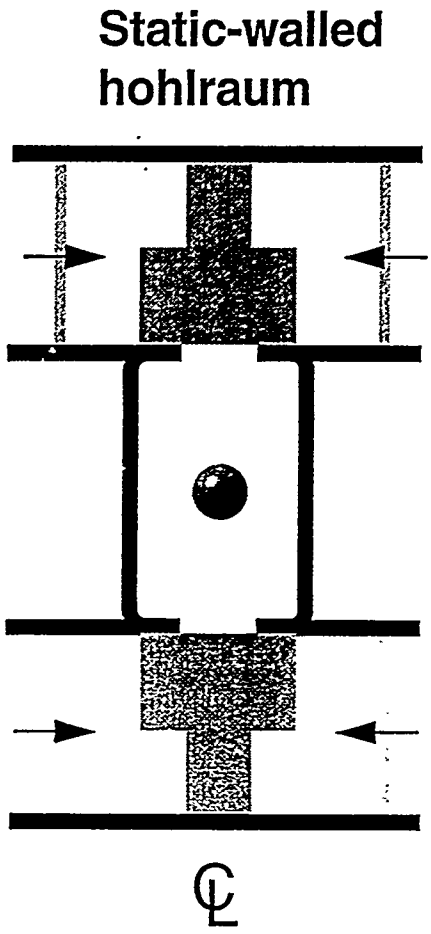

Fig. 35

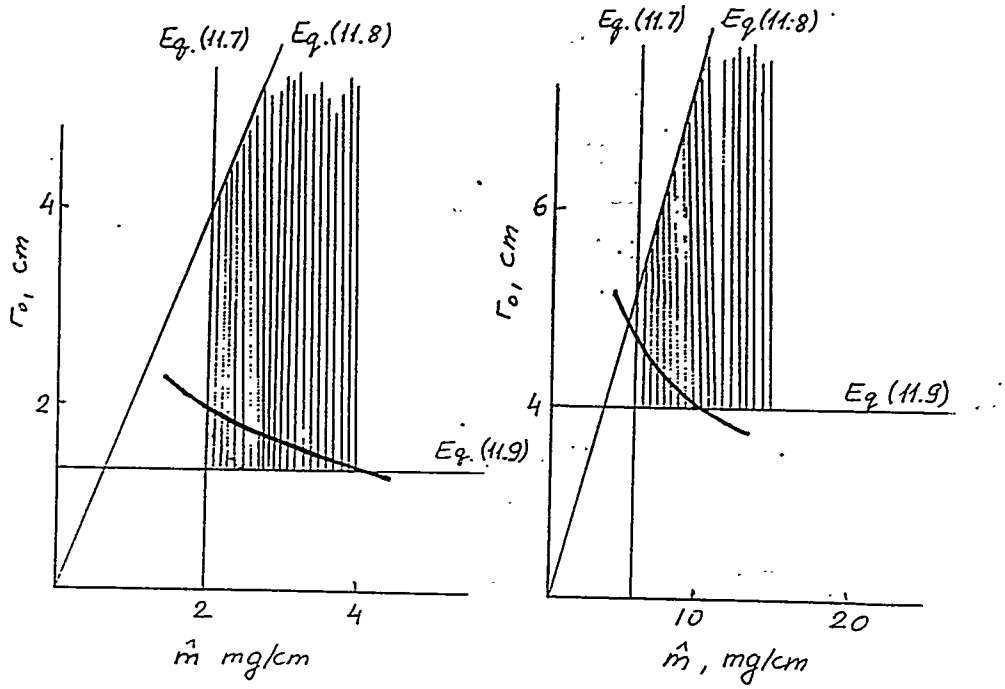
Eq. (11.7)
Eq. (11.8)
Eq. (11.9)
r_0, cm
4
2
2
4
$\hat{m}$ mg/cm
Eq. (11.7)
Eq (11.8)
Eq (11.9)
r_0, cm
6
4
10
20
$\hat{m}$, mg/cm